Copyright Warning & Restrictions

The copyright law of the United States (Title 17, United States Code) governs the making of photocopies or other reproductions of copyrighted material.

Under certain conditions specified in the law, libraries and archives are authorized to furnish a photocopy or other reproduction. One of these specified conditions is that the photocopy or reproduction is not to be "used for any purpose other than private study, scholarship, or research." If a, user makes a request for, or later uses, a photocopy or reproduction for purposes in excess of "fair use" that user may be liable for copyright infringement,

This institution reserves the right to refuse to accept a copying order if, in its judgment, fulfillment of the order would involve violation of copyright law.

Please Note: The author retains the copyright while the New Jersey Institute of Technology reserves the right to distribute this thesis or dissertation

Printing note: If you do not wish to print this page, then select "Pages from: first page # to: last page #" on the print dialog screen

ABSTRACT

THE DESIGN AND FABRICATION OF A THERMAL MICROPROBE INTEGRATED ON AN ATOMIC FORCE MICROSCOPE PROBE TIP

by
Yongxia Zhang

A thermal microprobe has been designed and built for high resolution temperature sensing. The thermal microprobe consists of a very-thin-film thermocouple junction confined to the very end of a low mass Atomic Force Microscope (AFM) probe tip. Essential to high resolution temperature sensing is the confinement of the thermocouple junction to a short distance at the AFM tip. This confinement is achieved by controlled photoresist coating.

Experimental prototypes have been made with the junction confined to within 0.3 μm of the tip. The couple is made of Au/Pd, and the two metals are electrically separated elsewhere by a thin insulating layer. The device is designed for insertion in an AFM instrument so that topographical and thermal images can be made with the same tip. Large contact pads permit mechanical and ohmic contacting with spring clamps.

Processing begins with double-polished, n-type, 4-inch-diameter, and 300 μm thick silicon wafers. Probe tips are formed by a combination of RIE, wet chemical etching, and oxidation sharpening, which makes the tips atomically sharp. The hot thermocouple junction is formed by controlled photoresist coating. The metal layers are sputtering deposited and the cantilevers are released by KOH etching and RIE.

The thermal microprobe gives a high temperature resolution and a high spatial resolution. The thermal mass is kept low in order to cause minimal disturbance of the

component under measurement. The thermal output of the microprobe is 5.6 $\mu V/^{o}C$ and is linear over the temperature range 25 ~ 110 ^{o}C.

THE DESIGN AND FABRICATION OF A THERMAL MICROPROBE INTEGRATED ON AN ATOMIC FORCE MICROSCOPE PROBE TIP

by
Yongxia Zhang

A Dissertation
Submitted to the Faculty of
New Jersey Institute of Technology
in Partial Fulfillment of the Requirements for the Degree of
Doctor of Philosophy

Department of Electrical and Computer Engineering

May 1997

APPROVAL PAGE

THE DESIGN AND FABRICATION OF A THERMAL MICROPROBE INTEGRATED ON AN ATOMIC FORCE MICROSCOPE PROBE TIP

Yongxia Zhang

Dr. Robert B. Marcus, Dissertation Advisor — Date
Professor of Electrical and Computer Engineering, NJIT

Dr. William N. Carr, Committee Member — Date
Professor of Electrical and Computer Engineering and Physics, NJIT
Director of Microelectronic Research Center, NJIT

Dr. Ken K. Chin, Committee Member — Date
Professor of Physics, NJIT
Director of NJIT/Rutgers-Newark Joint M.S./Ph.D. Program

Dr. Peter Engler, Committee Member — Date
Associate Professor of Electrical and Computer Engineering, NJIT

Dr. Nuggehalli M. Ravindra, Committee Member — Date
Associate Professor of Physics, NJIT

APPROVAL PAGE
(Continued)

THE DESIGN AND FABRICATION OF A THERMAL MICROPROBE INTEGRATED ON AN ATOMIC FORCE MICROSCOPE PROBE TIP

Yongxia Zhang

Dr. Roy H. Cornely, Committee Member — Date
Professor of Electrical and Computer Engineering, NJIT
Director of the Drexler Thin Films Microelectronics Laboratory, NJIT

BIOGRAPHICAL SKETCH

Author: Yongxia Zhang

Degree: Doctor of Philosophy

Date: May 1997

Undergraduate and Graduate Education:

- Doctor of Philosophy in Electrical Engineering,
  New Jersey Institute of Technology, Newark, NJ, 1997

- Master of Science in Semiconductor Physics and Device Physics,
  Fudan University, Shanghai, P. R. China, 1988

- Bachelor of Science in Physics,
  Fudan University, Shanghai, P. R. China, 1985

Major: Electrical Engineering

Presentations and Publications:

Yanwei Zhang, Yongxia Zhang, Dan Morrow, Dan Worsham, and Robert B. Marcus,
"A new MEMS wafer probe card,"
The 10th IEEE International Workshop on MEMS, Nagoya, Japan, Jan.26-30, 1997.

Yongxia Zhang, Yanwei Zhang, T. S. Sriram, and Robert B. Marcus,
"Formation of single tips of oxidation-sharpened Si,"
Applied Physics Letters, Vol.69, No.27, 4260(1996).

Yongxia Zhang, Yanwei Zhang, T. S. Sriram, and Robert B. Marcus,
"Formation of single tips of atomically sharp silicon,"
The 43rd National Symposium of the American Vacuum Society, Philadelphia, Pennsylvania, Oct.12-18, 1996.

Yongxia Zhang, Yanwei Zhang, and Robert B. Marcus,
"A new high resolution AFM thermal probe,"
Emerging Technologies Symposium, Princeton, New Jersey, Oct.26, 1995.

Yanwei Zhang, Yongxia Zhang, and Robert B. Marcus,
"CHIPP probe----A new MEMS wafer probe card,"
Emerging Technologies Symposium, Princeton, New Jersey, Oct.26, 1995.

This dissertation is dedicated to
my wife Xiaojing
and
my son Yucheng
and
my parents

ACKNOWLEDGMENT

I would like to express my deepest appreciation to Dr. Robert B. Marcus, who not only served as my research advisor, providing valuable and countless guidance, resources, and insight, but also constantly gave me support and encouragement.

Special thanks are given to Dr. William N. Carr, Dr. Ken K. Chin, Dr. Peter Engler, Dr. Nuggehalli M. Ravindra and Dr. Roy H. Cornely for actively participating in my committee.

I wish to acknowledge all the help and facilities made available to me at NJIT, which had a major role in completion of this dissertation. I wish to especially thank Dr. Dentcho Ivanov, Mr. Ken O'Brien and Mr. John Koons for their help in the clean room, and Dr. R. Levy for the use of his RF laboratory.

I wish to express my sincere thanks to Mr. Yanwei Zhang for his constant help, Dr. Jin-biao Huang for his mask making, Ms. Juliana Blaser and Dr. T. S. Sriram and Dr. Ahsan Enver at Digital Equipment Corporation for their help in the characterization and modelling, Dr. Paul Lin at Bellcore, and Mr. Leslie Hopkins and Mr. Gary Forsyth at Lucent Technology for their help of high resolution SEM.

I also wish to express my appreciation to Digital Equipment Corporation, Murray Hill Devices, Inc. and Digital Instruments, Inc. for financial support.

Last but not least, let me express my warmest thanks to my beloved family member in China and in the United States of America, for their overwhelming support.

TABLE OF CONTENTS

TABLE OF CONTENTS
(Continued)

Chapter **Page**

TABLE OF CONTENTS
(Continued)

Chapter **Page**

LIST OF TABLES

Table **Page**

LIST OF FIGURES

Figure **Page**

LIST OF FIGURES
(Continued)

Figure **Page**

LIST OF FIGURES
(Continued)

Figure **Page**

CHAPTER 1

INTRODUCTION

This research program has developed a high resolution thermal microprobe that is integrated on the sensing tip of an atomic force microscope (AFM) probe. Therefore the topographical and thermal images of the sample surface can be obtained simultaneously. The experimental work reported in this paper was done under the direction of Prof. R. B. Marcus in Electrical and Computer Engineering Department at New Jersey Institute of Technology.

1.1 Objective of this Research

In the microelectronics industry two factors drive a trend toward smaller microelectronic device components:

1) The growing need for high speed devices requires smaller components in order to operate devices at higher frequencies.
2) The trend toward more components on a chip drives a need for smaller components, since smaller component size means smaller chip area and higher device yield, and a lower unit cost.

Small size does not necessarily correlate with reduced power consumption since power requirements are in some cases dependent on the nature of the active component and not on its size. Decreased component size without a corresponding decrease in power leads to

an increase in power density which in turn produces Joule heating at sites of current crowding, charge injection, and in metal line. These unwanted thermal effects cause reliability problems, leading to device failure.

The successful diagnosis of potential failure modes caused by increased local power dissipation in increasingly smaller components requires a tool for measuring the temperature of these components during operation. In order to address this need we have designed and built a thermal microprobe for probing the temperature differences in various regions of components or devices at high resolution.

1.2 Brief Description of Thermal Microprobe

The thermal microprobe consists of a very-thin-film thermocouple junction confined to the tip region of a low-mass atomic force microscope probe. The device is designed for insertion in a Digital Instruments, Inc. scanning probe microscope (SPM) instrument and electrical contact to large thermocouple contact pads are made with spring clamp electrodes.

The main advantages of this thermal microprobe are:

1) It serves the dual function of an AFM probe for surface imaging and a thermal microprobe for probing the temperature of very small regions of the sample surface.
2) The thermal mass at the probe tip is kept low resulting in minimum perturbation of the temperature of the surface being measured with correspondingly high spatial resolution.

3) Abrasion or wearing of the probe tip surface does not alter the temperature measurement characteristics

4) It is fabricated monolithically by a sequence of mostly "standard" MEMS/IC processing methods.

1.3 Chapter Synopsis

Chapter 2 describes methods for measurement of surface temperature with very small probes, and also gives background information on the thermal microprobe developed in this research. Chapter 3 deals with the design of thermal microprobe. It includes atomic force microscope design, thermal microprobe design, processing steps and masks design. Chapter 4 details the steps for fabrication of the thermal microprobe. Chapter 5 describes the characteristics of the thermal microprobe developed in this research. Chapter 6 gives the summary. The Appendices describes the mask layout and the detailed processing parameters used in this research.

CHAPTER 2

BACKGROUND OF THERMAL MICROPROBE

With the current trends in microelectronics towards submicron scale devices, power dissipation and elevated temperature in high density chips are becoming increasingly important issues. To study thermal phenomena, such as "hot spots" during device operation, current crowding, electromigration, etc., on the microscopic scale and to assist in device and chip thermal design, it is essential to develop a technique to measure temperature at submicron scales.

There are many methods for sensing temperature of surface. Temperature is normally measured by thermoelectric devices such as thermocouples, semiconductor diodes and thermistors, metal film resistance[1], or optical techniques such as infrared thermometry[2], surface reflectance[3], liquid crystals[4] and Raman spectroscopy[5]. It is hard to get submicron spatial resolution with these methods. For example, optical techniques are diffraction limited by the wavelength of radiation involved which is about 5-10 μm for infrared thermometry and about 0.5 μm for Raman spectroscopy[5]. Since electrical devices can be built smaller than 0.5 μm with current microfabrication techniques, temperature measurement with a spatial resolution of at least 0.1 μm is desired.

2.1 Review of Thermal Microprobe

The inventions of the scanning tunneling microscope[6] (STM) and the atomic force microscope[7] (AFM) have spawned the development of different types of scanning probe microscopes (SPM) that can measure physical properties of materials with submicrometer and, at times, atomic scale spatial resolution. A thermal sensor built on AFM probe tip would offer the additional capability of thermal images of materials with small hot spots such as biased electronic devices and interconnects.

The AFM consists of a sharp tip mounted on a cantilever which is brought very close to, or in contact with, a substrate surface by piezoelectric actuators. The deflections of the cantilever due to tip-substrate interatomic forces (attractive or repulsive) are optically detected[8,9] by reflecting a laser beam from the cantilever onto a photodetector. With the spring constant of the cantilever known, the tip-substrate force can then be obtained. While maintaining a constant tip-substrate force of 10-20 nN by feedback control of the piezoelectric actuator, the tip is scanned over the substrate surface to obtain topographical images with atomic resolution capability.

It was recognized that one can also place a temperature, optical, magnetic, acoustic, or electrostatic sensor at the end of the sharp tip and use it as a scanning probe in an AFM. For such dual or multiprobing function, the AFM setup is attractive since the force feedback of an AFM can function independently of the sensor operation. The resolution of the multiprobing capability is often decided by the size of the sensor at the end of a probe tip.

The use of AFM for temperature measurement has a short history:

1) Majumdar *et al.*[10] developed a simple technique for making an AFM probe by joining two wires of a thermocouple. The wires provided the cantilever spring constant and the thermocouple junction was electrochemically etched to make a sharp tip which was used to simultaneously obtain thermal and topographical images of a single transistor and interconnect via structure. However, the thermocouple junction is as large as about 25 μm diameter.

2) Nakabeppu *et al.*[11] used differential thermal expansion of a composite AFM cantilever probe, made of a thin metal film (aluminum or gold) deposited on a regular silicon nitride AFM probe, to measure surface temperature contrast. During tip-surface contact, heat flow through the tip changes the cantilever temperature which bends the cantilever due to differential thermal expansion of the two probe materials.

3) Pylkki *et al.*[12] and Hammiche *et al.*[13] adapted a Wallaston wire to an AFM cantilever probe which can be used as a heater and a thermometer. The essential of the probe is a thermistor. The temperature of a surface is derived from a measurement of the resistance of the wire and the knowledge of the temperature coefficient of the resistance. One potential problem with this approach is that the abrasion or wearing of the probe surface may change the metal thickness and thus affect the output of the thermistor.

4) Most recently, Luo *et al.*[14] built a thin film thermocouple on AFM cantilever probe tip for scanning thermal microscope. The method uses voltage pulse to evaporate metal film and create a submicrometer scale hole at the very end of a metallized AFM cantilever probe tip. A thin metal film is deposited on a Si_3N_4 or Si cantilever probe. The probe tip is then brought in contact with a conducting surface using the AFM. A voltage pulse is applied between the tip and the surface. Due to the high electric field localized around the probe tip, the thin metal film evaporates and opens a hole only at the very end of the tip. The threshold voltage depends on the shape of the probe tip. It is difficult to know the threshold voltage due to the variability of the tip shape. Moreover, the fabrication is performed individually with each probe tip which is time-consuming and expensive.

2.2 The Development of this Research

Although the aforementioned thermal microprobes[10,11,12,13,14] can obtain thermal and topographical images simultaneously and some have very high spatial resolution, there are several problems with these devices. They were not reproducible since they were individually fabricated[10,12,13,14], or they were not reliable[11].

To overcome these problems, we developed a new method to build a very thin film thermocouple on the very end of the AFM cantilever probe tip. The hot junction of the thermocouple is at the end of the probe tip; the cold junction is an effective room

temperature junction at the contact pads on top of the probe chassis. When the AFM probe tip approaches the sample surface, it can perform its normal function as an AFM to reveal the topographical image of the sample surface. Meanwhile, the tiny thermocouple on the tip touches the hot spot on the sample surface and generates the Seebeck voltage which can be measured by the detection circuit. As the AFM probe tip scans across the sample surface, the temperature distribution and the topography of the sample surface can be obtained at the same time.

In our method the first thermocouple metal layer is deposited and patterned, and is followed by the deposition of an insulating layer (SiO_2, for example). Then the photoresist is coated in such a manner that there is no photoresist coverage at the region of the end of the probe tip. The exposed insulating layer is removed by wet or dry etching. The photoresist is removed and the second metal layer is deposited. This sequence of events produces a junction in the end region of the tip. Our method for restricting a junction to the end region only of the tip is more reproducible, more reliable, and is simpler.

CHAPTER 3

THERMAL MICROPROBE DESIGN

3.1 Atomic Force Microscope Design

3.1.1 Brief Description of Atomic Force Microscope

The atomic force microscope (AFM) probes the surface of a sample with a sharp tip, a couple of microns long and often less than 10 nm in diameter. The tip is located at the free end of a cantilever that is 100 to 200 μm long. Force between the tip and the sample surface cause the cantilever to bend, or deflect. In some cases, the tip touches the sample surface; in other modes, the tip is positioned hundreds of angstroms above the surface. A detector measures the cantilever deflection as the tip is scanned over the sample, or the sample is scanned under the tip. The measured cantilever deflections allow a computer to generate a map of surface topography. AFM can be used to study insulators and semiconductors as well as electrical conductors.

Several forces typically contribute to the deflection of an AFM cantilever. The force most commonly associated with atomic force microscopy is an interatomic force called the Van der Waals force. The dependence of the Van der Waals force upon the distance between the tip and the sample is shown in Figure 3.1.

Two distance regions are labeled on Figure 3.1: 1) the contact region; and 2) the non-contact region. In the contact region, the cantilever is held less than a few angstroms from the sample surface, and the interatomic force between the tip and the sample is

repulsive. In the non-contact region, the cantilever is held on the order of tens to hundreds of angstroms from the sample surface, and the interatomic force between the tip and the sample is attractive (largely a result of the long-range Van der Waals interactions).

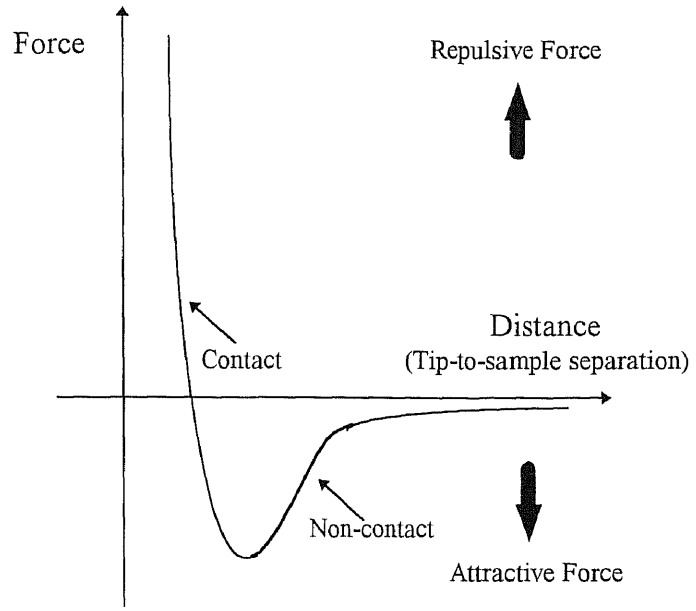

Figure 3.1 Interatomic force vs. distance curve

Most AFMs currently on the market detect the position of the cantilever with optical techniques[8,9]. In the most common scheme, shown in Figure 3.2, a laser beam bounces off the back of the cantilever onto a position-sensitive photodetector (PSPD). As the cantilever bends, the position of the laser beam on the detector shifts. The PSPD itself can measure displacements of light as small as 10 Å. The ratio of the path length between the cantilever and the detector to the length of the cantilever itself produces a

mechanical amplification. As a result, the system can detect sub-angstrom vertical movement of the cantilever tip.

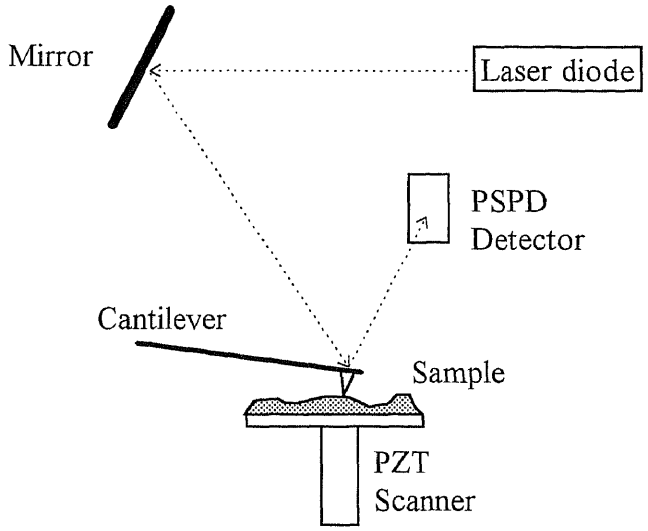

Figure 3.2 The AFM optical detection scheme

Other methods of detecting cantilever deflection rely on optical interference[15,16,17,18,19], or even a scanning tunneling microscope tip[7,20,21] to read the cantilever deflection.

3.1.2 Materials for Cantilever and Tip

Cantilever and its tip are critical components of an atomic force microscope system because they determine the force applied to the sample and the ultimate lateral resolution of the system. Silicon and silicon nitride are the two most common materials used in fabrication of cantilevers and tips[22,23]. Silicon nitride tips are fabricated by depositing a

layer of silicon nitride over an etched pit in a crystalline silicon surface. This method produces the pyramidal or tetrahedral tip geometry. The aspect ratio of a silicon nitride tip is thus limited by the crystallographic structure of the etch pit materials, silicon. The tips are broader than conical silicon tips, making them less suitable for imaging deep, narrow features. When cantilevers with high resonant frequencies call for thick films, silicon nitride films which contain residual stress make them deform as the film thickness increases.

Silicon cantilevers can be made with very sharp tips (radii of curvature down to 0.5 nm). Silicon conical tips are made commercially by etching into silicon around a silicon dioxide cap followed by oxidation sharpening. The high aspect ratio of conical tips makes them suitable for imaging deep, narrow features such as trenches and can provide atomic scale resolution. They are better for high frequency uses in the contact mode due to the large value of Young's modulus and can more easily be chemically modified for special application such as thermal microprobe. Therefore, we select silicon as our atomic force microscope material.

3.1.3 Operation Modes

In non-contact AFM, the tip is hovering a small distance away from the sample, vibrating near its natural resonant frequency; a high force constant is preferable as soft cantilevers tend to be pulled into the sample surface by attractive Van der Waals force. In contact AFM, the tip is in physical contact with the sample; a low force constant is required to avoid excessive pressure on the sample, thus avoiding scratching of the sample.

Typical values of force constants are 0.01 N/m to 1 N/m for contact AFM, and 1 N/m to 100 N/m for non-contact AFM[20,24].

In forming a thermal microprobe, a very thin film thermocouple is built on the tip of the AFM probe. In order to accurately measure the temperature of the sample surface, the thermocouple tip has to approach as closely as possible to the sample surface so that the temperature at the hot junction of the thermocouple is close to the temperature of the sample surface. In contact AFM operation mode, the tip is in contact with the sample and the contact mode is therefore preferred.

3.1.4 Geometry

The atomic force microscope is designed to be used with a Digital Instruments, Inc. AFM probe station, with the overall dimensions of 3.6 mm x 1.6 mm as shown in Figure 3.3.

The cantilever dimension in our contact AFM mode should meet the following criteria: (1) a low force constant, (2) a high resonant frequency, (3) short cantilever length, (4) a sharp protruding tip. The geometry parameters are shown in Figure 3.4 where l, w, and t are the cantilever length, width and thickness, respectively.

The cantilever force constant K is defined as the ratio (at the cantilever free end) of the force F applied to the deflection distance δ (Figure 3.5):

$$K = \frac{F}{\delta} \tag{3.1}$$

The relationship between force constant and cantilever geometry is[25]:

$$K = \frac{E}{4} \times \frac{wt^3}{l^3} \tag{3.2}$$

where E is Young's modulus.

For silicon Young's modulus E is 1.62×10^{11} N/m. The calculations of the force constant with cantilever width 20 μm and 40 μm are shown in Figure 3.6 and Figure 3.7. The force constant increases with the cantilever thickness and length. If the cantilever length is less than 200 μm, the force constant depends largely on the cantilever thickness and length. A little change in cantilever thickness will cause large force constant change. However, if the cantilever length is large than 200 μm, the force constant variation depends less on the cantilever thickness and length.

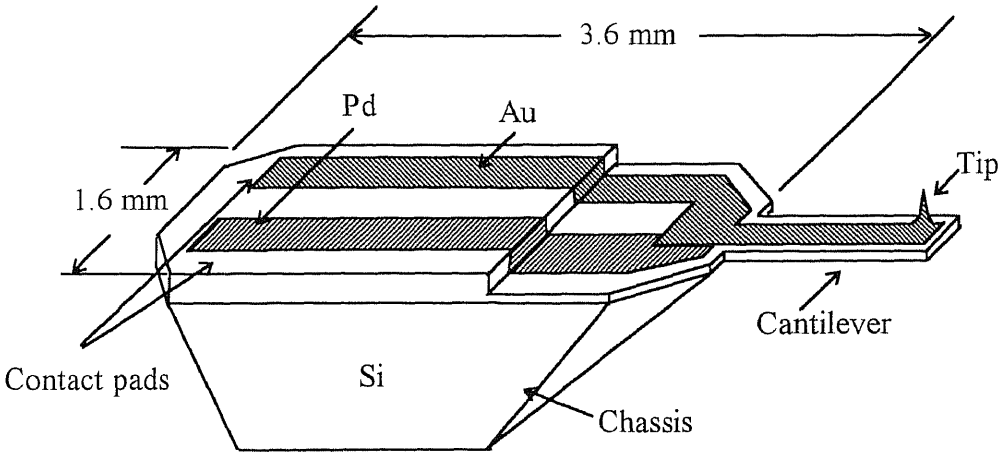

Figure 3.3 Overview of thermal microprobe

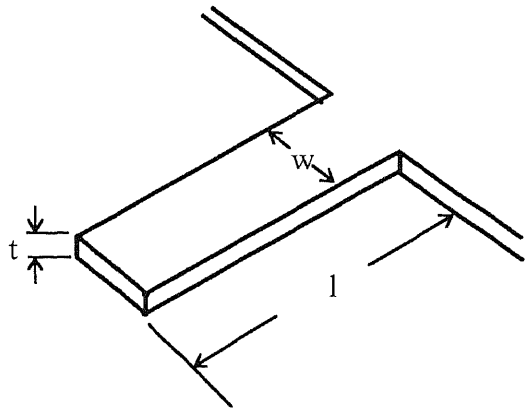

Figure 3.4 Cantilever geometry parameter: l (length) w (width), and t (thickness)

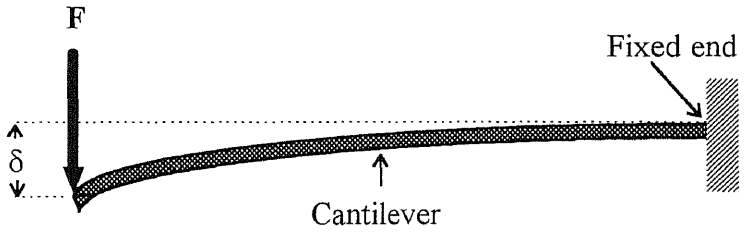

Figure 3.5 Cantilever deflection by applied force

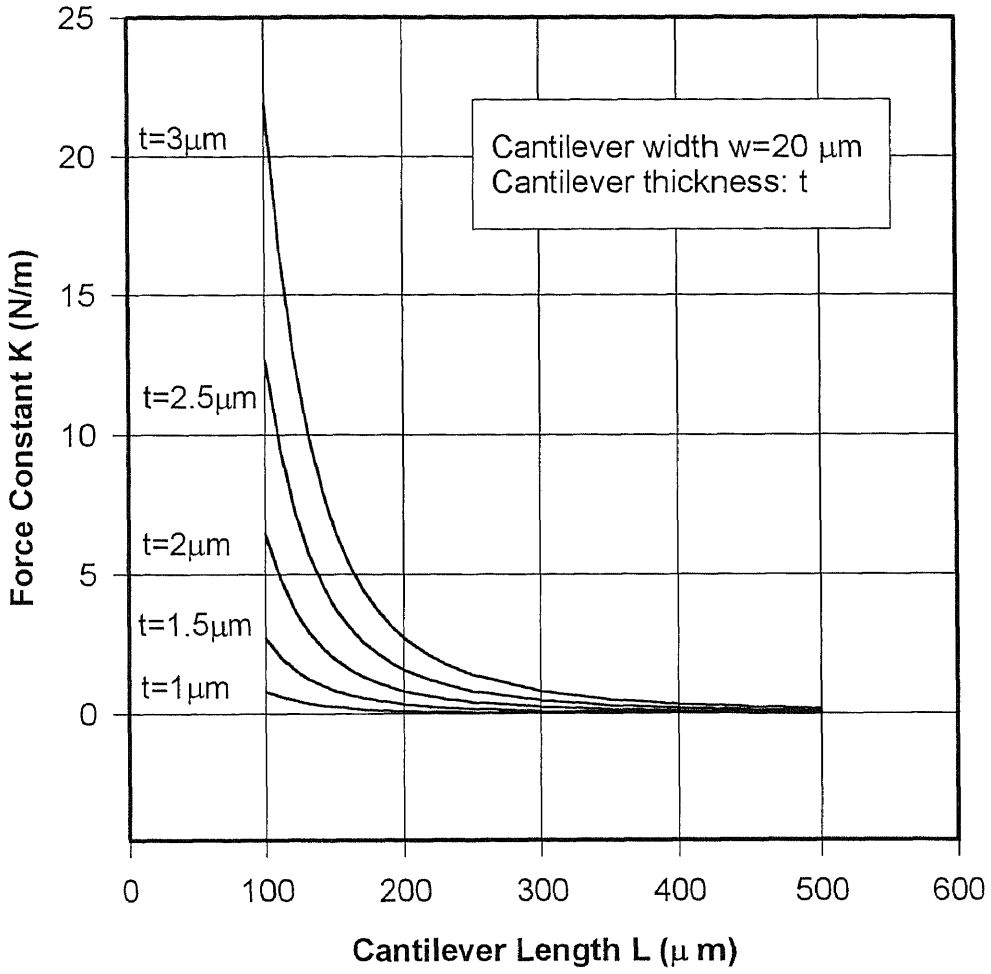

Figure 3.6 Force constant K vs. cantilever length l with w=20 μm

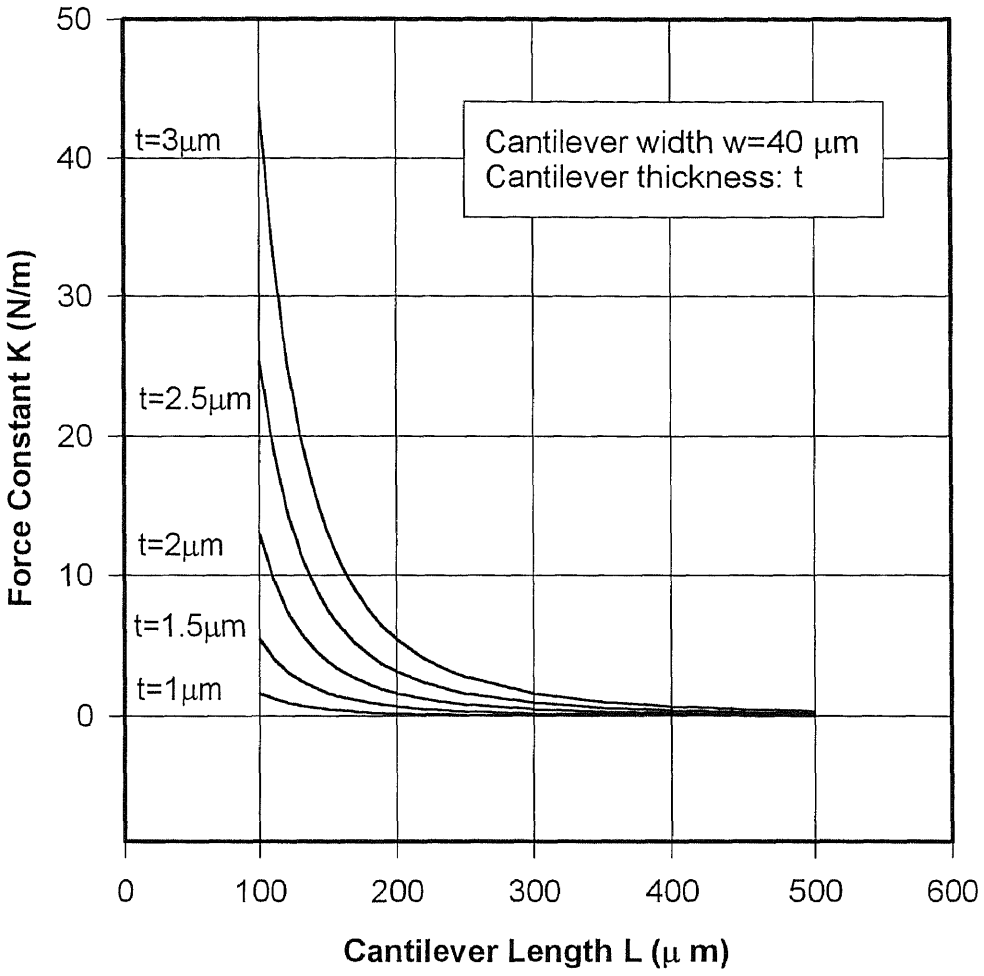

Figure 3.7 Force constant K vs. cantilever length l with w=40 μm

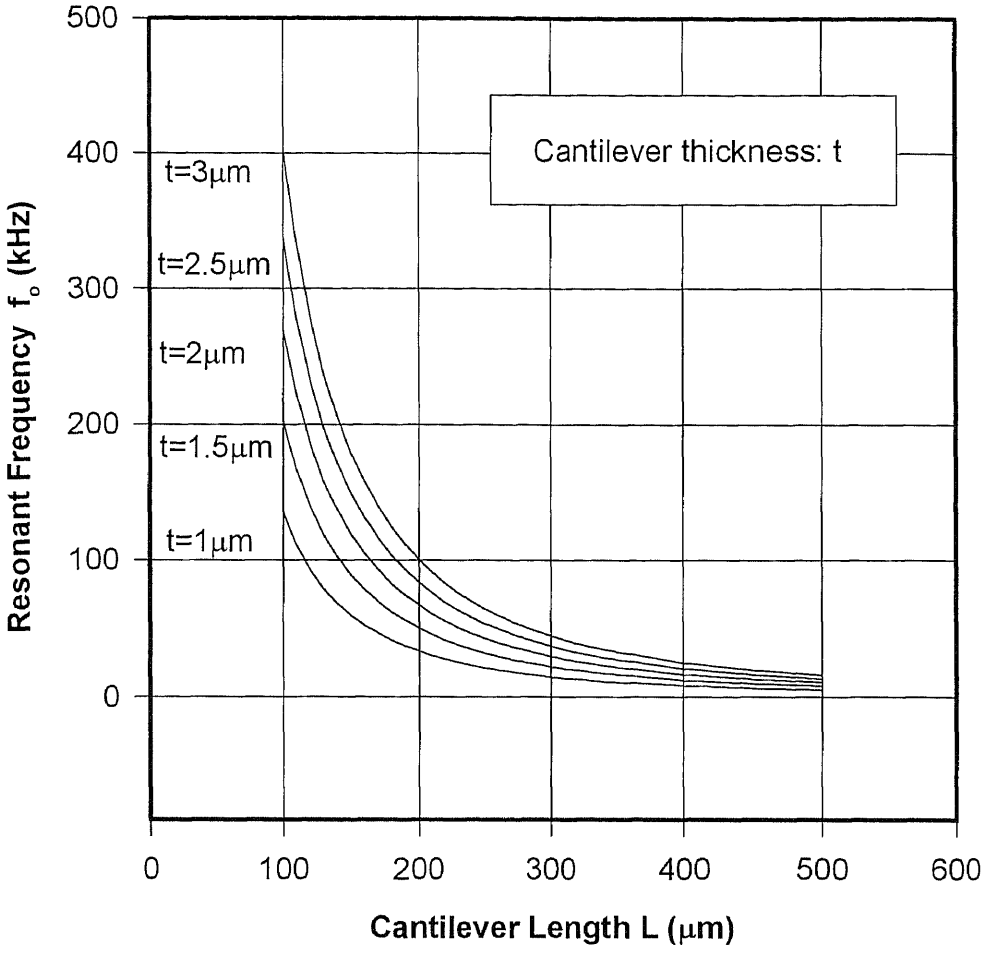

Figure 3.8 Cantilever resonant frequency vs. cantilever length

The resonant frequency of the cantilever is[25]:

$$f_o = \frac{3.52}{2\pi}\sqrt{\frac{EI}{ml^3}} \tag{3.3}$$

where I is area moment of inertia,

$$I = \frac{1}{12}wt^3 \tag{3.4}$$

m is cantilever mass,

$$m=\rho wtl \tag{3.5}$$

ρ is the density of the material. Therefore, the relationship between cantilever resonant frequency f_o and the cantilever dimension is:

$$f_o = 0.162\sqrt{\frac{E}{\rho}} \times \frac{t}{l^2} \tag{3.6}$$

For silicon ρ is 2.33 g/cm^3. The calculations in Figure 3.8 show that if the cantilever length is less than 200 μm, the increase in resonant frequency is strongly dependent upon the thickness and length.

Table 3.1 lists the cantilever dimensions and their force constant and resonant frequency of our designed devices. The lowest force constant is 0.03 N/m. The highest resonant frequency is 101.1 kHz. In order to meet the requirements of low force constant, high resonant frequency and short cantilever length, we have to trade off between these parameters. The optimum cantilever dimensions in our design are l=200 μm, w=40 μm and t=1.5 μm. The force constant and resonant frequency are 0.68 N/m and 50.5 kHz respectively.

The probe tip is designed 4 to 5 μm high extending from the cantilever surface (Figure 3.9). The tip is atomically sharp.

Table 3.1 Cantilever dimensions, force constant, and resonant frequency

Width	w=20 μm		w=40 μm			
Length	l=450 μm				l=200 μm	
Thickness	t=1.5 μm	t=3 μm	t=1.5 μm	t=3 μm	t=1.5 μm	t=3 μm
Force Constant (N/m)	0.03	0.24	0.06	0.48	0.68	5.47
Resonant Frequency (kHz)	10.0	20.0	10.0	20.0	50.5	101.1

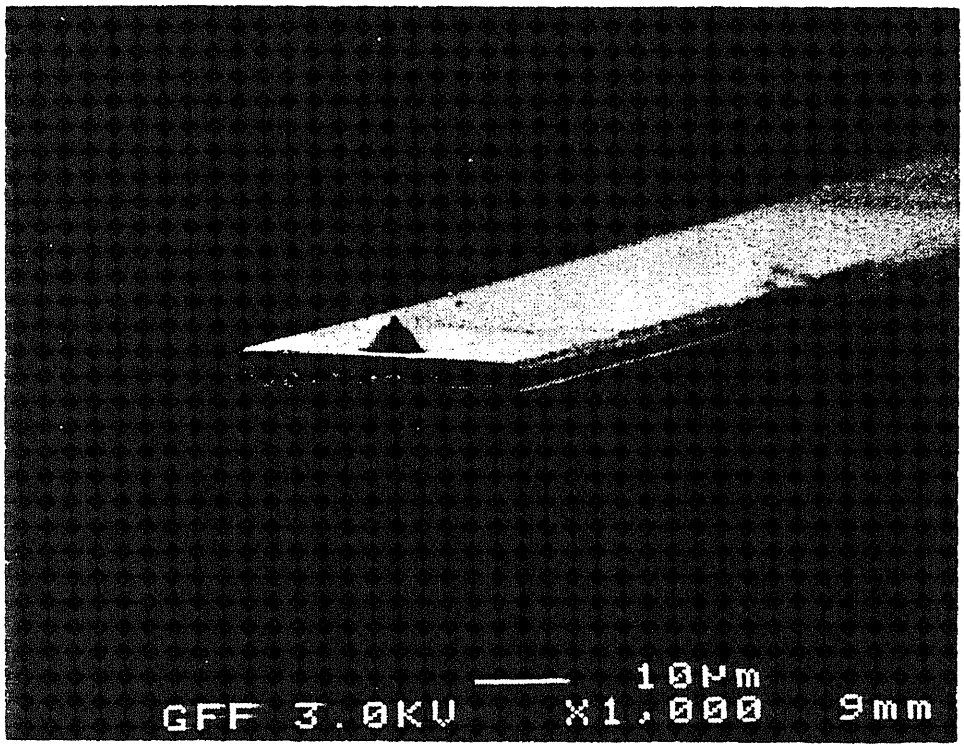

Figure 3.9 SEM photo: probe tip at the end of cantilever

3.2 Thermal Sensor Design

3.2.1 Electromotive Force (EMF)

Thermocouples are usually made from two dissimilar metal wires. The wires are connected at one end, and the electrical voltage is measured between the two remaining ends (see Figure 3.10). At thermal equilibrium, there will be a zero voltage. But if the temperature at the connection point is raised with respect to the ambient by an amount ΔT while the two remaining ends are still at ambient, an open-circuit voltage ΔV_s will be measured. This effect called the Seebeck effect[26]. This electromotive force (EMF) ΔV_s, known as the Seebeck voltage, can be mathematically expressed by:

$$\Delta V_s = \alpha_s \Delta T \tag{3.7}$$

with α_s as the Seebeck coefficient expressed in $V\ K^{-1}$.

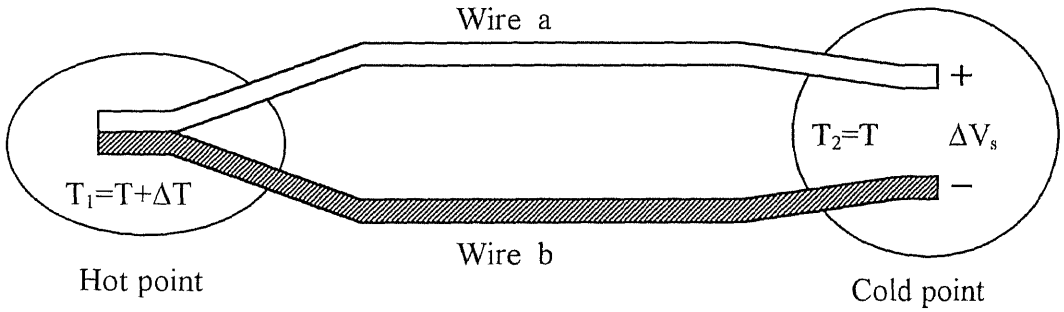

Figure 3.10 The Seebeck effect: an electrical voltage ΔV due to a temperature difference ΔT

The Seebeck effect results from two thermal phenomena, the Peltier and Thomson effects.

Peltier discovered[27] that when a small electric current is passed across the junction of two dissimilar metals in one direction, the junction is cooled and thus absorbs heat from its surroundings. When the direction of the current is reversed, the junction is heated and thus releases heat to its surroundings. This Peltier effect takes place whether the current is introduced externally or is induced by the thermocouple itself. The Peltier heat is proportional to the current and can be written

$$dQ_p=\pi I dt \tag{3.8}$$

where dQ_p is the heat delivered at a junction in time dt by a current I. The Peltier coefficient or Peltier voltage, π, depends only on the temperature and the two junction materials. It is the fundamental potential responsible for the Seebeck voltage. Thus the Peltier voltage for two materials, a and b, with junctions at temperatures T_1 and T_2, when current flow is zero, is

$$\pi_{ab}=(\pi_{ab})_{T1} - (\pi_{ab})_{T2} \tag{3.9}$$

The other thermal phenomenon is Thomson effect[28]. An electric current in a homogeneous wire delivers heat from the hot region to the cold region when the current flows from a hot region to a cold region; and in the opposite direction when the current was reversed. Such an effect would require an EMF to exist between the hot region and the cold region if no current flowed in a homogeneous conductor. That EMF is called the Thomson voltage. The Thomson voltage depends on the way the Fermi energy of each conductor varies with temperature. In simplest form it can be written

$$V_T = \int_{T1}^{T2} \sigma \, dT \tag{3.10}$$

where σ is Thomson coefficient.

The Seebeck voltage V_s for two materials, a and b, with junctions at temperatures T_1 and T_2, when current flow is zero, is the sum of the Peltier voltage π and the Thomson voltage V_T.

$$\begin{aligned} V_s &= \pi \; + V_T \\ &= (\pi_{ab})_{T2} - (\pi_{ab})_{T1} + \int_{T1}^{T2} \sigma_a dT + \int_{T2}^{T1} \sigma_b dT \\ &= (\pi_{ab})_{T2} - (\pi_{ab})_{T1} + \int_{T1}^{T2} \sigma_a dT - \int_{T1}^{T2} \sigma_b dT \\ &= (\pi_{ab})_{T2} - (\pi_{ab})_{T1} + \int_{T1}^{T2} (\sigma_a - \sigma_b) dT \end{aligned} \tag{3.11}$$

The Seebeck coefficient α_s, for materials a and b, is defined as

$$\alpha_s = \frac{dV_s}{dT} \tag{3.12}$$

Large thermal voltages are created by coupling elements with large differences in thermal electromotive force (Seebeck voltage). Table 3.2[29] lists some of the couple elements that were considered. The choice of junction elements was governed not only by the large differences of two elements in electromotive force (EMF) but also by the compatibility with processing steps necessary to form the device. Thus we chose gold and palladium as the two elements of the thermocouple. With the cold junction at 0 °C and hot junction at 100 °C, the EMFs of gold and palladium relative to platinum are 780 μV and -570 μV (Table 3.2). At 100 °C the junction is expected to deliver 13.5 μV for a temperature difference of 1.0 °C. The current generated in the thermocouple circuit is

estimated from the resistance of the circuit. The circuit includes resistance terms due to the thermocouple hot junction region at the end of the tip (R_J), electrical leads on the tip supporting the hot junction (R_T), electrical leads on the cantilever from the tip to the chassis (R_L), and electrical leads on the chassis (R_C). The calculated resistances are shown in Figure 3.11 and Table 3.3, giving a total resistance of 96.4 Ω. The thermal EMF produced by a temperature difference of 0.01 °C is 0.135 μV. The current produced by a temperature difference of 0.01 °C is therefore calculated to be 1.4 nA. Since this level of current well above the noise level for a potentiometric measurement scheme using null detection, 0.01 °C sensitivity therefore is reasonable and obtainable.

In the device fabrication, there is a very thin layer of Cr between Pd and Au for improving Au adhesion to SiO_2. However, both the Au/Cr couple and the Cr/Pd couple are in the same hot temperature region and the Cr therefore will have minimum effect on the thermoelectric voltage of the Pd/Au thermocouple[30]. Thus, we will still refer to our thermocouple as a Pd/Au junction.

Table 3.2 Thermal EMF of some materials relative to platinum*

materials	EMF (μ V)
Ta	330
Pd	-570
Au	780
Cu	760

* cold junction at 0 °C; hot junction at 100 °C

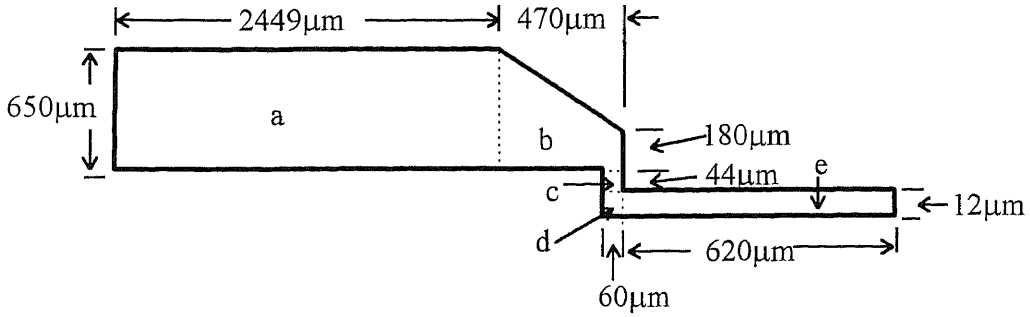

Resistivity of Pd: ρ_1=10.8 μΩ cm
Thickness: t=800 A
Sheet resistance: R_{s1}= ρ_1/t=1.35 Ω/square
R'_{Pd}= R'_L+R'_C=79.3 Ω

(a) Resistance of metal 1: Pd

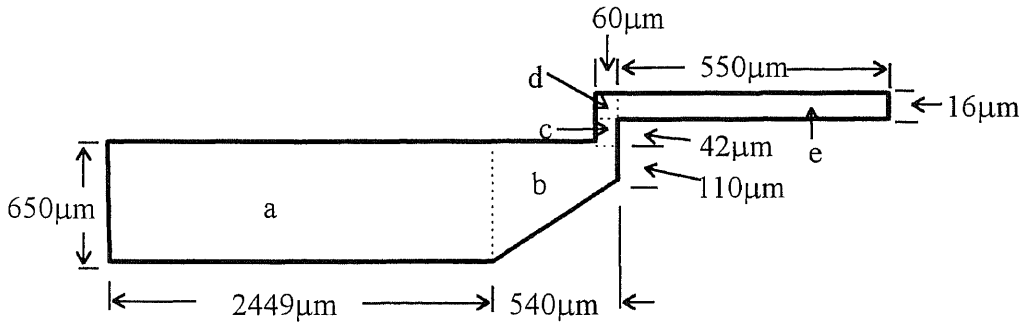

Resistivity of Au: ρ_2=2.2 μΩ cm
Thickness: t=800 A
Sheet resistance: R_{s2} = ρ_2/t=0.28 Ω/square
R'_{Au}= R''_L+R''_C=11.7 Ω

(b) Resistance of metal 2: Au

Figure 3.11 Resistance estimation of two layers metal

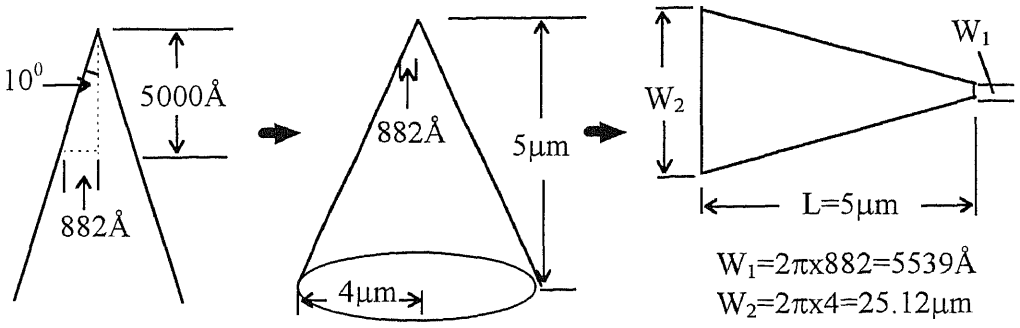

Thickness: t=400Å

Sheet resistance: R_{sPd}=2.7 Ω/square

R_{sAu}=0.55 Ω/square

$\mathbf{R_{pPd}}$**= 4.4 Ω**

$\mathbf{R_{pAu}}$**= 1.0 Ω**

(c) Resistance on the tip

The total resistance of two layers metal:

$$\mathbf{R_{total}} = R'_{Pd} + R'_{Au} + R_{pPd} + R_{pAu}$$
$$= 79.3 + 11.7 + 4.4 + 1.0$$
$$= \mathbf{96.4\ \Omega}$$

Figure 3.11 (continued) Resistance estimation of two layers metal

Table 3.3 Estimation of resistance for thermocouple circuit

Material	$R_J(\Omega)$	$R_T(\Omega)$	$R_L(\Omega)$	$R_C(\Omega)$	$R_{total}(\Omega)$
Pd	trivial	4.4	72.0	7.3	83.7
Au	trivial	1.0	10.1	1.6	12.7
				Total R (Ω)	**96.4**

3.2.2 Thermocouple Junction

The thermocouple circuit consists of a cold junction and a hot junction. The cold junction is an effective room temperature junction at the contact pads on the chassis of the probe; the hot junction is at the end of the tip (see Figure 3.3). Both the extents of the hot thermocouple junction and the thermal mass of the probe must be kept small. The junction in the vertical direction must be short in order to minimize the temperature gradient throughout the junction. A small thermal mass is required to reduce heat transfer from the sample surface under test in order to obtain a more accurate temperature reading. A reduction in heat transfer also means an improvement in temperature resolution and in spatial resolution.

The shape and dimensions of the hot junction are shown in Figure 3.12. The vertical height of the junction **a** is about 0.5 μm. The thickness of Pd ($\mathbf{t_{11}}$) and Au ($\mathbf{t_{21}}$) on the tip is 50 nm. The Pd and Au away from the junction are separated by silicon dioxide with thickness $\mathbf{t_{ox2}}$=240 nm. The Pd and silicon are separated by silicon dioxide with thickness $\mathbf{t_{ox1}}$=25 nm. The radius **r** at the end of silicon tip is about 5 nm. The height **h** of the tip is about 5 μm. The lateral radius $\mathbf{r_c}$ of the tip at base is 4 μm. The detailed parameters of the thermocouple hot junction are listed in Table 3.4.

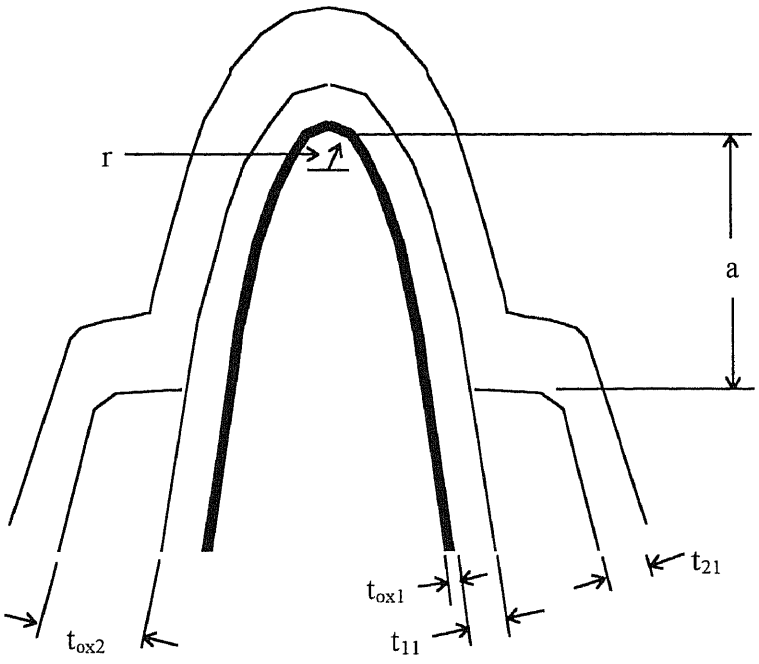

(a)

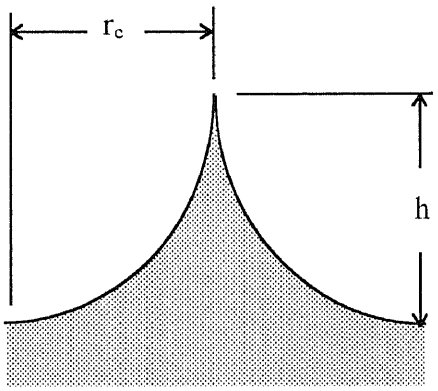

(b)

Figure 3.12 Thermocouple geometry and its parameters

Table 3.4 Parameters of components of the thermal microprobe

Parameter	Symbol	Values
radius at the end of Si tip	r	5 nm
vertical height of thermocouple	a	500 nm
thickness of metal 1 on tip	t_{11}	50 nm
thickness of metal 2 on tip	t_{21}	50 nm
thickness of oxide 1	t_{ox1}	25 nm
thickness of oxide 2	t_{ox2}	240 nm
lateral radius of tip at base	r_c	4 μm
height of tip	h	5 μm
width of Si cantilever	w	20 μm, 40 μm
length of Si cantilever	l	200 μm, 450 μm
thickness of Si cantilever	t	1.5 μm, 3 μm
electrical resistivity of metal 1 (Pd)	ρ_1	10.5 μΩ cm
electrical resistivity of metal 2 (Au)	ρ_2	2.24 μΩ cm
thermal conductivity of metal 1 (Pd)	κ_1	0.72 W/cm K
thermal conductivity of metal 2 (Au)	κ_2	3.18 W/cm K
thermal conductivity of oxide	κ_{oxide}	0.0266 W/cm K
thermal conductivity of silicon	κ_{Si}	1.39 W/cm K

Using the parameters in Table 3.4, a finite element analysis model was created[31] as shown in Figure 3.13. The model simulates the test condition of the thermal microprobe in air. Figure 3.14 gives the temperature when the thermal microprobe touches the test sample surface at 56 °C in air while the base of the tip remains at 30 °C. The simulation shows a significant loss in temperature from the end of the tip towards the cantilever. This gives us the following important suggestions:

1) The hot junction should be confined to as short a vertical distance at the end of the tip as is practical in order to minimize the temperature loss along this direction.
2) The thermocouple must be calibrated against known temperatures in order to be able to use the microprobe for accurate temperature measurements.
3) It is reasonable to conclude that the cold junction at the contact pads stays at room temperature during a measurement. The steeply falling temperature from the hot sample surface will not affect the cantilever temperature. Therefore the contact pads far away from the cantilever will remain at room temperature.

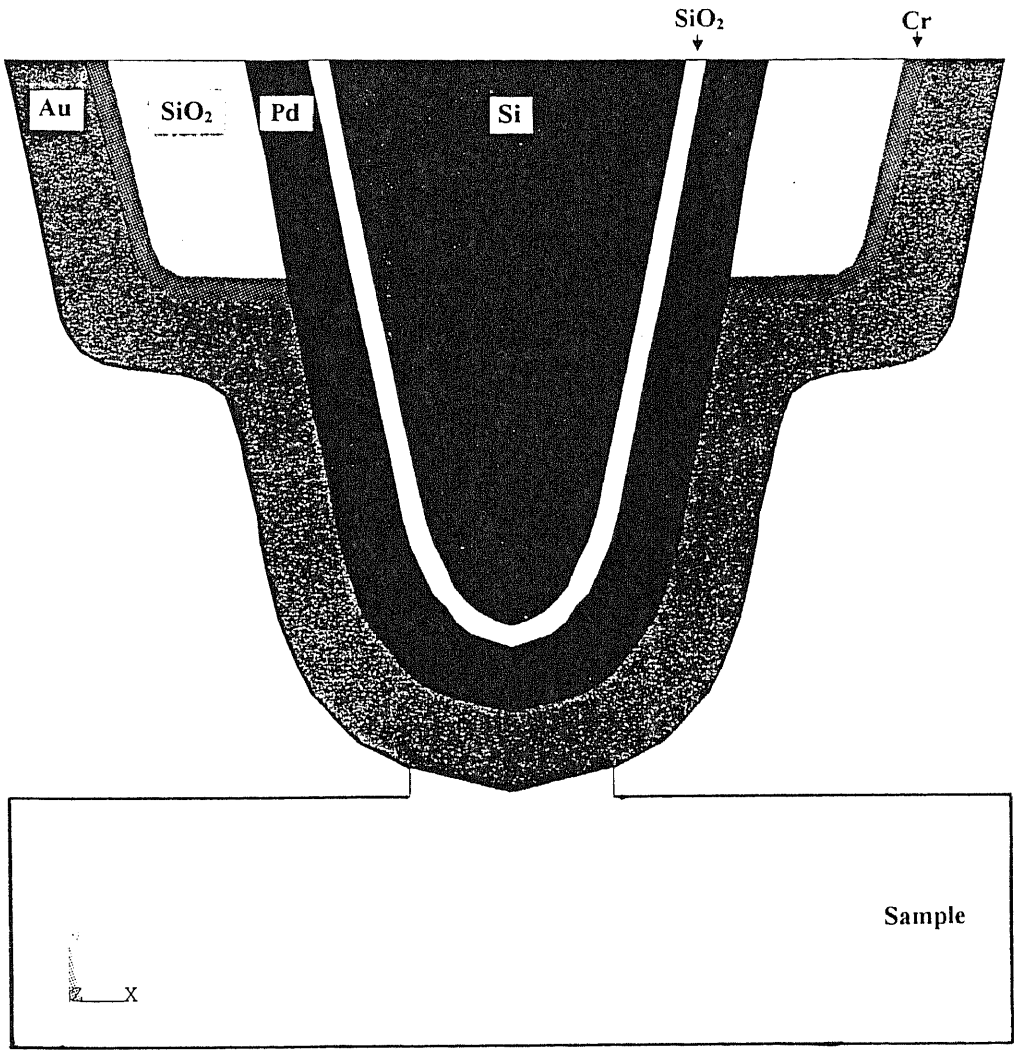

Figure 3.13 Thermal finite element analysis model of microprobe tip

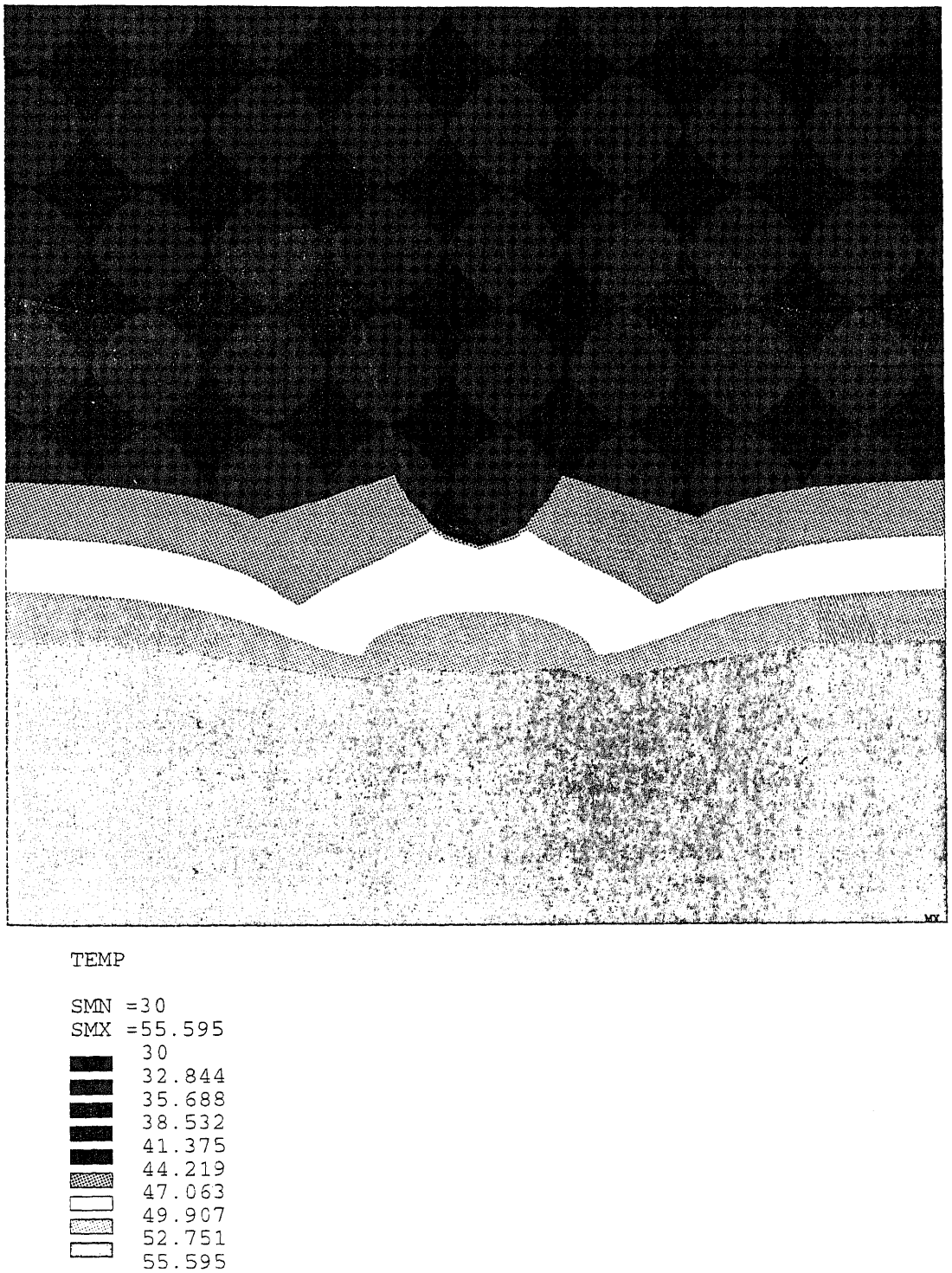

Figure 3.14 Temperature distribution between the microprobe tip and the test sample

3.3 Processing Steps

In this section, we briefly summarize the processing scheme. The details will be described in Chapter 4.

The processing begins with double-polished n-type 4" silicon wafers. The major steps are summarized as following:

1. Grow thermal oxide.
2. Form the tip by photolithography followed by a careful combination of RIE and wet chemical etching.
3. Define the size of the chassis, cantilever, and tabs (for function of tabs see Section 3.4) by RIE.
4. Sharpen the tip by oxidation sharpening.
5. Grow a thin thermal oxide layer followed by deposition of 50 nm Pd.
6. Deposit 300 nm LPCVD oxide on Pd.
7. Coat the wafer with photoresist except the end of the tip.
8. Etch off the exposed oxide with RIE. Then strip the photoresist.
9. Deposit 50 nm Au.
10. Release the cantilever from back side by KOH etching.

3.4 Masks Design

The mask design is done on the IC station of the MENTOR GRAPHICS version 8.4. There are total seven masks including Disk, Cantilever, Backside Etching, Metal 1, Metal 2, Window and Contact Pad. The layouts of the mask are shown in Appendix A.

The first mask (Disk) defines the tip region which has 8 μm diameter (Figure A.1). Dry and wet etching are used to form a 5 μm high tip. It also forms 4 tabs at two sides of the device chassis (Figure 3.15a, arrows) to connect the device to the silicon wafer frame after backside etching. It is easy to take the individual device off the wafer frame by slightly pressing the tabs down when the test of device is needed. The thickness of the tabs is equal to the height of the tip plus the thickness of the cantilever.

The second mask (Cantilever) defines the cantilever (Figure A.2). There are three cantilever sizes (450 μm x 20 μm, 450 μm x 40 μm and 200 μm x 40 μm) as shown in Figure 3.15. The two corners at the front edge of the device are truncated and the tip is located as close as possible to the cantilever free end. These will allow the probe tip to probe a textured surface with minimum interference from the end of the cantilever and chassis.

The third mask (Backside) is used for backside etching to release the cantilever (Figure A.3). At the four corners of the rectangle, compensation patterns are designed. This satisfies the problem created by KOH etching at a convex corner. More details will be presented in Chapter 4.

The fourth and fifth masks (Metal 1 and Metal 2) are used with "lift off" to form the metal patterns (Figure A.4 and Figure A.5). The leads on the chassis also serve as the contact pads which are designed as large as possible to reduce the resistance.

The sixth mask (Window) is used to etch the silicon dioxide on Pd, allowing the external spring contact to make ohmic contact with Pd (Figure A.6).

The seventh mask (Contact Pad) is designed to increase the thickness of both metal layers on the chassis (Figure A.7) to provide better ohmic contact with the external spring contacts.

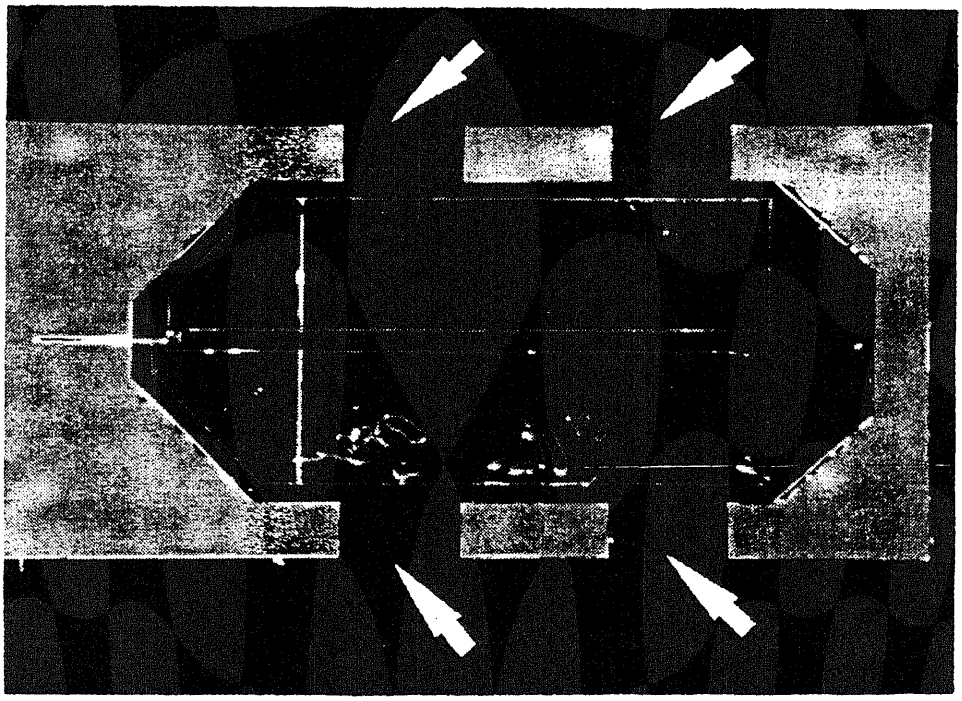

(a) Cantilever size: 450 μm x 20 μm

Figure 3.15 Optical microscope photos showing devices with three different cantilever sizes

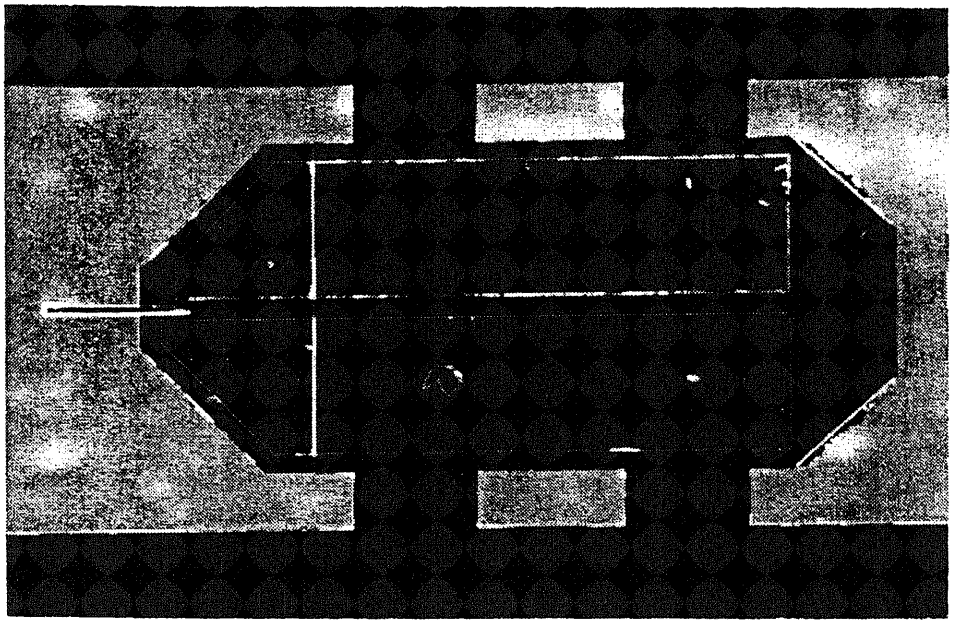

(b) Cantilever size: 450 μm x 40 μm

Figure 3.15 (cont.) Optical microscope photos showing devices with three different cantilever sizes

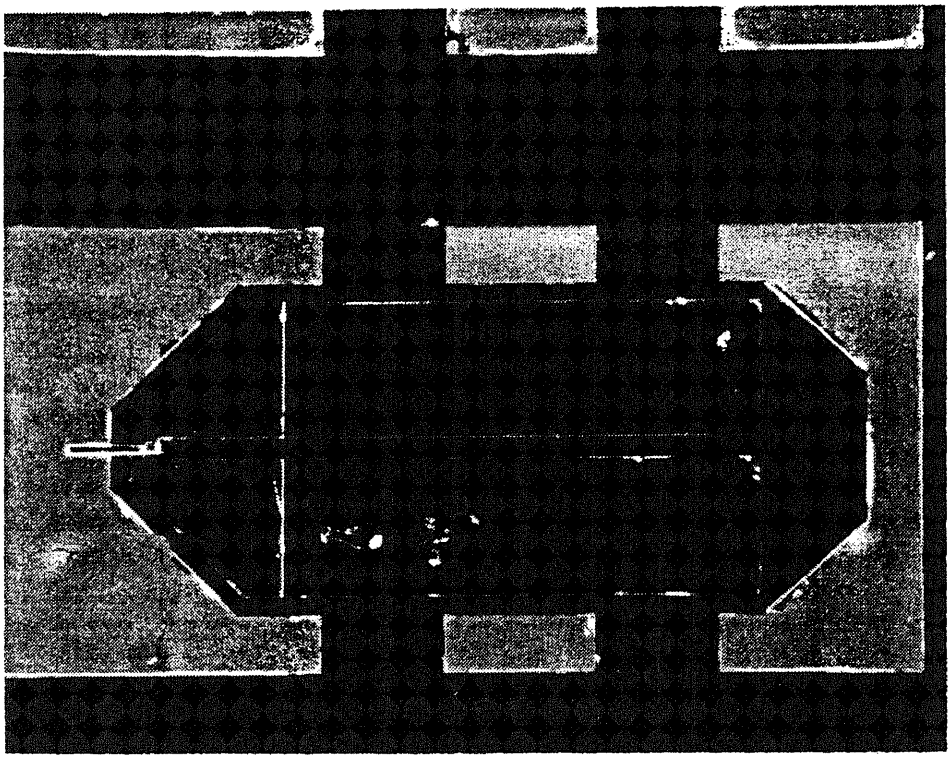

(c) Cantilever size: 200 μm x 40 μm

Figure 3.15 (cont.) Optical microscope photos showing devices with three different cantilever sizes

CHAPTER 4

FABRICATION OF THERMAL MICROPROBE

4.1 Formation of Single Tips of Atomically Sharp Silicon[32,33]

A crucial component of atomic force microscope (AFM) and our thermal microscope is the formation of an atomically-sharp tip, usually positioned at the end of a flexible cantilever[7]. Silicon is an attractive material for forming both the cantilever and integrated tip because of its good mechanical properties and ease of fabrication[34]. Si cantilevers with Si tips are formed by dry or wet etching followed by oxidation sharpening[35,36,37]. Atomically-sharp silicon tips with radius < 1 nm are produced by the oxidation sharpening method[35,36].

However, the oxidation sharpening method sometimes leads to the formation of multiple tips instead of the desired single tips[36,38]. A typical example is shown in Figure 4.1. Multiple tips can seriously affect the spatial resolution of AFM images and also influence the resolution of thermal microscope. In this section we analyze the mechanisms likely to be responsible for forming multiple tips. We find that the likely mechanism involves the presence of sharp corners before oxidation sharpening and the subsequent generation of atomically sharp points at these corners. Therefore we developed a processing scheme that eliminates the sharp corners and produces only single tips of silicon with typical atomic sharpness.

Figure 4.1 SEM photo of multiple tips resulting from standard oxidation sharpening method

4.1.1 Multiple Tips Formation

The overall processing scheme used as the starting point in this study was essentially the standard method for oxidation sharpening. The starting material was n-type (100) silicon wafers. Precursor shapes before oxidation sharpening were formed by dry reactive ion etching (RIE) and wet isotropic etching, and final tip configuration was controlled by oxidation. Silicon etching masks were made of 200 nm thermal SiO_2. Wafers were oxidized in steam and oxygen at 1050 °C for 30 minutes followed by photolithography patterning to define 8 μm diameter round pads of SiO_2 (Figure 4.2a). Anisotropic RIE was used to form a steep wall (Figure 4.2b). The wafer was then etched in a solution consisting of 2% HF, 3% CH_3COOH, and 95% HNO_3 (vol%). This is an isotropic silicon etchant with the oxide etch rate only 0.01 times the silicon etching rate. The etching was stopped after 2~3 minutes when the width of the silicon supporting the oxide mask was less than 500 nm (Figure 4.2c). After the oxide mask was stripped in buffered HF solution, sharp corners on the top were evident (Figure 4.2d and Figure 4.3). Finally, dry oxidation at 950 °C of the sample produced the double-tipped structure shown in Figure 4.1 and Figure 4.2e. Double-tipped structures sometimes form even when the width of the silicon before oxidation is as small as 200 nm.

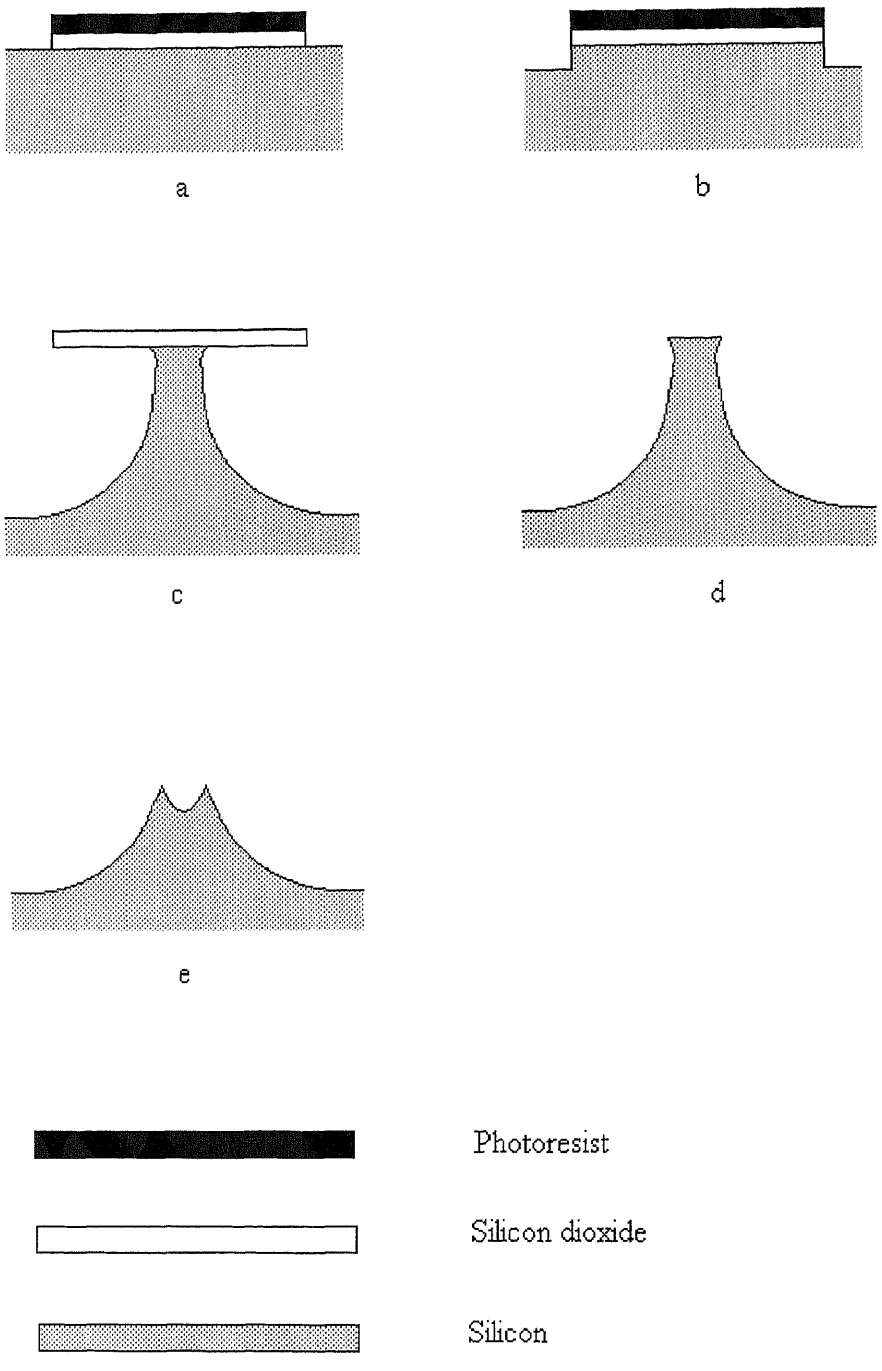

Figure 4.2 Illustration of multiple tips formation

Figure 4.3 SEM photo of precursor tip ready for oxidation sharpening

4.1.2 Single Tip Formation

Experiments showed that single tips only form if the sharp corners shown in Figure 4.2d and Figure 4.3 are eliminated. The processing procedure is shown in Figure 4.4. After the oxide mask was stripped in buffered HF solution (Figure 4.4d), we removed the sharp corners by dipping samples in the isotropic etch solution for several seconds immediately before oxidation sharpening (Figure 4.4e). The structure produced by this procedure is also shown in Figure 4.5. The pre-oxidation sharpening treatment produced single tips as shown in Figure 4.6. Although the limiting resolution of the scanning electron microscope (SEM) cannot examine the tip morphology with atomic-scale resolution, earlier work[35,36] has demonstrated that this basic procedure forms an atomically sharp tip (Figure 4.7).

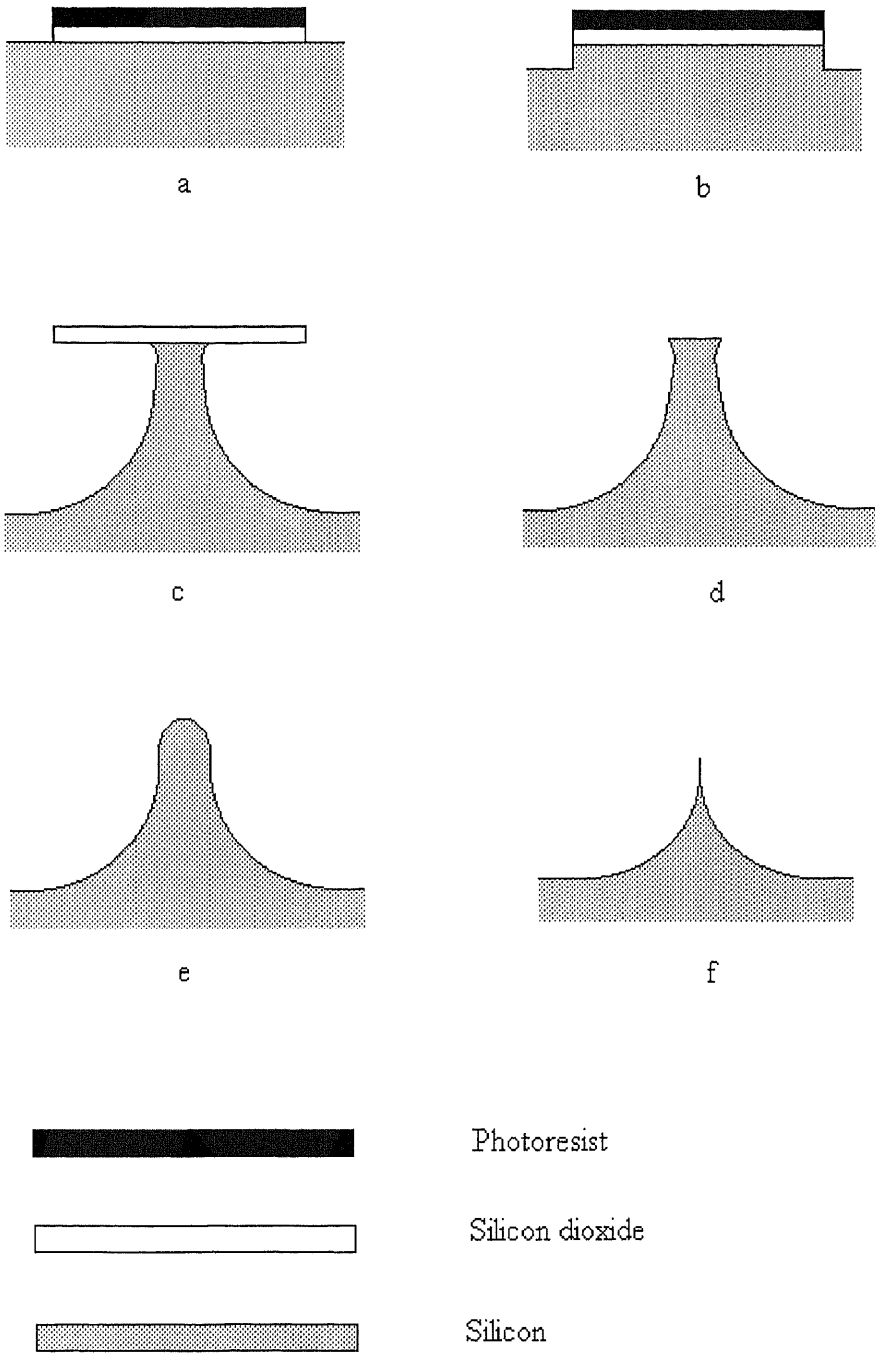

Figure 4.4 Illustration of single tip formation

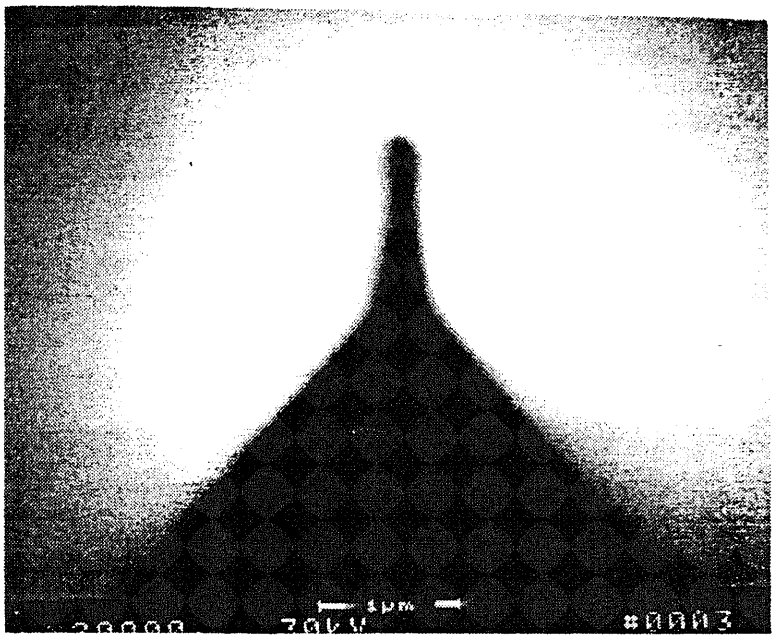

Figure 4.5 SEM photo of side view of precursor tip after pre-sharpen etching treatment

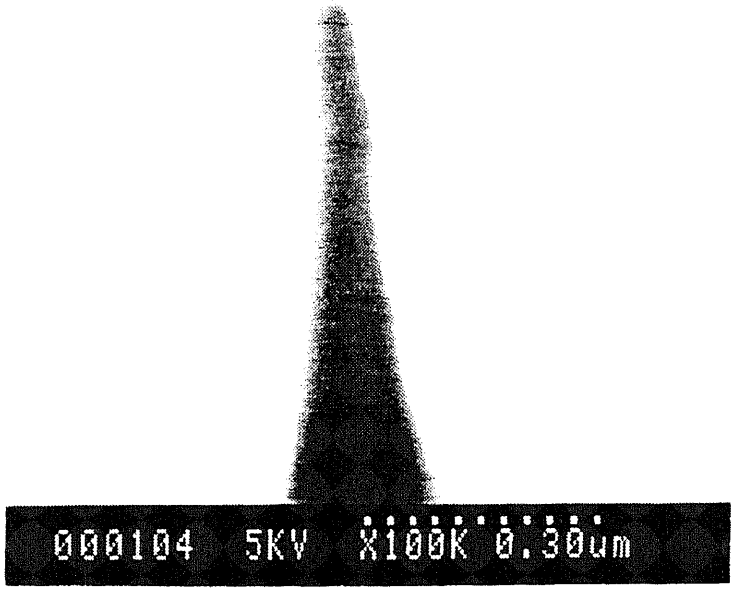

Figure 4.6 SEM photo of a single tip formed after using pre-sharpen treatment

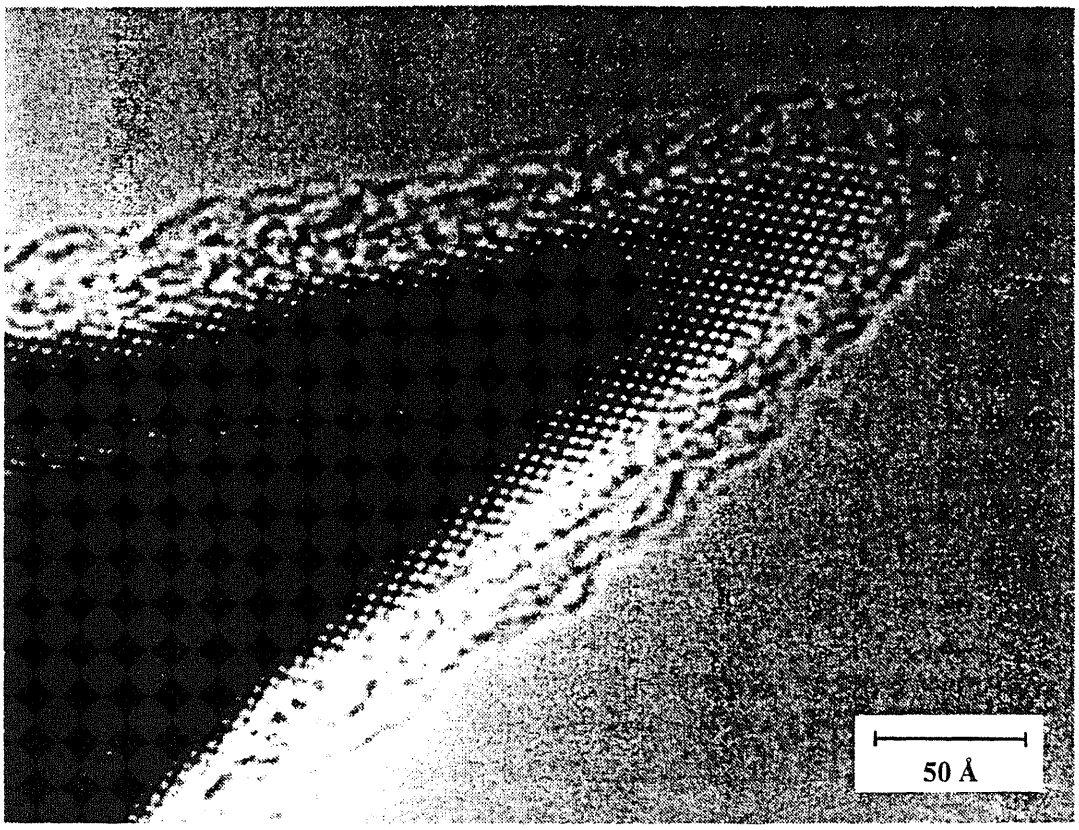

Figure 4.7 TEM photo showing atomically sharp silicon tip made by oxidation sharpening

4.1.3 The Mechanism of Multiple and Single Tip Formation

An analysis of the problem shows that the likely cause of multiple tip formation is related to the presence of the sharp corners. The classical model of planar oxidation of silicon consists of two regimes[39]. In the first linear regime the rate limiting step during the oxidation is the interfacial reaction of an oxygen-containing species with the silicon surface. Beyond a critical oxide thickness, the rate limiting step becomes the diffusion of oxygen across the already grown oxide, and the reaction follows a parabolic rate law. For silicon wedges and other regions of high curvature, the stress buildup results in a suppression of interfacial reaction, and hence the oxidation rate slows down in the linear region [40]. The stress is largely a result of specific volume difference of silicon oxide with respect to the silicon and cannot be relieved at temperature <~1050 °C due to the high viscosity of the oxide which prevents oxide flow for stress relief.

Multiple and single tip formation can be described and explained with the aid of Figure 4.8. After the oxide mask is stripped, the top of the tip is rectangular (Figure 4.8[left]) with length to width ratio about 2:1.5, often with sharp corners on the top (Figure 4.3). After initial oxidation, the structure becomes a wedge with a rather flat ridge on the top (Figure 4.8a[center]). During the final oxidation, the oxidation rate on the ridge and at the side of the post is faster than the high curvature corners, which results in two tips in the corners (Figure 4.1 and Figure 4.8a[right]). But if the sharp corners are eliminated before oxidation by dipping the silicon wafer in the isotropic etchant for several seconds, the top view of the tip becomes an oval-like shape and the side view of the tip shows that the sharp corners have been eliminated (Figure 4.5 and Figure 4.8b[center]).

There is no flat top existing and the apex of the post is high curvature. During the final oxidation, the oxidation rate is faster at the side of the post than on the top. Finally a single atomically sharp silicon tip forms (Figure 4.6, Figure 4.7 and Figure 4.8b[right]).

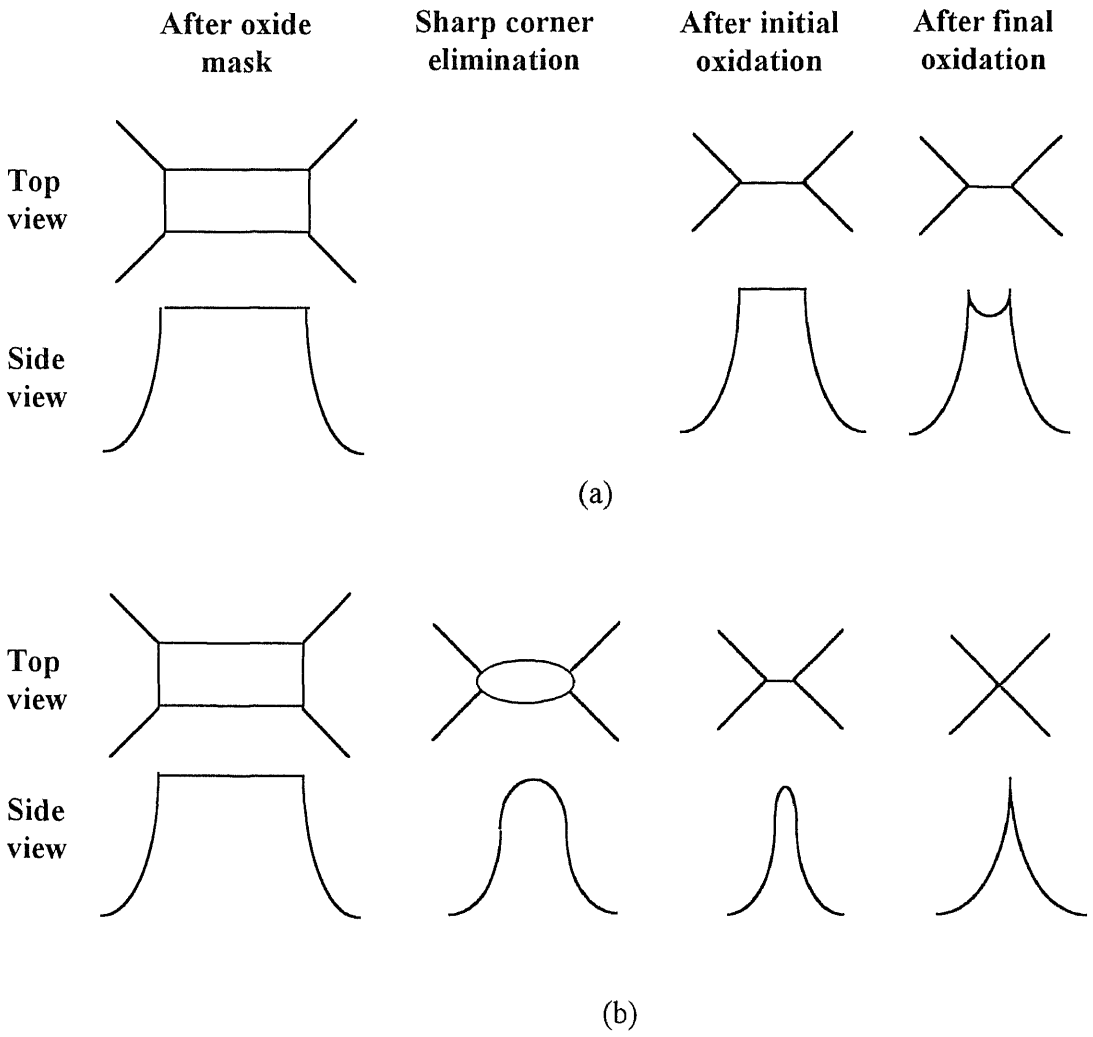

Figure 4.8 The illustration of top and side view for
(a) double tips and (b) single tip formation

4.2 Formation of Thermocouple Junction on the Tip

The critical point to make the thermal microprobe is the formation of hot thermocouple junction on the probe tip. The hot junction acting as the thermal sensor consists of two layers of very thin metal film. These two layers of metal film are confined to the very end of the tip. Less than 0.5 μm in the vertical direction on the tip is desired (Figure 3.6). As mentioned in Chapter 2, Luo *et al.*[14] built a thin film thermocouple on AFM cantilever probe tip for scanning thermal microscope. Their method to form the hot junction is using voltage pulse to evaporate metal film and create a nanometer scale hole at the very end of a metallized AFM cantilever probe tip. It is hard to control the conditions and devices cannot be batch fabricated.

Recently, R.C Davis *et al.*[41,42] used a batch fabrication method to build the Near-field Photodetection Optical Microscope (NPOM). We find this method also suitable to form hot thermocouple junction on the probe tip.

The fabrication procedure is shown in Figure 4.9. The sharp silicon tip is formed following the processes described in Section 4.1 (Figure 4.9a). The next step is to construct the hot thermocouple junction at the end of the tip. First a thin layer of oxide (about 25 nm) is grown in dry oxygen at 950 °C (Figure 4.9b). This thin oxide layer insulates the silicon substrate electrically from the metal 1 (palladium) subsequently deposited. Then a layer of 50 nm thickness palladium is sputtering deposited on the tip (Figure 4.9c). Next a layer of 300 nm low temperature silicon dioxide (LTO) is deposited on the tip by low pressure chemical vapor deposition (LPCVD) (Figure 4.9d).

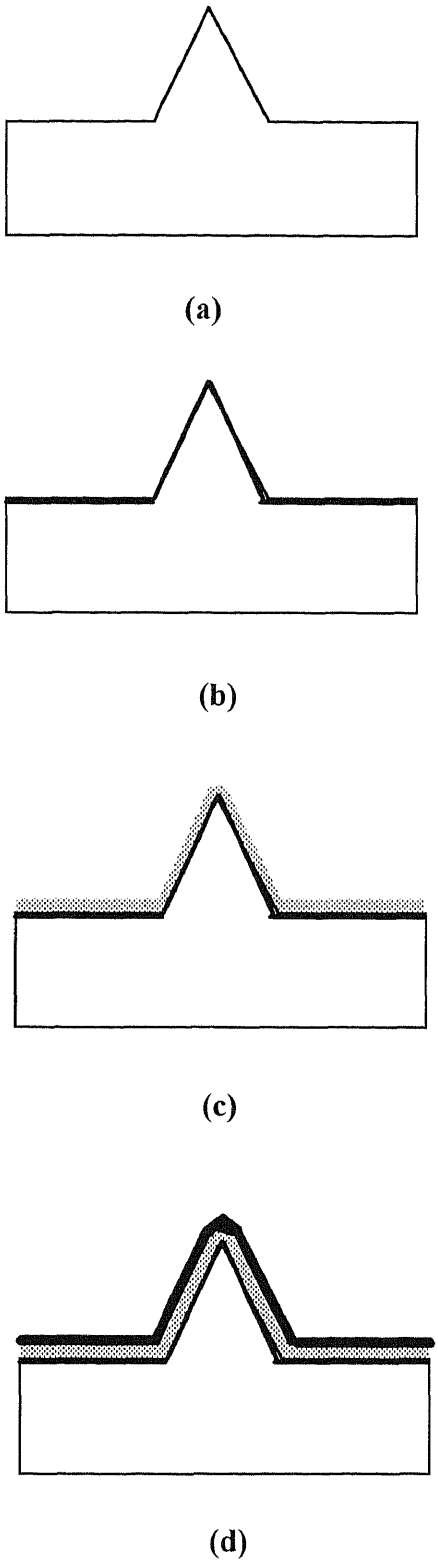

Figure 4.9 Process procedure to form thermocouple junction on the tip

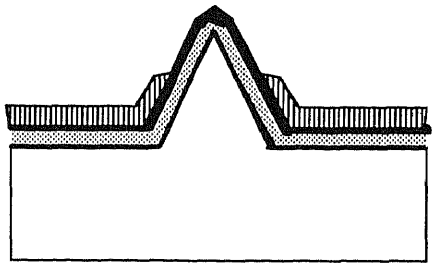

(e)

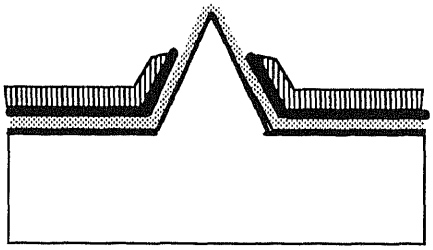

(f)

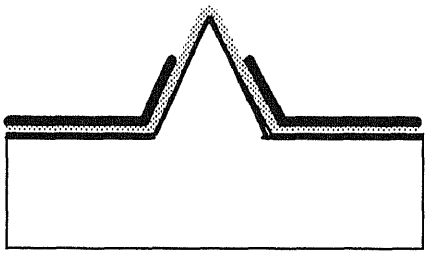

(g)

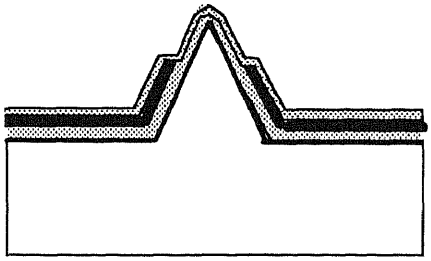

(h)

Figure 4.9 (cont.) Process procedure to form thermocouple junction on the tip

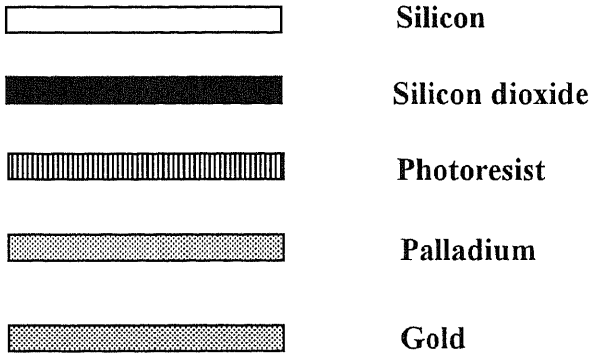

Figure 4.9 (cont.) Process procedure to form thermocouple junction on the tip

Now we remove the low temperature silicon oxide from a small region on end of the tip. Under certain conditions the photoresist can be spun on the wafer without completely covering the conical tip. The photoresist (Shipley 827) is placed on the wafer and spun for only 0.5 second, resulting in a very thick layer of photoresist. The xylene in the photoresist is allowed to evaporate for 10 seconds. The wafer is then spun for 30 seconds at the speed varied depending on the different height of the conical tips. This gives the desired result, i.e., only the end of the tip protrudes through the photoresist (Figure 4.9e). If the photoresist is spun on conventionally, omitting the intermediate evaporation step, a large nonsymmetrical portion of the tip will not be covered with photoresist.

Following the photoresist coating step, the oxide is etched from the exposed tip region with buffered HF or reactive ion etching (RIE) (Figure 4.9f) and the resist is removed (Figure 4.9g). Then a layer of 50 nm thick metal 2 (gold) is sputtering deposited over the tip (Figure 4.9h). The hot thermocouple junction is confined to a region less than 500 nm at the end of the tip. The two layers of metal are electrically separated elsewhere by the thin oxide layer. Figure 4.10 shows the SEM photo after the hot thermocouple junction formation. The arrow in the Figure 4.10 points the location of the hot thermocouple junction. About 0.3 μm of the tip protrudes on the top. Therefore, the hot thermocouple junction is confined to only 0.3 μm at the end of the tip.

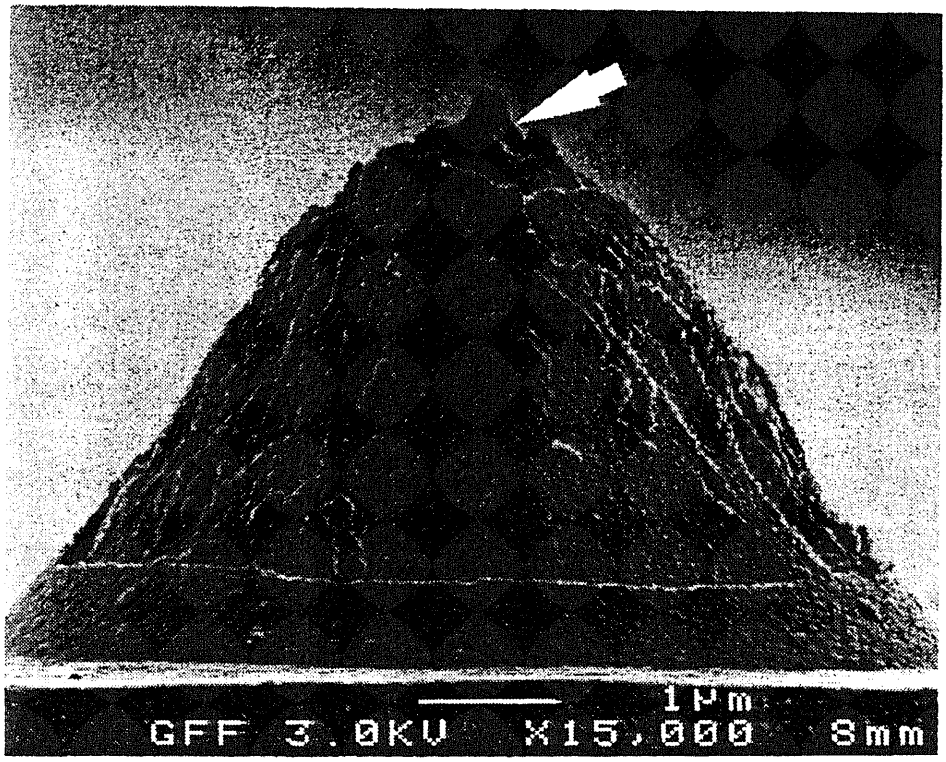

Figure 4.10 SEM photo showing 0.3 μm-high junction at the top of the tip (arrow)

4.3 Cantilever Releasing by Silicon Wafer Backside Etching

4.3.1 KOH Etching Mechanism

At the last step of the process to make thermal microprobe, the cantilever is released by anisotropic KOH etching from backside of the wafer. Potassium hydroxide (KOH) is the most frequently used anisotropic etchant. A basic feature of the KOH etching is that its etch rate is strongly dependent on crystallographic orientation. The (111) surfaces etch at a slower rate than other crystallographic planes[43]. Considering a (100)-oriented silicon wafer with an etched hole in a layer of silicon nitride that covers the surface, when exposed to KOH etching solution this will create a truncated pyramidal shaped pit. The pit side wall is bounded by (111) crystallographic planes that exhibit a very low etch rate.

The thermal microprobe is fabricated from 4-inch-diameter, 300-μm-thick, (100) surface, double side polished silicon wafer. When the processing step reaches the cantilever release step, a patterned Si_3N_4 film is used to expose the regions to be etched. Then the wafer is placed in 45% KOH etching solution at 80 °C for several hours. After cantilever release, the probe chassis side wall is bounded by (111) crystallographic planes. The (111) planes have an inclination of 54.7° (see Figure 4.11).

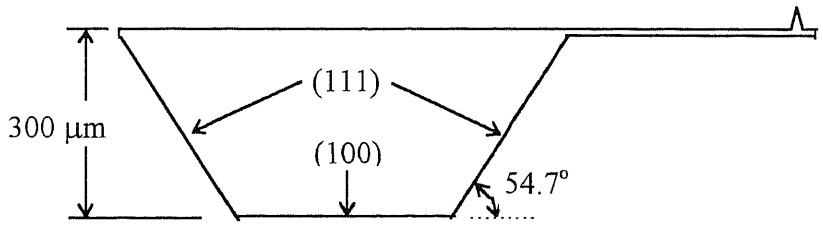

Figure 4.11 Schematic side view of the thermal microprobe

The mechanism of KOH anisotropic etching of silicon can be described by the general unifying electrochemical model[43,44]. The main features are outlined in the following reaction from (4.1) to (4.8).

Two hydroxide ions can bind with two dangling bonds of a silicon atom on a (100) surface, injecting two electrons into the conduction band, (4.1).

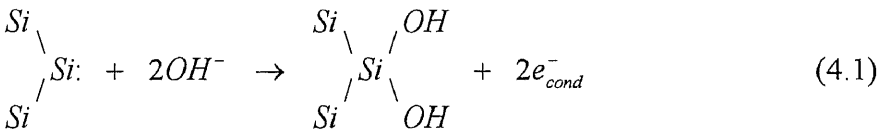

(4.1)

Next the Si-Si backbones of the $Si(OH)_2$ neighboring lattice atoms have to be broken to obtain a soluble silicon complex, which is positive charged, (4.2).

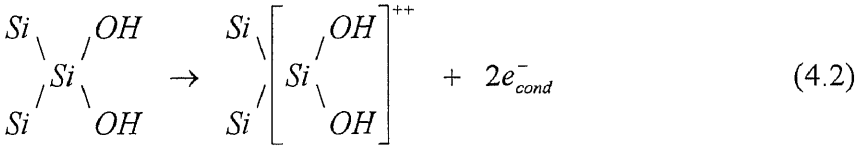

(4.2)

The silicon-hydroxide complex reacts further with two more hydroxide ions to give orthosilicic acid, (4.3).

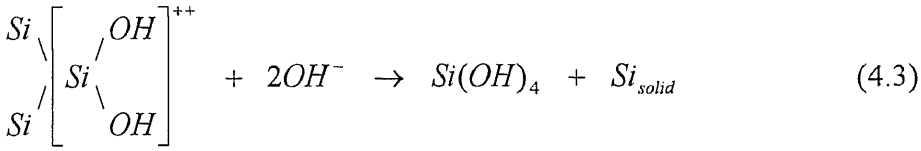

(4.3)

The $Si(OH)_4$ can leave the solid surface by diffusion, but in the bulk electrolyte, it is unstable due to the high pH value of the solution. In this environment, the complex in (4.4) can form.

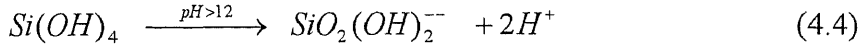

(4.4)

The excess electrons in the conduction band can be transferred to water molecules producing hydroxide ions and hydrogen, (4.5) to (4.7).

$$2H^+ + 2OH^- \rightarrow 2H_2O \tag{4.5}$$

$$4H_2O + 4e \rightarrow 4H_2O^- \tag{4.6}$$

$$4H_2O^- \rightarrow 4(OH)^- + 4H \rightarrow 4(OH)^- + 2H_2 \tag{4.7}$$

The overall reaction is represented in (4.8).

$$Si + 2OH^- + 2H_2O \rightarrow SiO_2(OH)_2^{--} + 2H_2 \tag{4.8}$$

4.3.2 Compensation Structure for Convex Corner

When etching rectangular convex corners in silicon using KOH anisotropic etchant, deformation of the edges always occurs due to underetching. Figure 4.12 shows the device backside pattern after KOH etching to release the cantilever. The underetching effect is obvious. This is an unwanted effect in our device. Thus a rectangular compensation structure is implemented to prevent over etching of the convex corners.

For KOH etching solution, the <130> direction is predominant in the under etched structure[45]. Figure 4.13 shows compensation structure, which are based on the idea of having <130> direction as preferential etch planes. A new 90° convex corner is created on the original rectangular convex corner. When the wafer is placed in KOH etching solution,

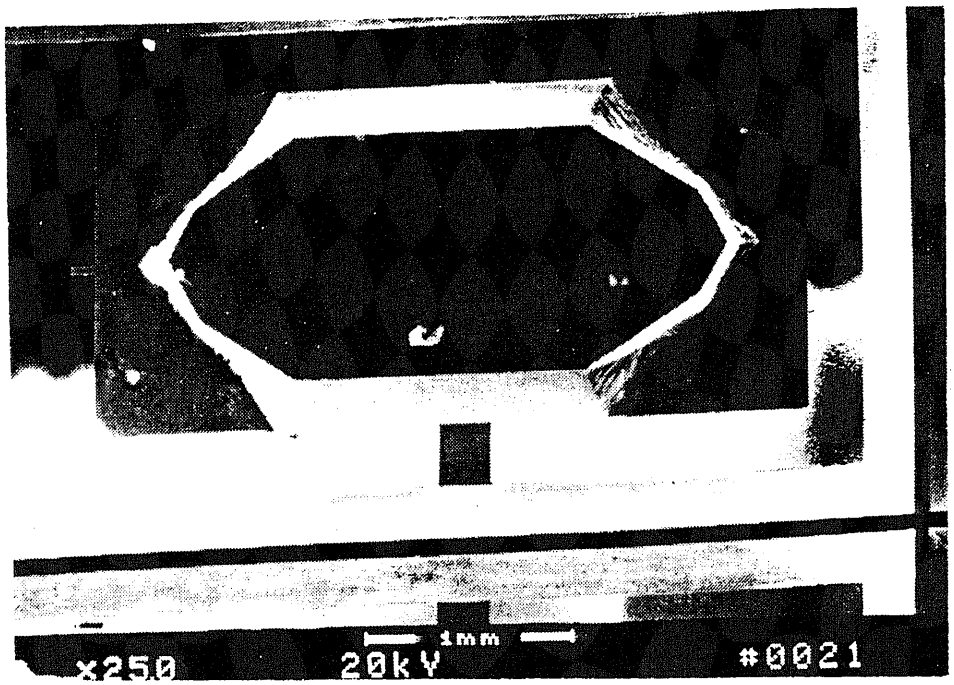

Figure 4.12 SEM photo of the device backside: severe overetching after KOH etching without compensation pattern

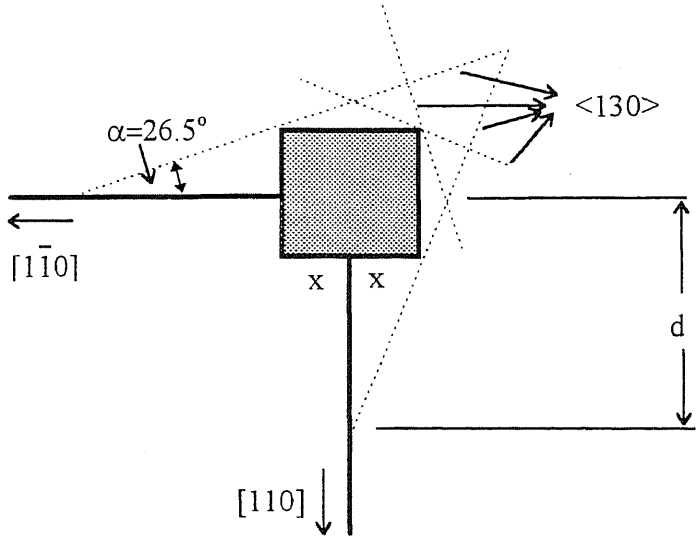

Figure 4.13 KOH anisotropic etching compensation structure

the etchants attack the convex corners of the compensation rectangle from four different <130> orientations until it is entirely 'consumed' to leave the desired 90° corner. The relationship between undercutting length d and etch depth ed is[45]

$$d=5.7+3.72ed\ (\mu m) \tag{4.9}$$

The compensation square side length 2x is

$$x = d\frac{tg\alpha}{1+tg\alpha} \tag{4.10}$$

where α is the angle between the [110] direction and a <130> direction. For a 300 μm thick wafer, the etch depth is 300 μm. To get complete compensation, the compensation square half side length x should be 374 μm. Figure 4.14 indicates the convex corner shapes after KOH etching. These shapes are shown with their corresponding mask patterns and give uncompensation, complete compensation and part compensation, respectively. In our device, the corners are already truncated and therefore only part compensation is enough. The two convex corners at the head of the device (Figure 4.15 right) are compensated with x=250 μm and the two convex corners at the tail of the device (Figure 4.15 left) are compensated with x=150 μm. The result after etching is shown in Figure 4.15. Comparing Figure 4.12 and Figure 4.15, the difference between the KOH etching of uncompensated corners and corners with square compensation structures is obvious. The compensation structures proved to be successful.

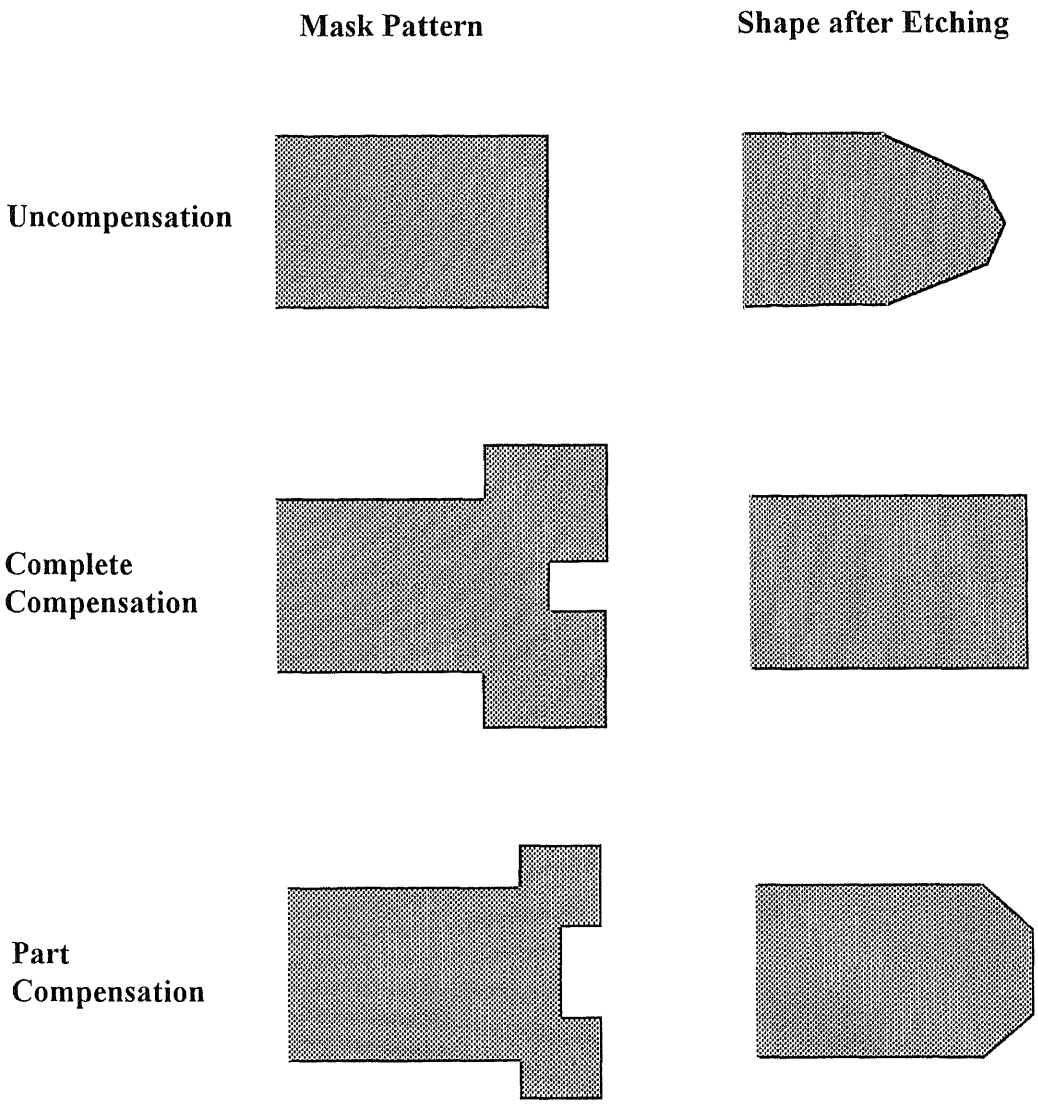

Figure 4.14 Silicon convex corner shapes after KOH etching and their mask pattern

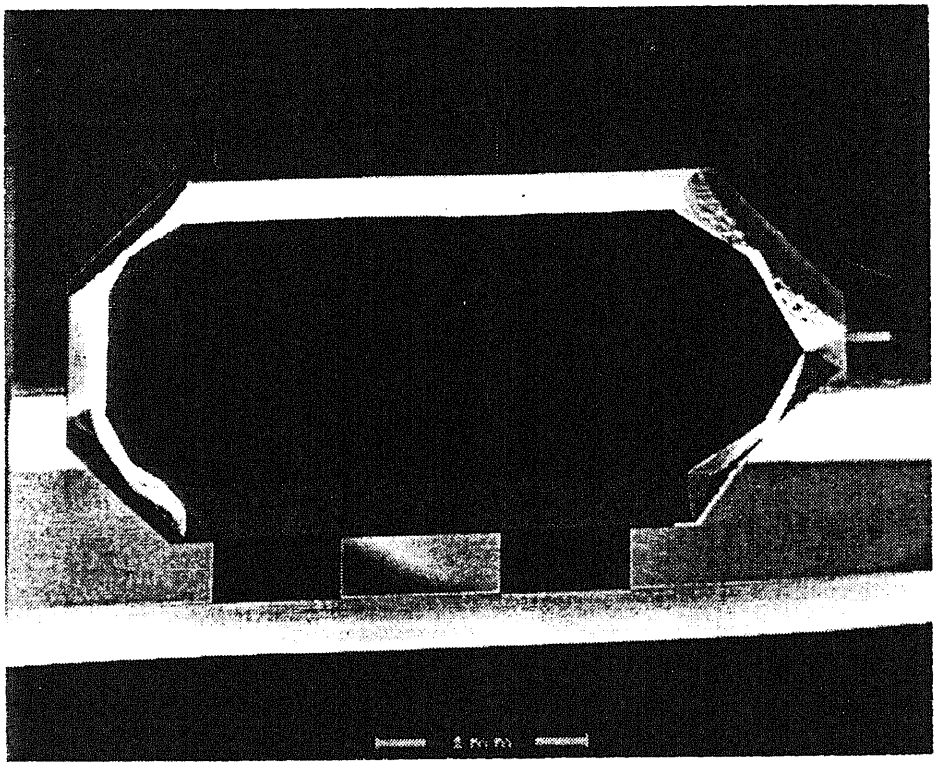

Figure 4.15 SEM photo of the device backside: good compensation after KOH etching with compensation pattern

4.4 General Fabrication of Thermal Microprobe

The method we developed to fabricate thermal microprobe includes many silicon planar processes. We use thermal oxidation, wet etching, dry etching, LPCVD deposition, DC sputtering deposition, photolithography, lift-off, etc. The major fabrication steps are described in Figure 4.16.

1. Starting material

The starting material is 4-inch-diameter, n-type, double polished silicon wafer with (100) orientation. The thickness of the wafer is 300 μm for two reasons. In the later process steps, we will use backside photolithography by infrared alignment and release the cantilever by KOH etching silicon from backside. Infrared alignment is easier and the cantilever releasing time by KOH etching will decrease for thinner wafers.

2. Patterning the small disk which will form the probe tip later

A layer of 2000 Å silicon dioxide is thermally grown at 1050 °C in steam (Figure 4.16a). The photoresist is coated on oxide and patterned by mask 1 (Disk) to define the 8 μm diameter disk which will form the probe tip later (Figure 4.16b). Then the exposed oxide is etched in buffered HF and the mask 1 pattern is transferred to the wafer (Figure 4.16c).

3. The formation of the probe tip

The probe tip is formed by several steps of dry etching and wet etching.

Two steps of reactive ion etching (RIE) are used with photoresist and silicon dioxide as mask to get a tip 5 μm high. The first RIE step is isotropic etch with SF_6 (Figure 4.16d). The second RIE step is pseudo-anisotropic etch with Cl_2 and BCl_3 (Figure

4.16e). These two etch steps leave a tip with a rather thick neck under the oxide mask as shown in Figure 4.17.

To further reduce the tip neck under the oxide mask, wet isotropic etching is used to get the proper precursor for oxidation sharpening (Figure 4.16f). The wet isotropic etchant is in mixtures of nitric acid (HNO_3) and hydrofluoric acid (HF). The reaction is initiated by the HNO_3 which forms a layer of silicon dioxide on the silicon, and the HF dissolves the oxide away. The overall reaction is:

$$Si + HNO_3 + 6HF \rightarrow H_2SiF_6 + HNO_2 + H_2 + H_2O \qquad (4.11)$$

Water can be used to dilute the etchant, but acetic acid (CH_3COOH) is preferred as a buffering agent, since it causes less dissociation of HNO_3, and thus yields a higher concentration of the undissociated species.

The mixture compositions can be varied to yield different etch rates. At high HF and low HNO_3 concentration, the etch rate is controlled by the HNO_3 concentration, because in such mixtures there an excess of HF to dissolve the SiO_2 created during the reaction. On the other hand at low HF and high HNO_3 concentrations, the etch rate is limited by the ability of the HF to remove the SiO_2 as it is created. In such etchants the etching is isotropic. We desire the etch rate to be slow and uniform, so the ratio of the mixture composition is HNO_3 : HF : CH_3COOH = 95% : 2% : 3%. At room temperature, the etch rate is about 0.25~0.3 μm per minute. The wafer is dipped in this isotropic etchant until the silicon neck supporting the oxide mask is less than 0.4~0.5μm (Figure 4.18).

4. Defining the cantilever

Mask 2 (Cantilever) is used to pattern the cantilevers by photolithography. There are three sizes of cantilevers. The length x width is 200 μm x 40 μm, 450 μm x 40 μm and 450 μm x 20 μm, respectively. The RIE with reactive gas SF_6 is used to etch down about 1.5 μm from wafer surface, forming the cantilever thickness of 1.5 μm (Figure 4.16g).

5. Sharpening the probe tip

The probe tip is sharpened by typical dry thermal oxidation process.

As described in section 5.1, to get the single tip, we have to treat the precursor of the tip chemically before sharpening. After the oxide mask is stripped in buffered HF solution (Figure 4.19), we remove the sharp corners of the precursors by dipping the wafer in the isotropic etch solution for several seconds immediately before oxidation sharpening. Then the wafer is oxidation sharpened at 950 °C for 2~5 hours and the oxide is stripped in buffered HF solution. This may repeat for several times until atomic sharp silicon tip formed (Figures 4.16h and 4.20).

6. Defining backside etching mask.

The cantilever will be released at the last step by KOH etching from wafer backside. Si_3N_4 is used as KOH etching mask. After a thin layer of thermal oxide growing, the wafer backside is deposited 2000 Å Si_3N_4 by LPCVD at 775 °C. Then the Si_3N_4 is patterned by photolithography of infrared alignment with mask 3 (Backside). And the Si_3N_4 is etched by RIE using photoresist as mask (Figure 4.16i).

7. The formation of thermocouple junction

The thermocouple junction is formed by depositing two layers of metal (Pd an Au) on the tip. The metals are deposited by DC sputtering and patterned by lift-off. To increase the adhesion of Pd and Au to oxide, we deposit a very thin layer of Ti or Cr (about 100 Å ~ 200 Å) before Pd and Au deposition.

First, we deposit 100 Å Ti and then about 500 Å Pd on thin oxide (Figure 4.16j). Second, a layer of 2400 Å low temperature oxide is deposited on Pd by LPCVD (Figure 4.16k). Third, photoresist is coated on the wafer except the end of the tip (Figure 4.16l). Fourth, the oxide on the end of the tip is etched off by RIE (Figure 4.16m). Fifth, the photoresist is stripped (Figure 4.16n). Sixth, we deposit 100 Å Cr and about 500 Å Au on the end of the tip, forming the hot junction of the thermocouple (Figures 4.16o, 4.16p and 4.21).

8. Releasing of the cantilever

The last step is to release the cantilever. The wafer front side is protected in a special chlorinated polyvinyl chloride (CPVC) holder (see Figure 4.22) and only the wafer backside is exposed in the KOH etching solution. After several hours of KOH etching, the wafer is almost etched through. Then RIE is used to etch the remaining Si. The device is formed (Figure 4.16q). Figure 4.23 shows photos of the device array in the wafer before and after releasing.

The detailed thermal microprobe fabrication processing flow is shown in Appendix B.

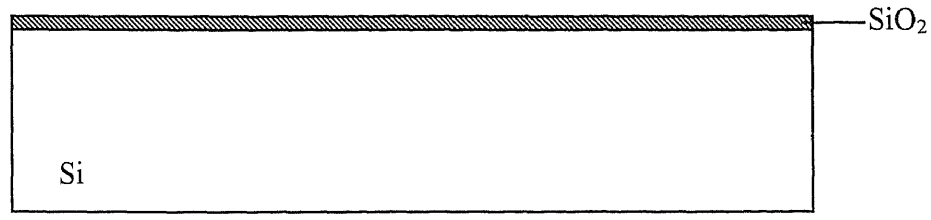

(a)

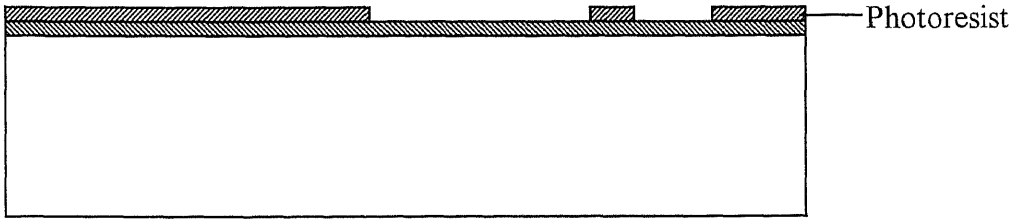

(b)

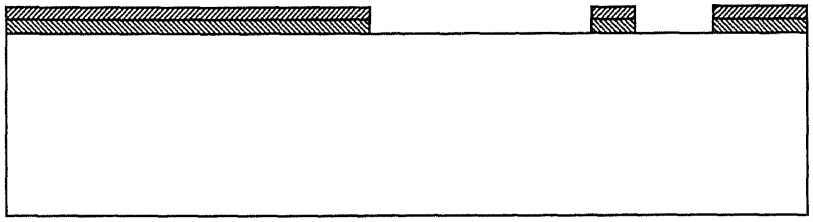

(c)

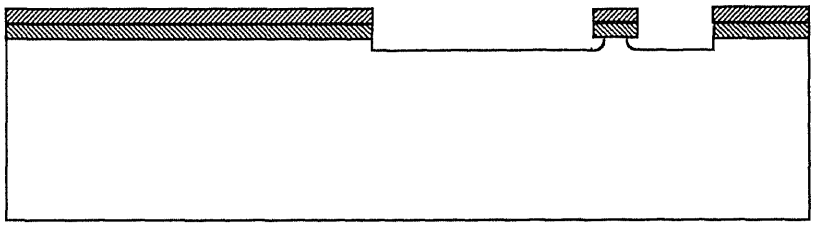

(d)

Figure 4.16 The major steps to fabricate thermal microprobe

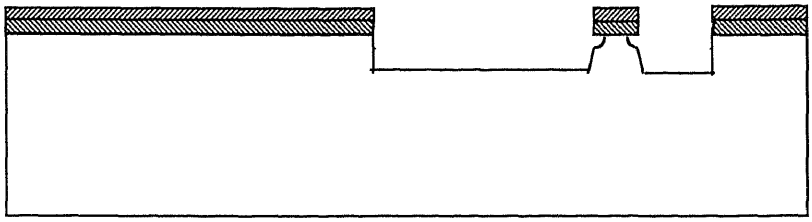

(e)

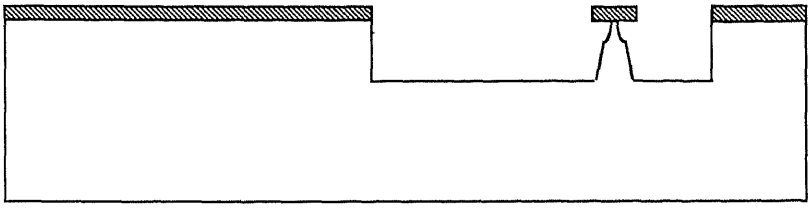

(f)

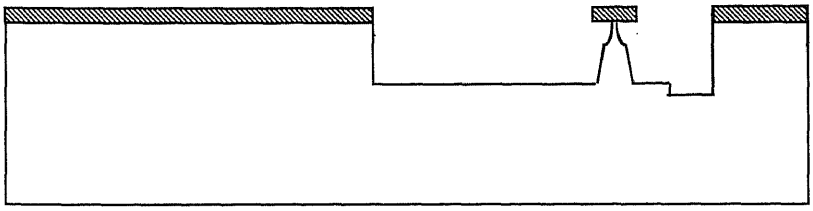

(g)

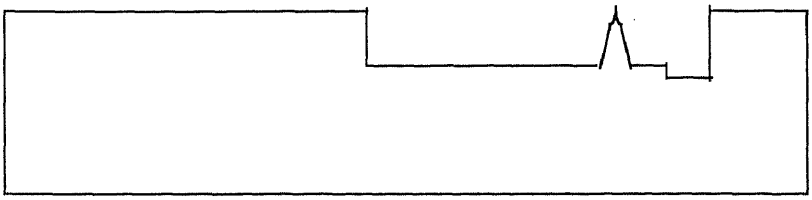

(h)

Figure 4.16 (cont.) The major steps to fabricate thermal microprobe

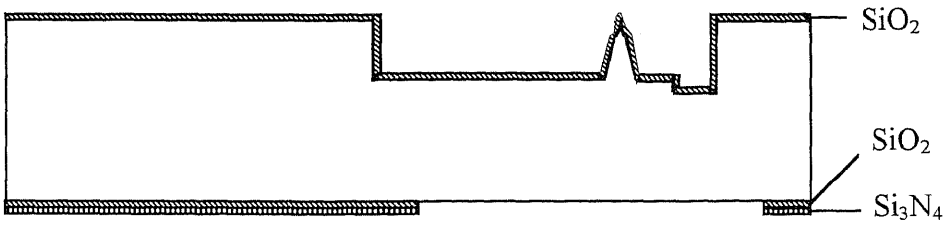

(i)

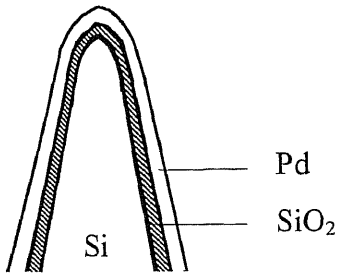

(j)

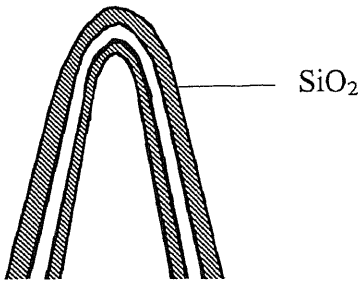

(k)

Figure 4.16 (cont.) The major steps to fabricate thermal microprobe

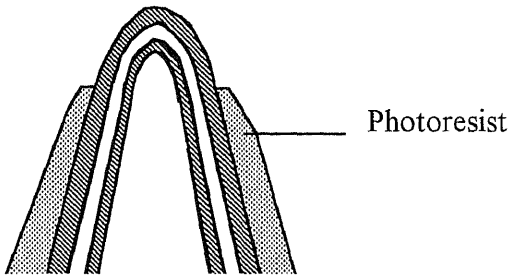

(l)

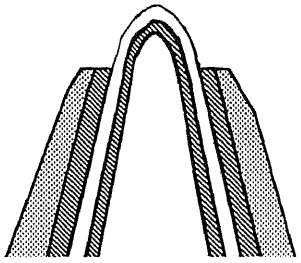

(m)

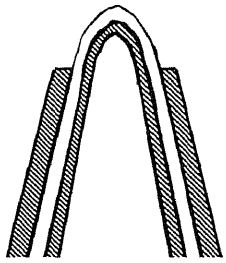

(n)

Figure 4.16 (cont.) The major steps to fabricate thermal microprobe

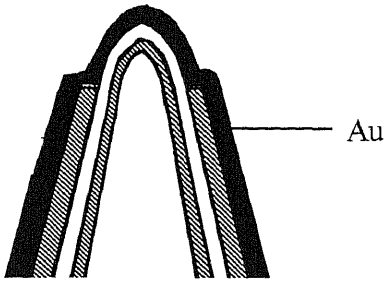

(o)

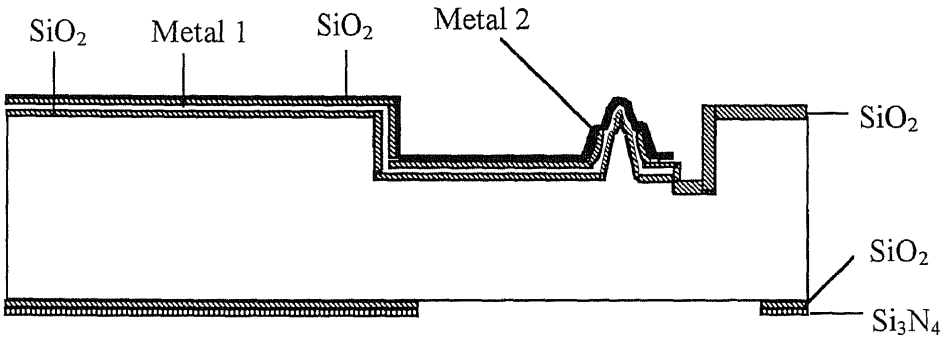

(p)

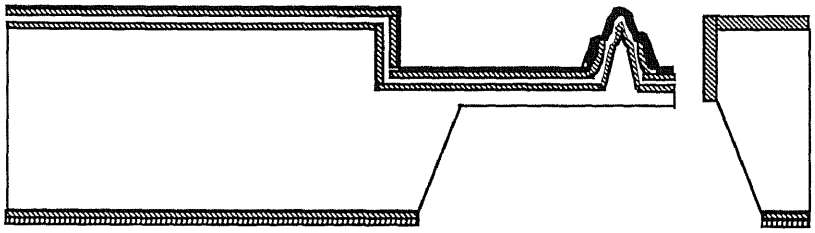

(q)

Figure 4.16 (cont.) The major steps to fabricate thermal microprobe

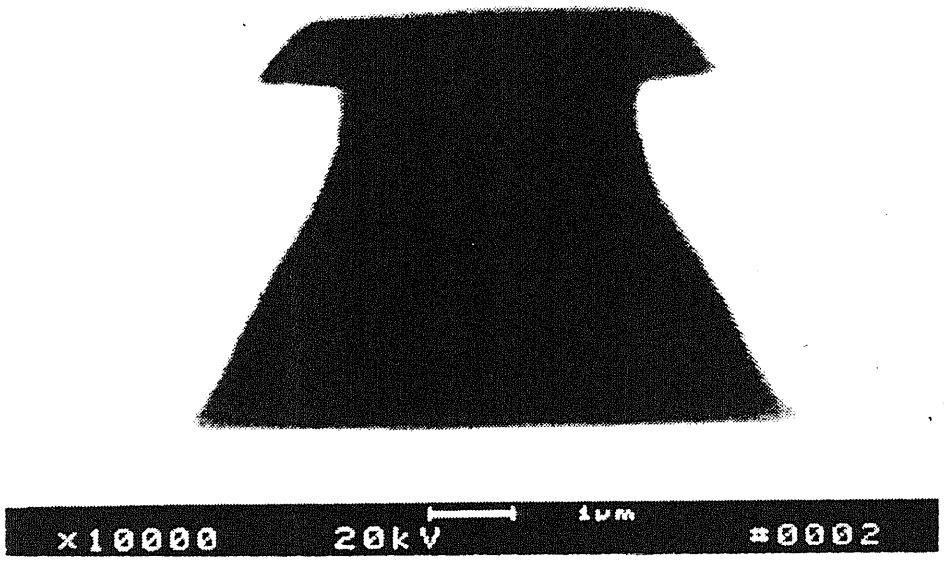

Figure 4.17 SEM photo of the tip after two steps RIE etching (Figure 4.16e)

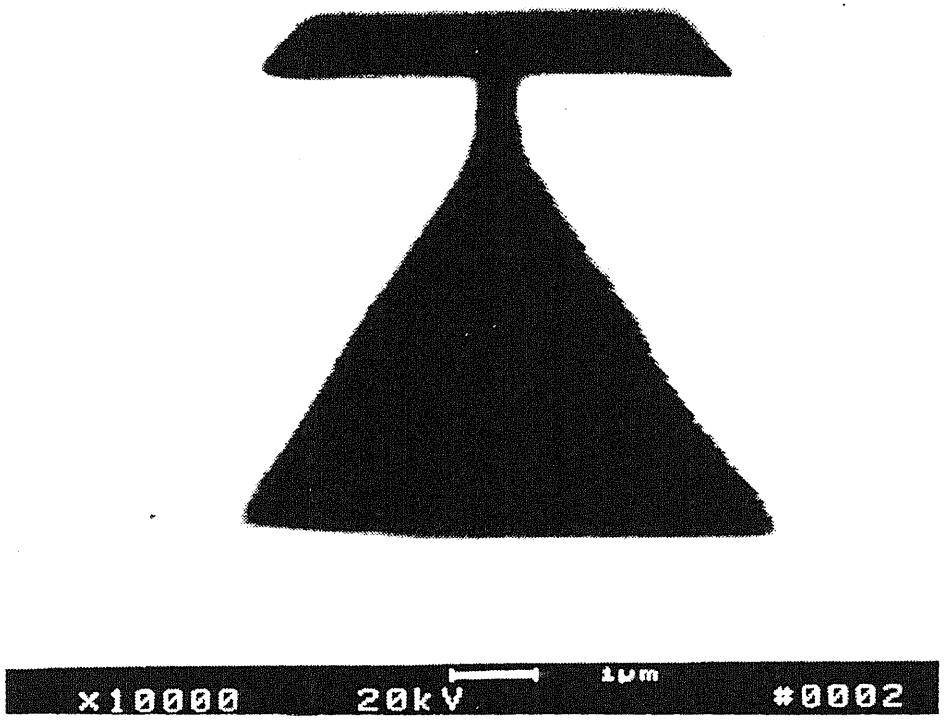

Figure 4.18 SEM photo of the tip after wet isotropic etching (Figure 4.16f)

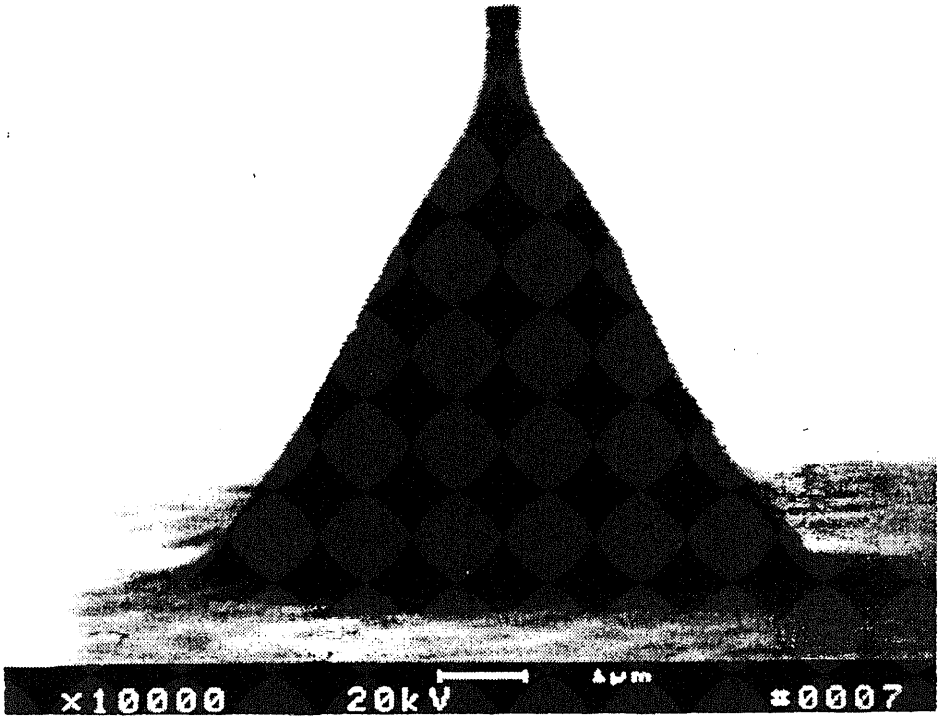

Figure 4.19 SEM photo of the tip after oxide mask stripped

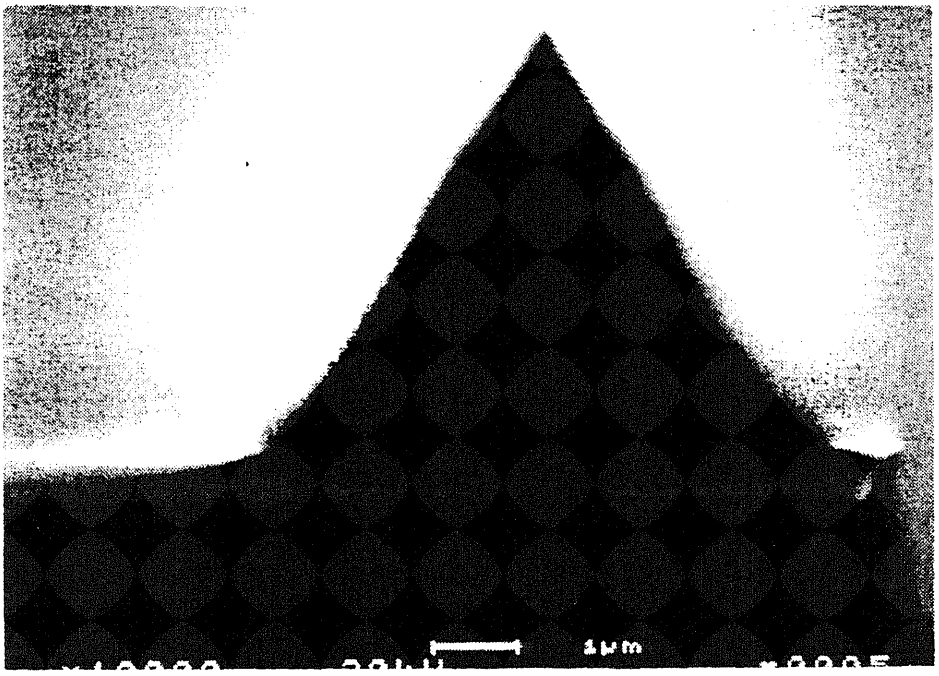

Figure 4.20 SEM photo of the tip after oxidation sharpening (Figure 4.16h)

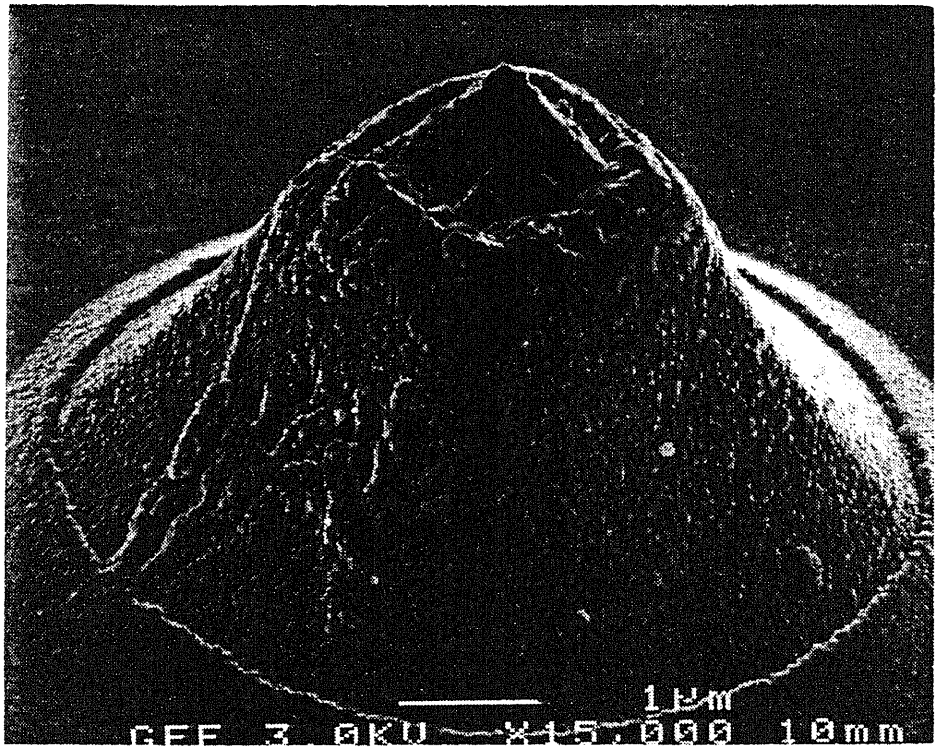

(a) Top view

Figure 4.21 SEM photos of the tip after forming hot thermocouple junction

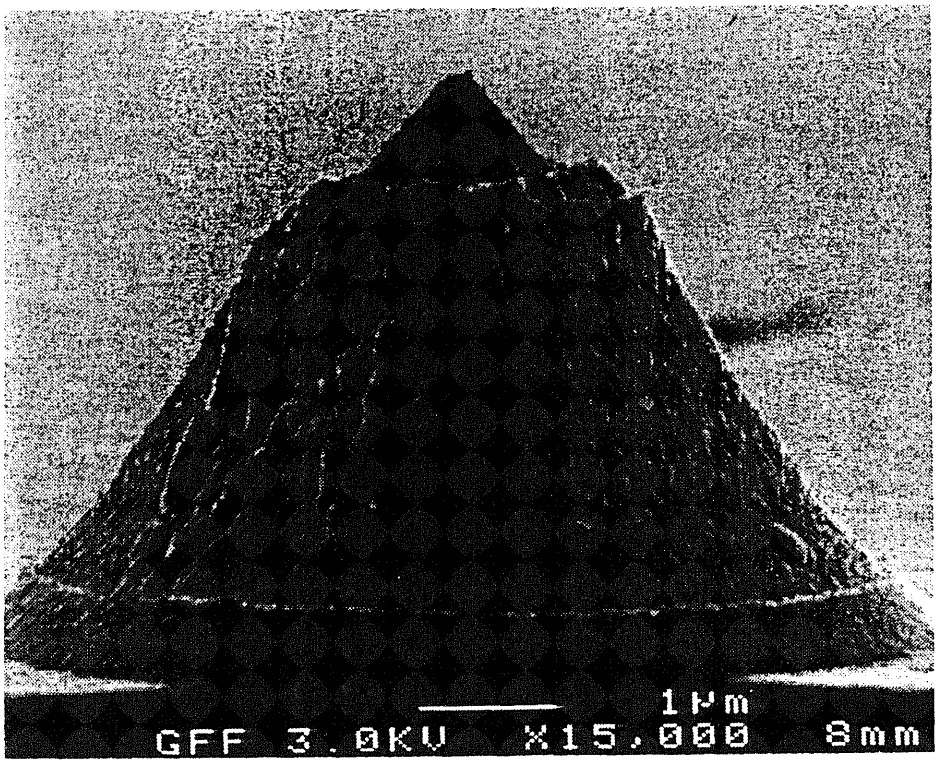

(b) Side view

Figure 4.21 (continued) SEM photos of the tip after forming hot thermocouple junction

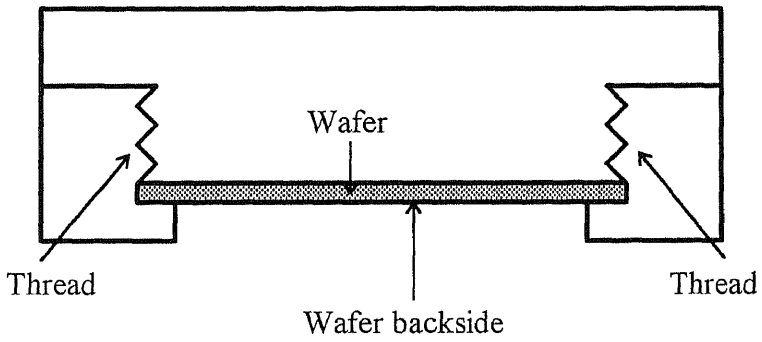

Figure 4.22 Special holder to protect front side of wafer during KOH etching

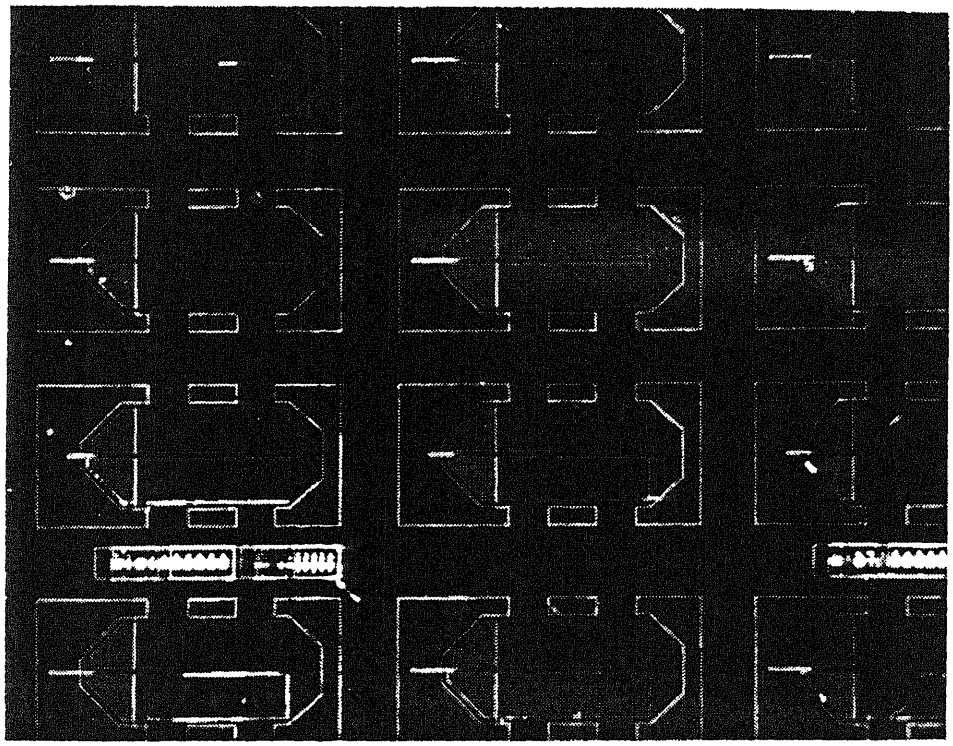

(a) Before releasing

Figure 4.23 Optical microscope photos of device array before and after releasing

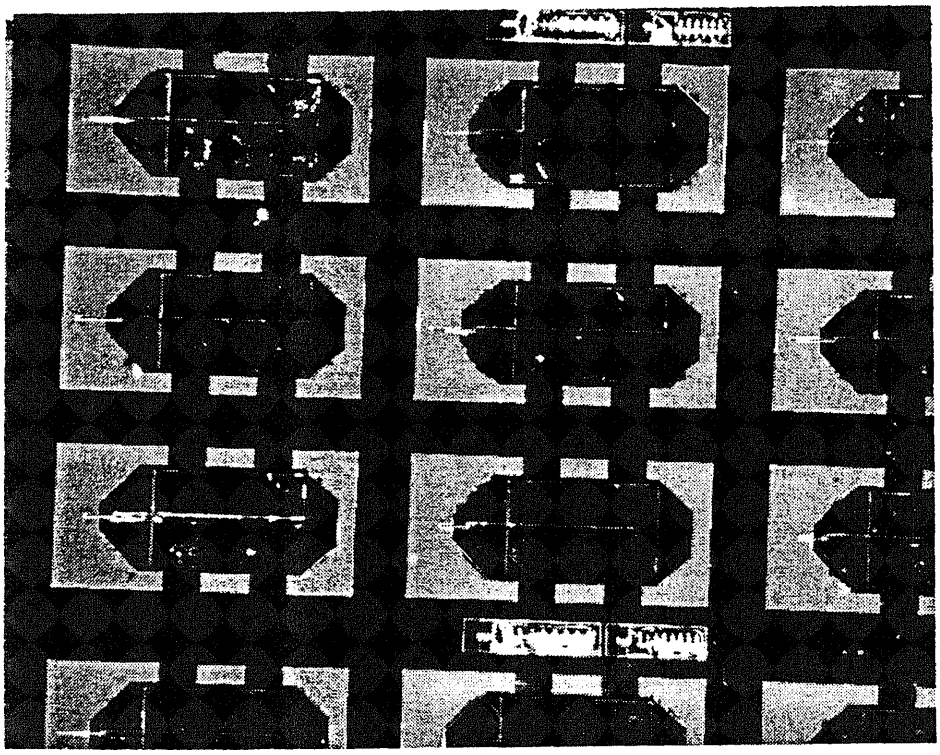

(b) After releasing

Figure 4.23 (cont.) Optical microscope photos of device array before and after releasing

CHAPTER 5

CHARACTERIZATION OF THE THERMAL MICROPROBE

5.1 Calibration of the Thermal Microprobe

5.1.1 Calibration Scheme

To evaluate the thermal microprobe performance, a method for calibrating the thermal microprobe EMF response against a known temperature is necessary. The approach to this technical objective is to make a test device that contains a thin platinum film resistor on its surface. The resistance of platinum thin film resistor is sensitive to temperature changes due to its large temperature coefficient of resistivity (3920 ppm/K). Heating the platinum thin film resistor to various temperatures in the range of 25~110 °C in an oil temperature bath, a calibration curve of resistance vs. temperature is obtained. The platinum thin film resistor then is Joule heated, the thermal microprobe is applied to the heated resistor surface, and the EMF output of the thermal microprobe is measured with a microvoltmeter. Measurement of the resistance of the platinum thin film resistor during Joule heating combined with the previous calibration curve of resistance vs. temperature gives a tool for making EMF vs. temperature calibrations for a large number of thermal microprobes.

5.1.2 The Design of Platinum Thin Film Resistor

The thin film resistor design has to satisfy the following requirements:

1) When it is heated in the oil temperature bath, its resistance change can be measured easily.

2) It can be effectively Joule heated by applying electrical power, and its resistance change can be measured easily.

Both of the requirements call for a thin film resistor with large resistance and large temperature coefficient of resistivity (TCR).

We chose Pt as the thin film resistor material since Pt has rather large TCR and high electrical resistivity. To increase the resistance of the resistor within a finite area, we designed a meander pattern to increase the length of the resistor. The layout of the resistor is shown in Figure 5.1. Two large square contact pads (2 mm x 2 mm) make it easy to connect lead wires by soldering. The dimensions and parameters of the resistor are listed in Table 5.1. The designed resistance is 16.88 kΩ.

The processing flow of the Pt thin film resistor is:

1) Thermally grow 4000 Å SiO_2 on 4-inch-diameter silicon wafer.

2) Pattern the wafer with the mask as Figure 5.1 for lift-off

3) DC sputter deposit 2400 Å Pt.

4) Lift-off in acetone.

Table 5.1 Dimensions and parameters of the Pt thin film resistor

Material	TCR	Resistivity	Length	Width	Thickness	Resistance
Pt	3900×10^{-6}/K	10.58 μΩ cm	383 mm	10 μm	2400 Å	16.88 kΩ

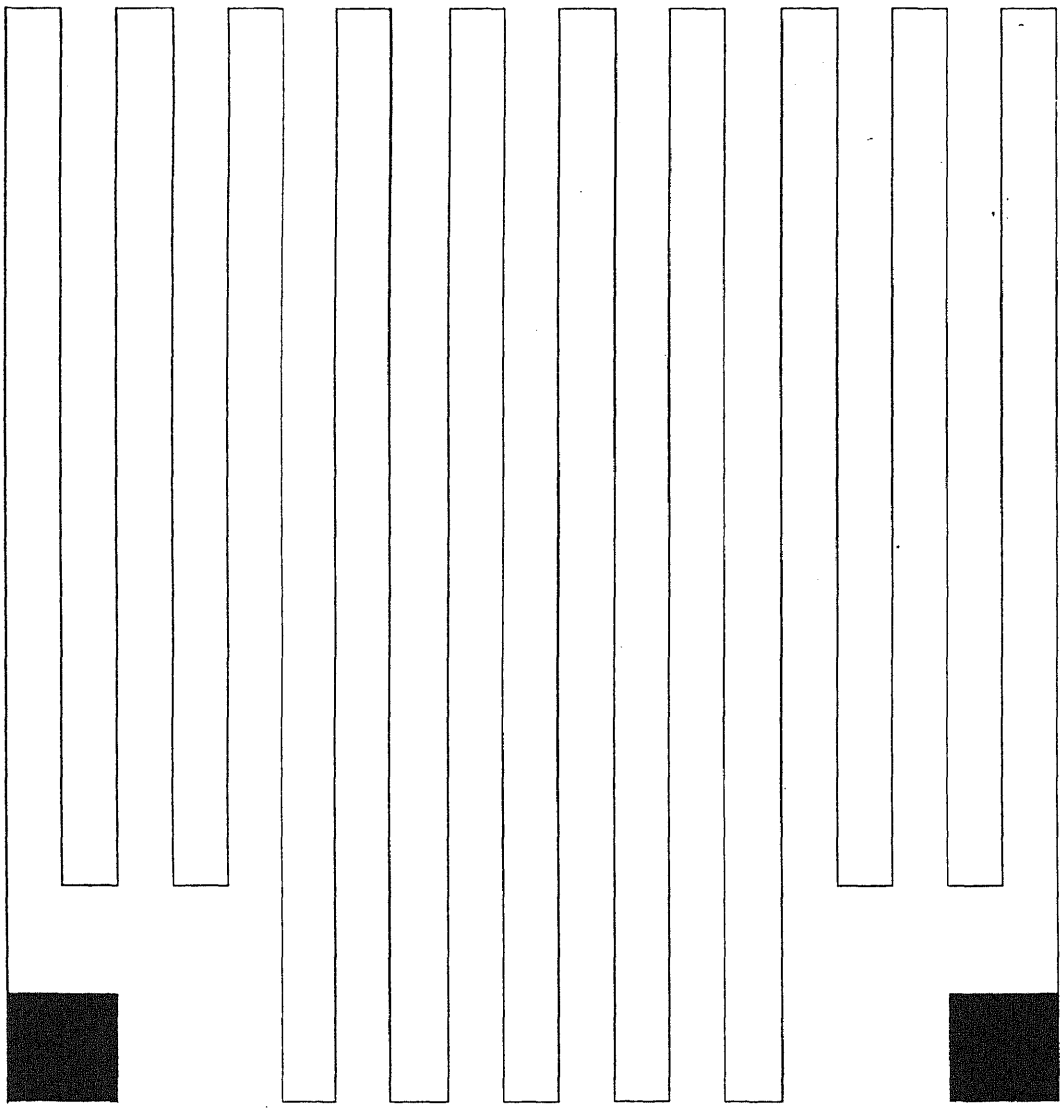

Figure 5.1 Layout of the Pt thin film resistor

5.1.3 Calibration of the Thermal Microprobe

At the first step of the calibration, a Pt thin film resistor was immersed in an oil temperature bath. Increasing the bath temperature from 21 °C to 110 °C, the corresponding resistance of the Pt thin film resistor was recorded and the resistance vs. temperature curve was obtained as shown in Figure 5.2. The resistance change per degree of the Pt thin film resistor is 35.3 Ω.

In the second step, we applied electrical power to the Pt thin film resistor and positioned the thermal microprobe tip on the heated Pt thin film resistor wire. After increasing the applied power (therefore increasing the temperature of the resistor) to a new level and waiting for thermal equilibration, the resistance of the resistor and the corresponding EMF voltage of the thermal microprobe were recorded. The curve of EMF voltage vs. resistance is shown in Figure 5.3.

In the third step, by combining Figure 5.2 and a line giving the best fit to the data shown in Figure 5.3, we get the curve of EMF voltage of the thermal microprobe vs. temperature (Figure 5.4). This is the calibration curve of the thermal microprobe. It is linear over the temperature range 25 ~ 110 °C. The sensitivity of this thermal microprobe is 5.6 μV/°C. A second thermal microprobe was found to have a sensitivity of 4.5 μV/°C. The EMF is measured by a microvoltmeter with the smallest scale of 10 μV. This limits the temperature resolution to about 2 °C. However, it is reasonable for the temperature resolution to reach 0.01 °C with a low noise pre-amplifier to measure the EMF.

Compared to the sensitivity of 13.5 μV/°C for bulk materials in reference [28], our sensitivity value is smaller most likely due to the following reasons:

1) Our thermal microprobe is a thin film thermocouple instead of a bulk wire thermocouple in reference [28]. Thin films often have properties different from bulk materials.
2) Our thermocouple cold junction temperature is fixed at room temperature instead of 0 °C in reference [28].

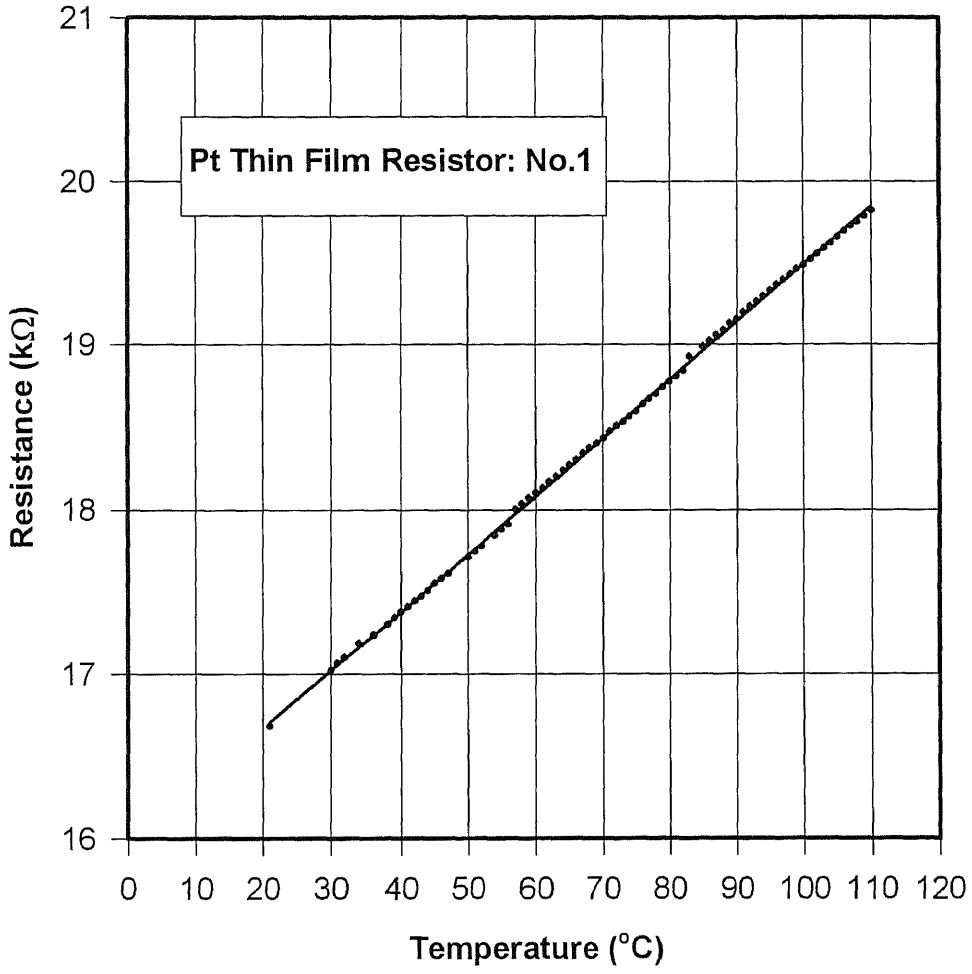

Figure 5.2 The curve of resistance vs. temperature of the Pt thin film resistor

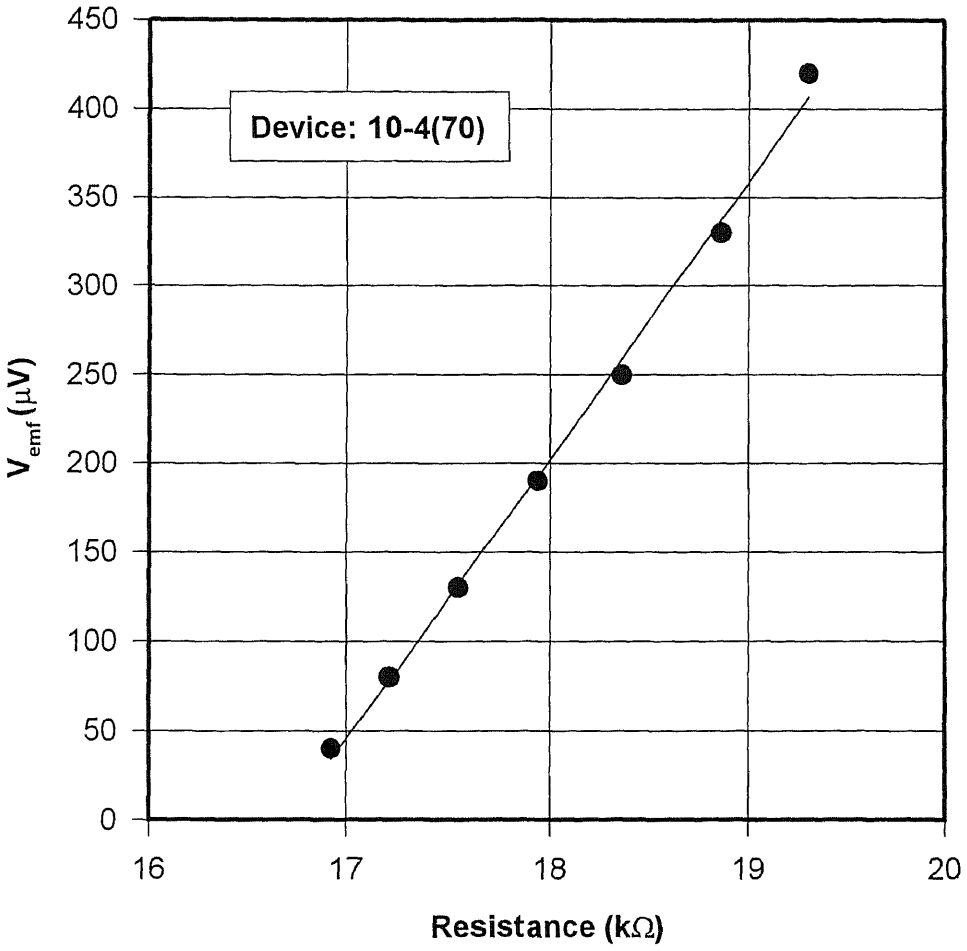

Figure 5.3 EMF voltage of the thermal microprobe vs. resistance of the Pt thin film resistor

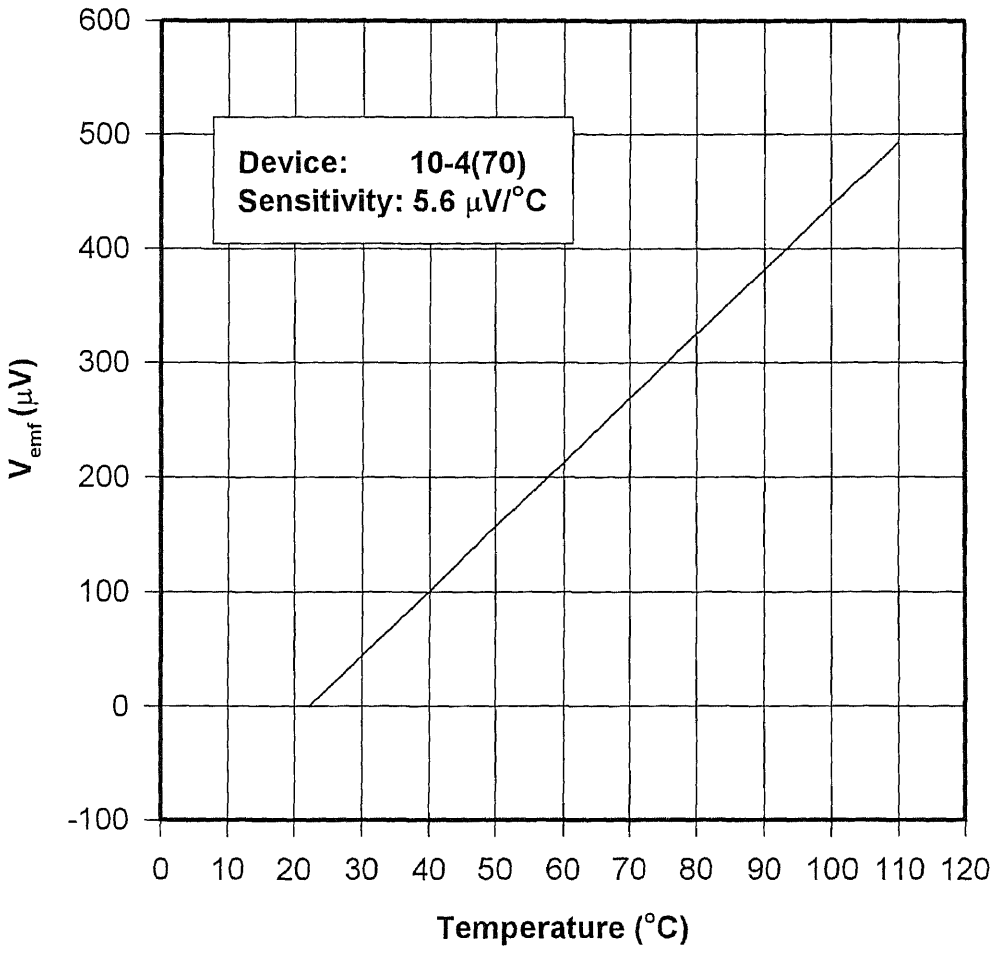

Figure 5.4 EMF voltage vs. temperature of the thermal microprobe

5.2 Topographical and Thermal Images of the Thermal Microprobe

To get the topographical and thermal images, the thermal microprobe tip was scanned across a thin tungsten film fuse structure (courtesy Digital Instruments, Inc.). The fuse structure is shown in Figure 5.5. The fuse size is 19 μm x 9 μm with 3 μm wide leads at two ends. All tungsten was deposited by focused ion beam (FIB). The thickness of tungsten in the fuse area is much thinner than in the leads.

When electrical current is applied, the fuse becomes heated. The larger the current, the higher the temperature in the fuse area. Electrical currents of 4 mA, 6 mA and 8 mA were applied to the fuse and the thermal microprobe was scanned across the fuse during each application. The topographical and thermal images of the fuse that were obtained are shown in Figure 5.6. The lower images in Figure 5.6 are the topographical images, clearly showing the structure of the tungsten thin film structure. The upper images in Figure 5.6 are the thermal images. The brighter the thermal image, the higher the temperature. Combined with the topographical image, we can see from the thermal images that the temperature in the fuse area is higher than in the leads to the fuse. Moreover, we also can see from Figure 5.6 that the electrical current increased from 4 mA, 6 mA to 8 mA, the brightness of the thermal image is increased showing that the temperature also increased.

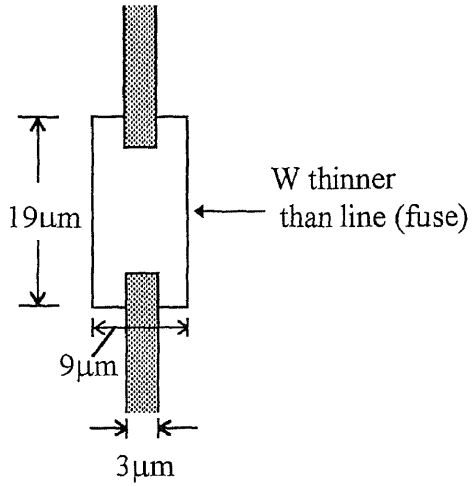

Figure 5.5 W thin film fuse structure

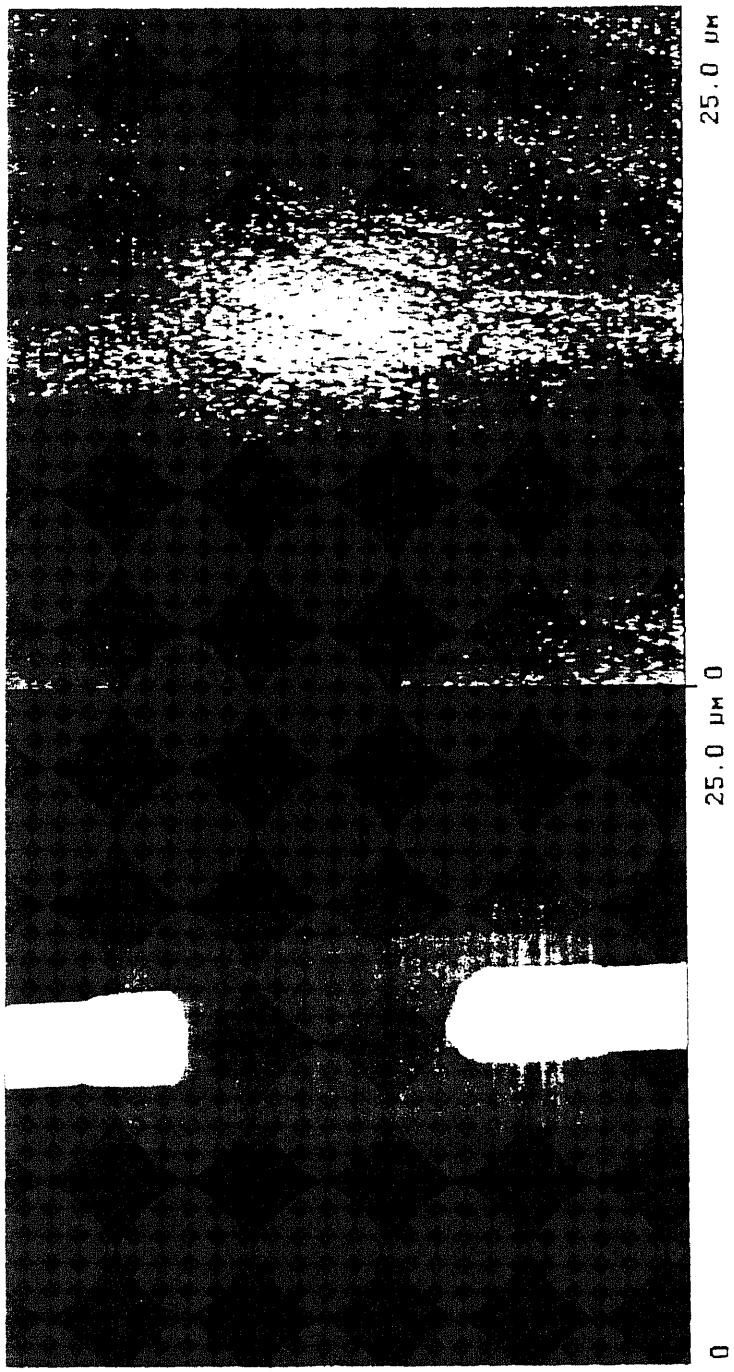

(a) Applied electrical current: 4 mA

Figure 5.6 Topographical (lower) and thermal (upper) images of W thin film fuse

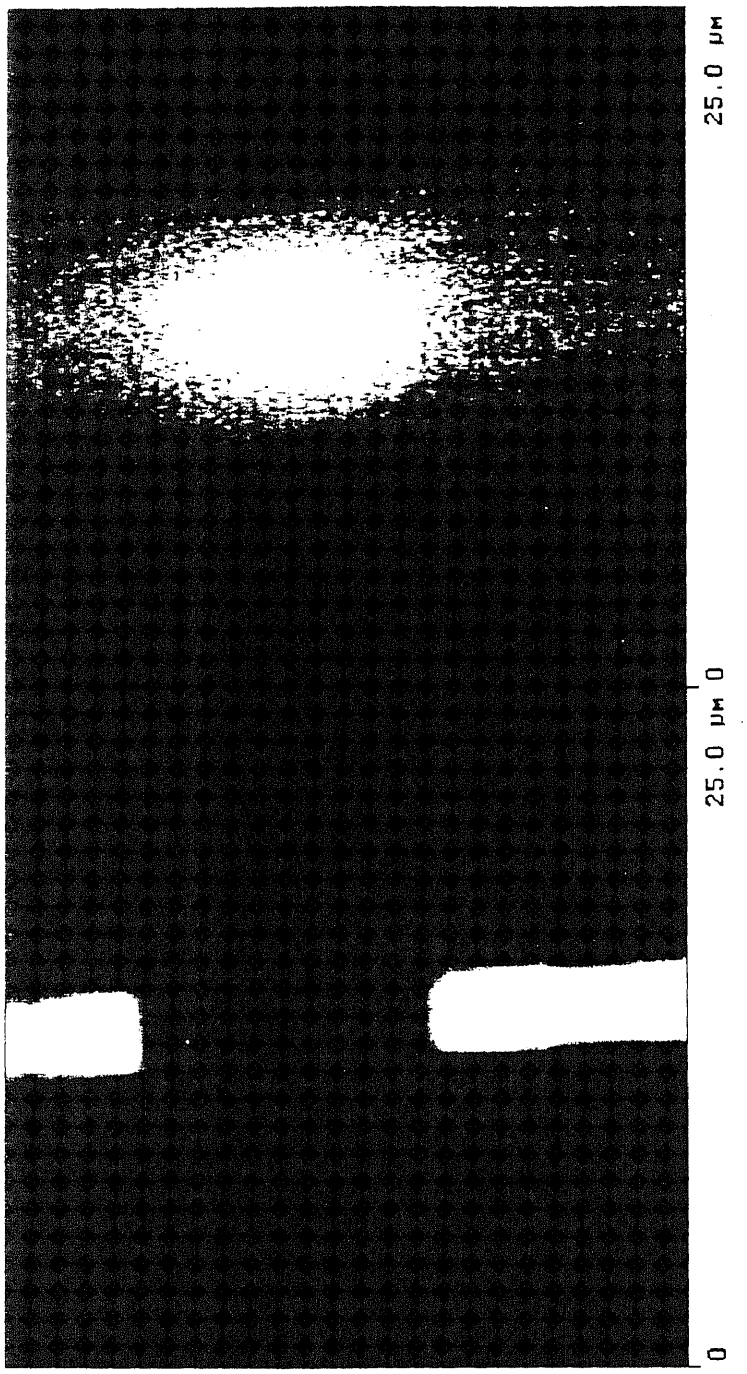

(b) Applied electrical current: 6 mA

Figure 5.6 (continued) Topographical (lower) and thermal (upper) images of W thin film fuse

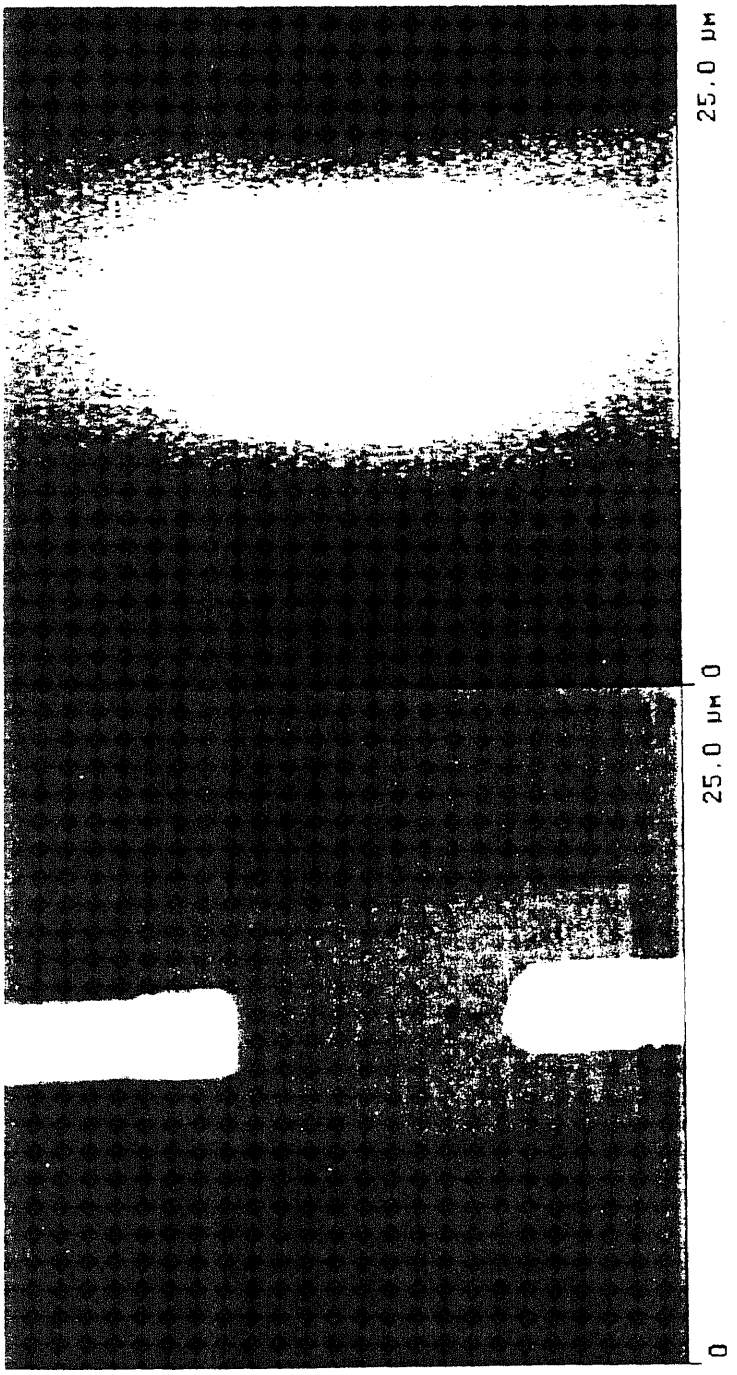

(c) Applied electrical current: 8 mA

Figure 5.6 (continued) Topographical (lower) and thermal (upper) images of W thin film fuse

5.3 Discussions and Suggestions

The Seebeck effect results from the temperature dependence of the Fermi energy E_f. If the temperature distribution in the thermocouple junction is uniform, the Fermi energy of two metals in the junction area both before and after junction formation is also uniform (Figure 5.8). The EMF is decided by the temperature difference (T_1-T_2) between the hot and cold junctions, and the temperature resolution is not related to the size of the junction area. However, if the temperature distribution in the thermocouple junction is nonuniform, the Fermi energy of each metal is also nonuniform before contact, but after contact the Fermi energy becomes constant and an average of the two (Figure 5.9). Thus, the hot junction temperature is an average temperature T_3 instead of T_1. T_3 is related to the size of the junction area, and the temperature resolution is therefore controlled in part by the area of the thermocouple. The smaller the sensor, the higher the temperature resolution.

In previous work where probes were individually fabricated[10,11,12,13], the thermal sensors were larger than 25 μm and the thermal resolution of the much smaller junctions made in this research is expected to be superior. Other recent research made submicron-meter size thermocouple junctions by the use of high electrical fields[14], but those devices required individual fabrication. The research presented here using wafer-stage processing steps with controlled photoresist coating to form the thermocouple has an advantage over methods requiring individual fabrication. This method is more reproducible, and a large number of probes can be obtained at the same time from a 4-inch-diameter silicon wafer. This method confines the thermocouple junction to a region less than 0.5 μm from the end of the probe tip.

The sensitivity (4.5 ~ 5.6 μV/°C) of the Au/Pd thin film thermocouple in our thermal microprobe is similar to the Au/Pt thin film thermocouple in reference [14] (6 μV/oC). However, the spatial and thermal resolution can still be improved. Suggestions for a next generation thermal microprobe is as follows:

1) Increase the aspect ratio of the probe tip by deep anisotropic RIE to form the probe tip. This will allow the probe to better follow the surface of a highly-textured sample.
2) Decrease the thickness of two metal layers at the end of the tip to reduce the curvature radius and get better spatial resolution.
3) Improve the electronics of the EMF measuring system to reduce the electrical noise and get better temperature resolution.

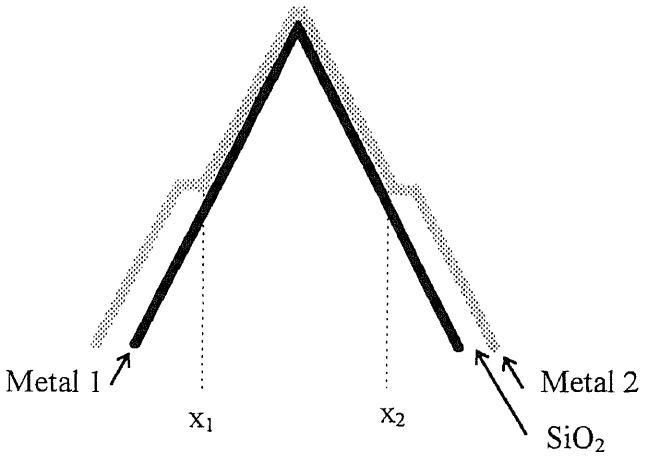

Figure 5.7 Illustration of thermocouple structure, defining limits used in Figures 5.8 and 5.9

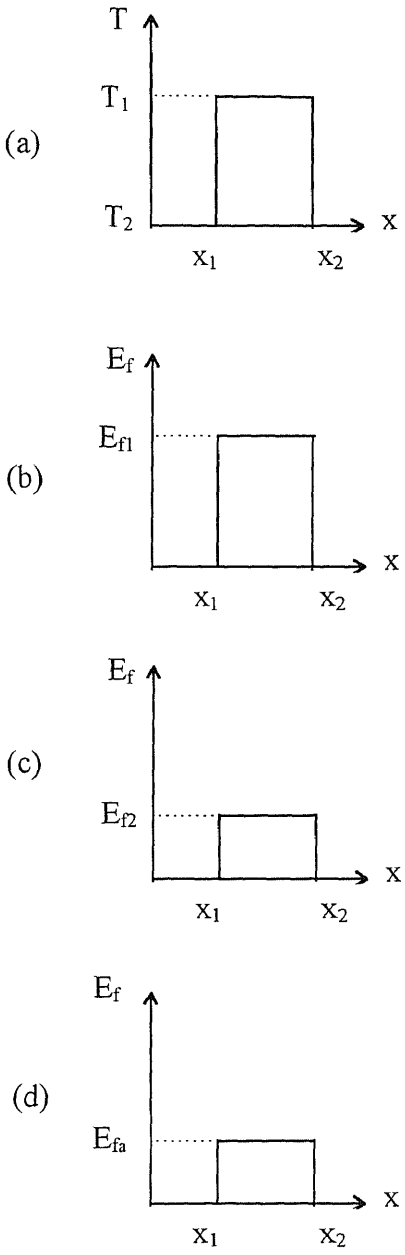

Figure 5.8 Illustration of Fermi energy level in the thermocouple junction (a) is the assumed linear temperature distribution between points x_1 and x_2 (Figure 5.7), (b) and (c) show Fermi levels in the two metals before contact, and (d) shows the resulting Fermi level after contact.

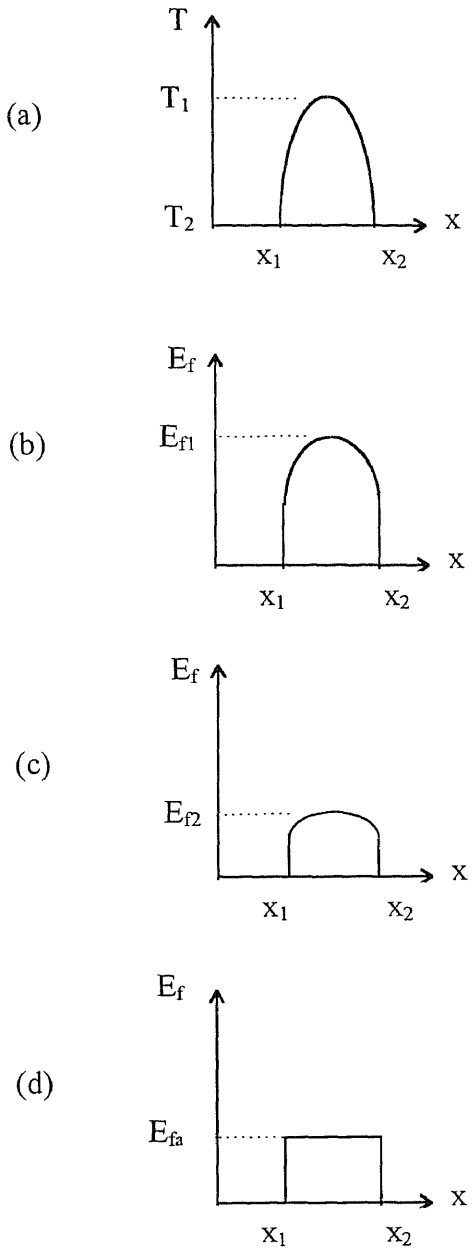

Figure 5.9 Illustration of Fermi energy level in the thermocouple junction In this case a nonuniform temperature distribution is assumed.

CHAPTER 6

SUMMARY OF THE RESULTS

This research program is concerned with the design, fabrication and characterization of a thermal microprobe. The main results of this dissertation are as follows:

1. An atomic force microscope with silicon cantilever and tip has been designed with a thin film Au/Pd thermocouple on the end of an AFM silicon probe tip. The overall dimension of the device is 3.6 mm x 1.6 mm. The cantilever size is 200 μm long, 40 μm wide and 1.5 μm thick; this meets the requirements of low force constant, high resonant frequency and short cantilever length.
2. A method was devised for making single, atomically sharp silicon tips, which avoids the formation of multiple tips.
3. The hot thermocouple junction was confined to a small region 0.3 ~ 0.5 μm at the end of the tip by a specially developed method of controlled photoresist coating. This method is reproducible, reliable and simple.
4. A compensation pattern was designed at convex corners to give the desired shape after backside KOH etching to release the silicon cantilever.
5. A complete processing procedure was designed for fabricating a thermal microprobe on a 4-inch-diameter silicon wafer. This process is reproducible and productive.

6. A method was devised to calibrate the thermal microprobe over the temperature range 25 °C ~ 110 °C. The measured sensitivity on two thermal microprobes is 4.5 and 5.6 μV/°C.
7. Thermal images and topographical images were obtained from a heated tungsten thin film fuse. The thermal images show a rise in fuse temperature after increasing the applied electrical current.
8. Improvements are suggested for a "next generation" thermal microprobe:

   (1) Increase the aspect ratio of the probe tip.

   (2) Decrease the thickness of two metal layers at the end of the tip.

   (3) Improve the electronics of the EMF measuring system.

APPENDIX A

MASK LAYOUT

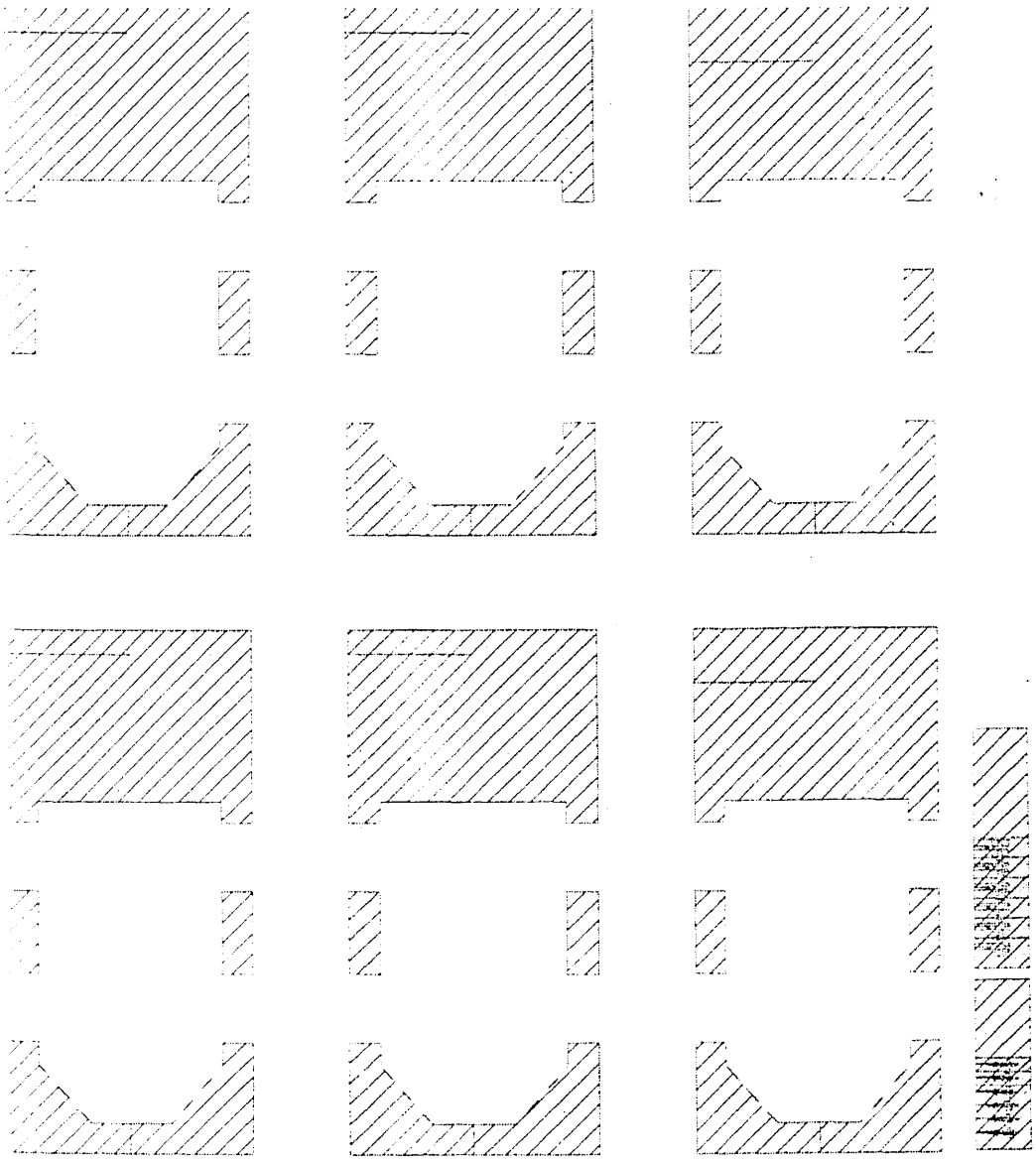

Figure A.1 Mask 1: Disk

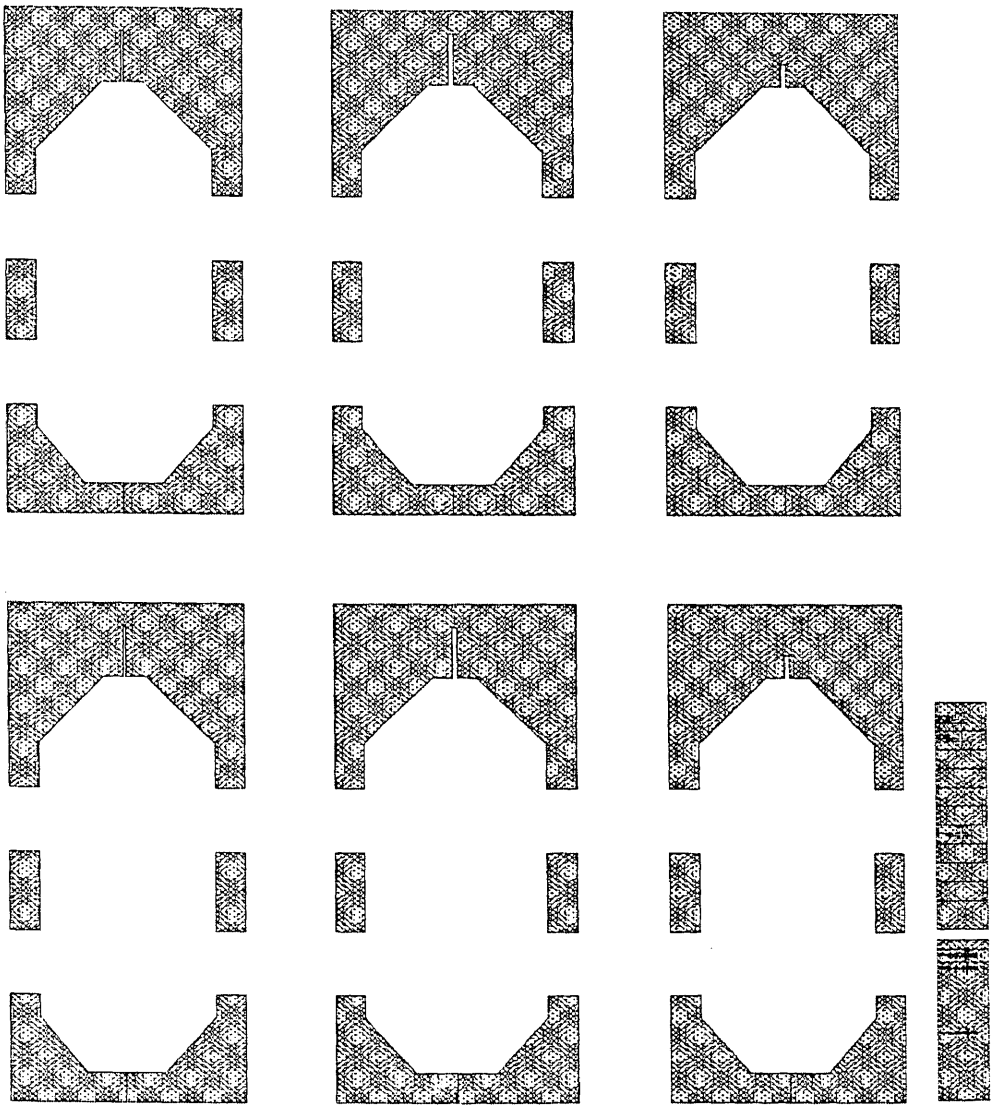

Figure A.2 Mask 2: Cantilever

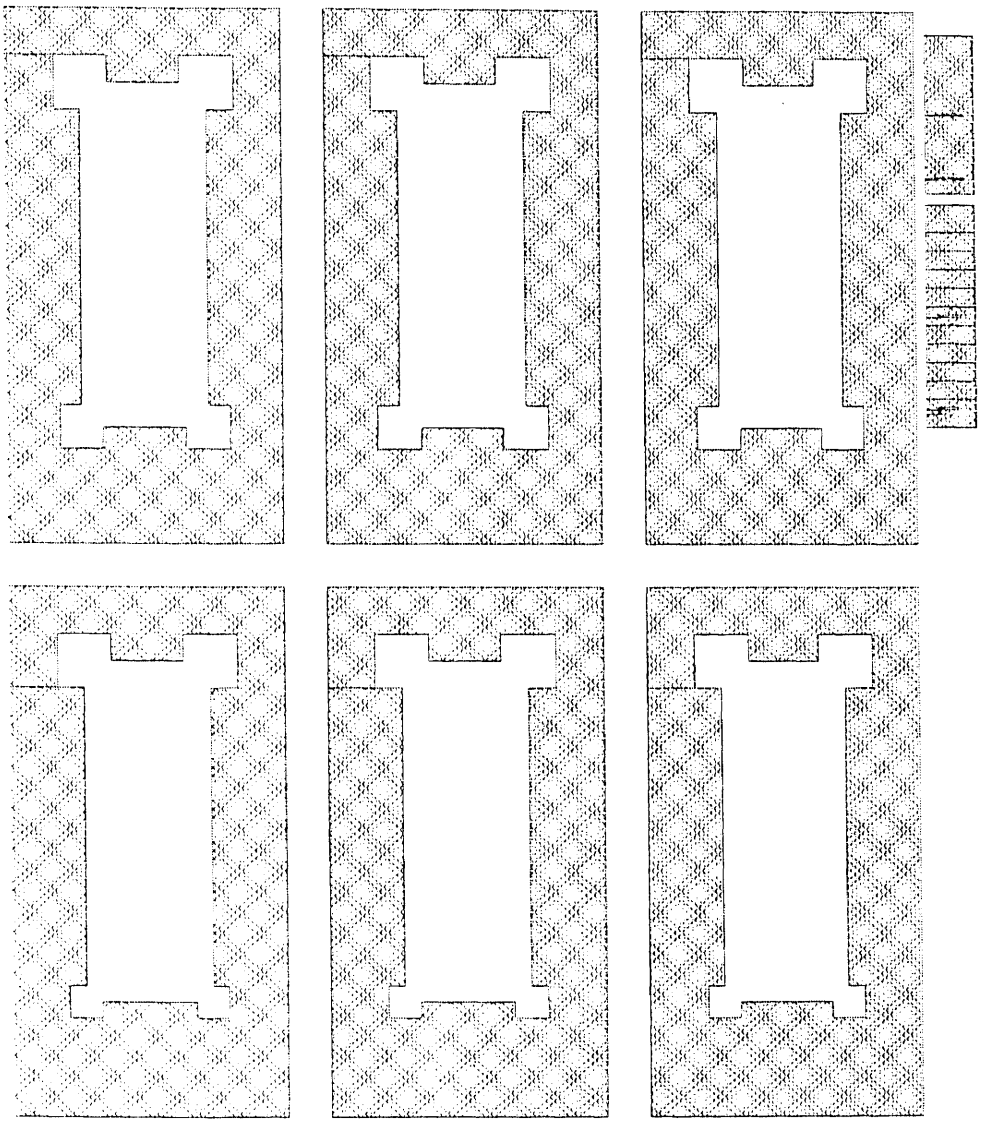

Figure A.3 Mask 3: Backside

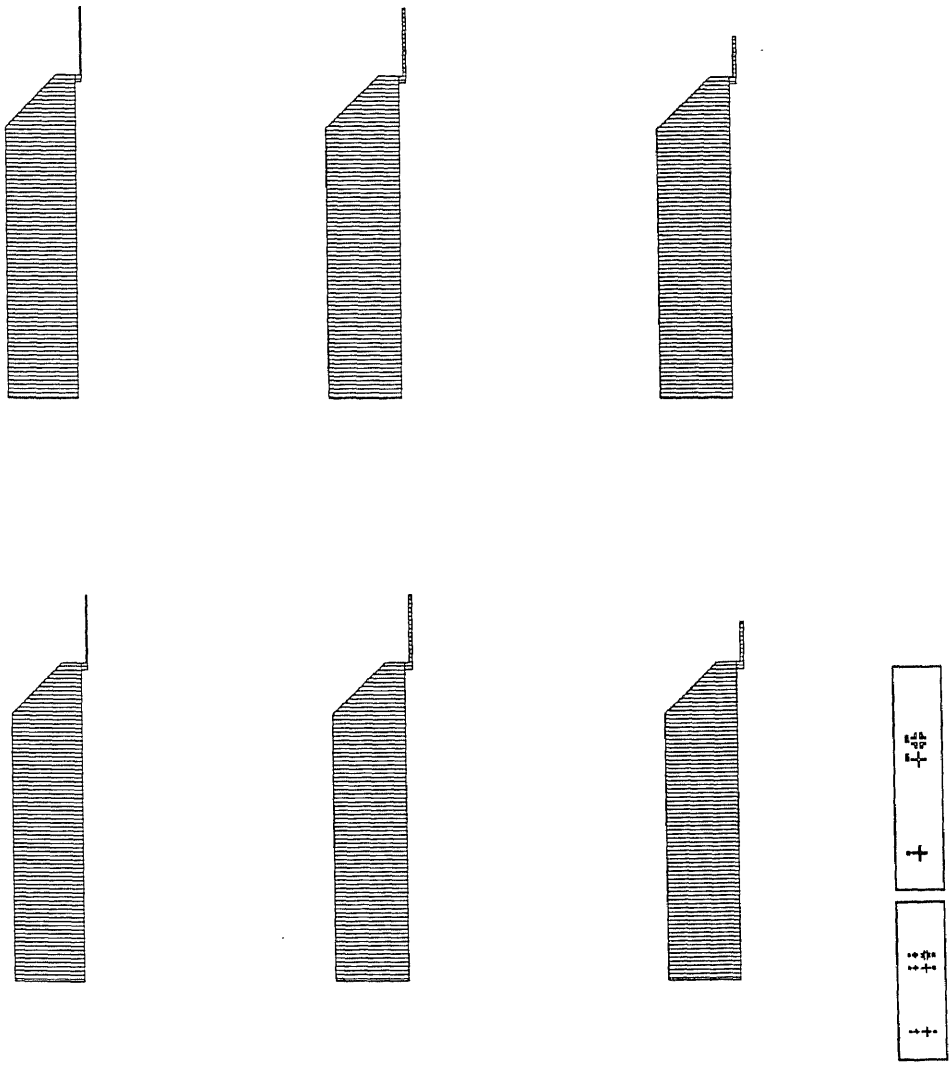

Figure A.4 Mask 4: Metal 1

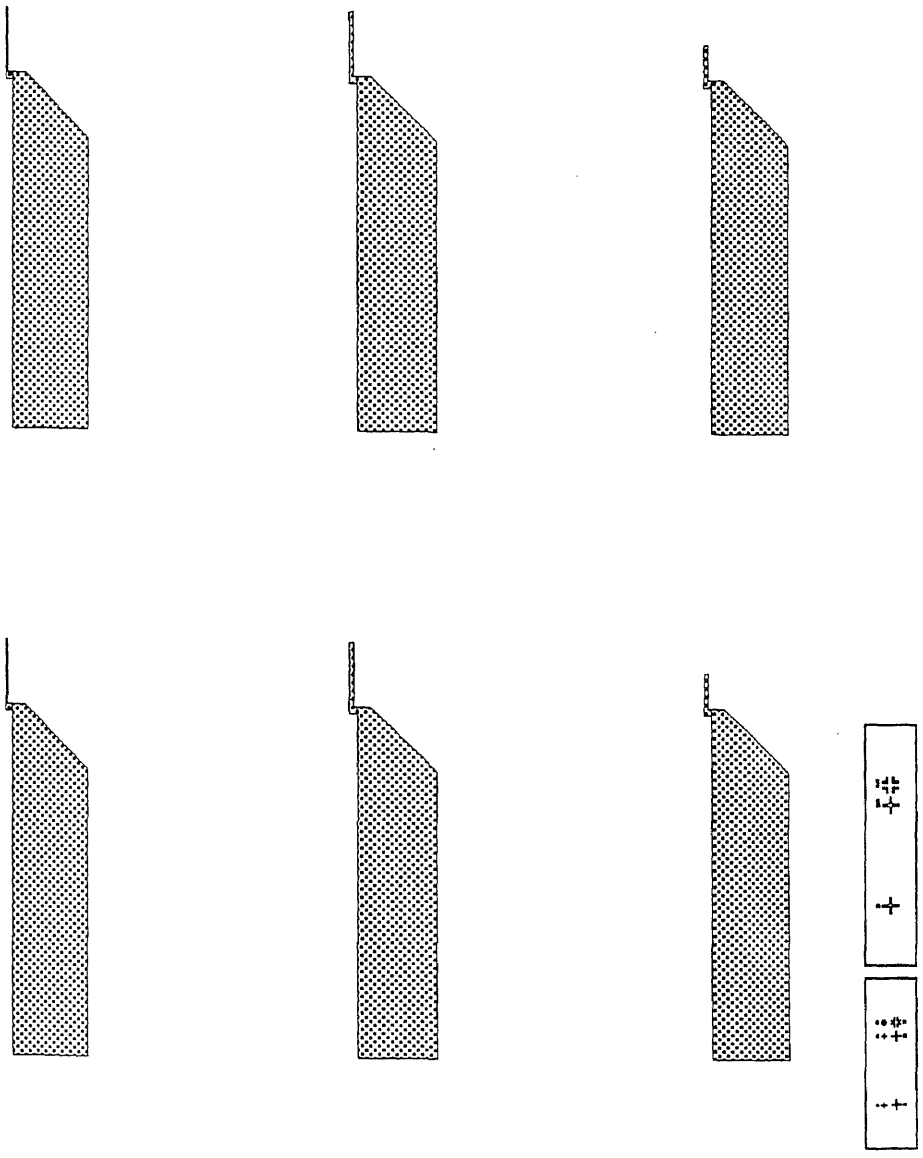

Figure A.5 Mask 5: Metal 2

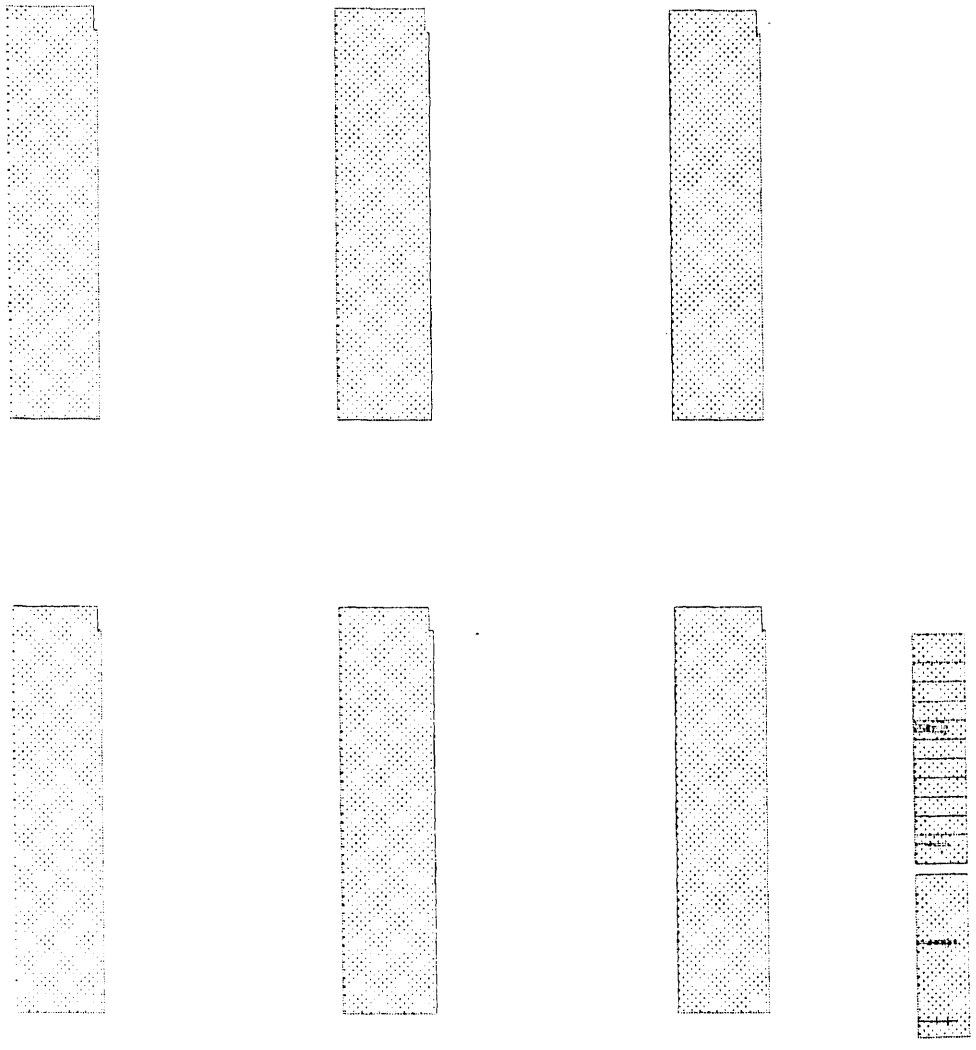

Figure A.6 Mask 6: Window

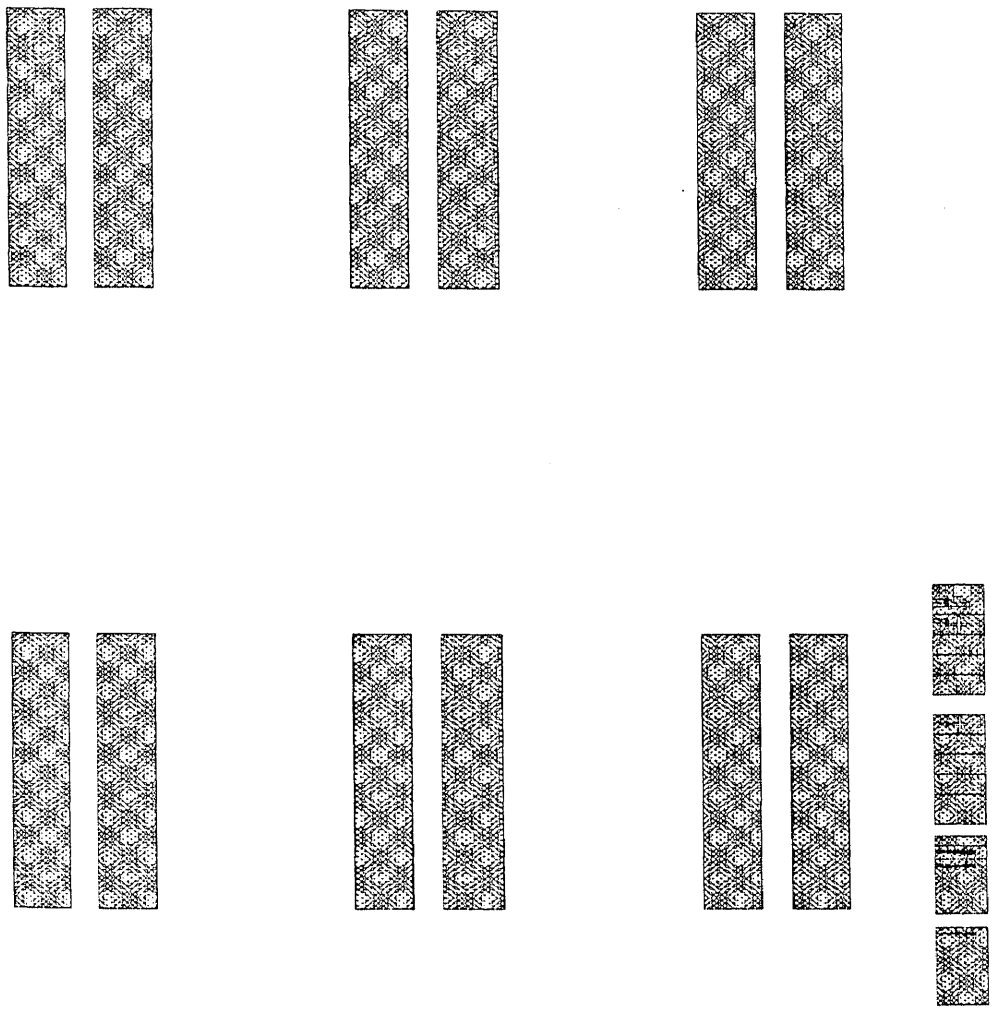

Figure A.7 Mask 7: Contact Pad

APPENDIX B

THERMAL MICROPROBE FABRICATION PROCESSING FLOW

1. **P-clean**: 5:1 H_2SO_4:H_2O_2, temperature: 110 °C, time: 10 minutes, rinse hot DI water 10 minutes, rinse cold DI water 5 minutes, blow dry.

2. **Furnace pre-clean**: 100:1 H_2O:HF, time: 1 minute, rinse cold DI water 10 minutes, blow dry.

3. **Steam oxidation**: O_2: 7.5 SLM, bubbler: 530 sccm, temperature: 1050 °C, time: 30 minutes (target: 2000 Å).

4. **Photolithography**: apply photoresist (Shipley 3813): 2000 rpm, 30 seconds. Box oven soft bake: 115 °C, 20 minutes. Align and expose (Mask 1): 20 seconds. Develop (MF 319): 30 seconds + 30 seconds. Box oven hard bake: 115 °C, 20 minutes.

5. **Wet etch oxide**: 7:1 BOE, 25 °C, 2 minutes, rinse cold DI water 10 minutes, blow dry.

6. **RIE Si**: 40 sccm SF_6, 250 mtorr, 50 watts, 25 °C, 12 minutes.

7. **RIE Si**: 25 sccm Cl_2, 10 sccm BCl_3, 180 mtorr, 175 watts, 25 °C, 15 minutes.

8. **Strip photoresist**: 5:1 H_2SO_4:H_2O_2, temperature: 110 °C, time: 10 minutes, rinse hot DI water 10 minutes, rinse cold DI water 5 minutes, blow dry.

9. **Wet isotropic etch Si**: 95% vol:2% vol:3% vol HNO_3:HF:CH_3COOH, 25 °C, about 100 seconds. Rinse cold DI water 10 minutes. Blow dry.

10. **Photolithography**: apply photoresist (Shipley 827): 2000 rpm, 30 seconds. Box oven soft bake: 115 °C, 20 minutes. Align and expose (Mask 2): 30 seconds. Develop (MF 319): 30 seconds + 30 seconds. Box oven hard bake: 115 °C, 20 minutes.

11. **RIE Si**: 75 sccm SF_6, 105 mtorr, 400 watts, 25 °C, 11 minutes.

12. **Strip photoresist**: 5:1 H_2SO_4:H_2O_2, temperature: 110 °C, time: 10 minutes, rinse hot DI water 10 minutes, rinse cold DI water 5 minutes, blow dry.

13. **Wet etch oxide**: 7:1 BOE, 25 °C, 2 minutes, rinse cold DI water 10 minutes, blow dry.

14. **Pre-sharpening treatment**: 95% vol:2% vol:3% vol HNO_3:HF:CH_3COOH, 25 °C, about 5 seconds. Rinse cold DI water 10 minutes. Blow dry.

15. **P-clean**: 5:1 H_2SO_4:H_2O_2, temperature: 110 °C, time: 10 minutes, rinse hot DI water 10 minutes, rinse cold DI water 5 minutes, blow dry.

16. **Furnace pre-clean**: 100:1 H_2O:HF, time: 1 minute, rinse cold DI water 10 minutes, blow dry.

17. **Dry oxidation sharpening**: O_2: 7.5 SLM, temperature: 950 °C, time: 5 hours.

18. **Wet etch oxide**: 7:1 BOE, 25 °C, 2 minutes, rinse cold DI water 10 minutes, blow dry.
    (Step 17 and step 18 will be repeated several times until getting atomic sharp tips.)

19. **P-clean**: 5:1 H_2SO_4:H_2O_2, temperature: 110 °C, time: 10 minutes, rinse hot DI water 10 minutes, rinse cold DI water 5 minutes, blow dry.

20. **Furnace pre-clean**: 100:1 H_2O:HF, time: 1 minute, rinse cold DI water 10 minutes, blow dry.

21. **Dry oxidation**: O_2: 7.5 SLM, temperature: 950 °C, time: 20 minutes (target: 250 Å).

22. **LPCVD deposit Si_3N_4** (both side): 50 sccm DCS, 120 sccm NH_3, 400 mtorr, 775 °C, 40 minutes (target: 2000 Å).

23. **Low temperature oxide (LTO) deposit** (both side): 300 sccm SiH_4, 75 sccm O_2, 500 mtorr, 425 °C, 3 hours (target: 3000 Å).

24. **Front side wet etch oxide** (back side photoresist protection): 7:1 BOE, 25 °C, 2 minutes, rinse cold DI water 10 minutes, blow dry.

25. **Front side wet etch Si_3N_4**: H_3PO_4, 170 °C, 25 minutes. Rinse hot DI water 10 minutes, rinse cold DI water 5 minutes, blow dry.

26. **Back side wet etch LTO** (front side photoresist protection): 7:1 BOE, 25 °C, 2 minutes, rinse cold DI water 10 minutes, blow dry.

27. **Photolithography** (back side): apply photoresist (Shipley 3813): 2000 rpm, 30 seconds. Box oven soft bake: 115 °C, 20 minutes. Align (infrared) and expose (Mask 3): 18 seconds. Develop (MF 319): 30 seconds + 15 seconds. Box oven hard bake: 115 °C, 20 minutes.

28. **RIE Si_3N_4**: 50 sccm SF_6, 150 mtorr, 400 watts, 25 °C, 4 minutes.

29. **Thin oxide strip**: 100:1 H_2O:HF, time: 3 minute, rinse cold DI water 10 minutes, blow dry.

30. **Strip photoresist**: 5:1 H_2SO_4:H_2O_2, temperature: 110 °C, time: 10 minutes, rinse hot DI water 10 minutes, rinse cold DI water 5 minutes, blow dry.

31. **Photolithography**: apply photoresist twice (Shipley 827): 2000 rpm, 30 seconds. Box oven soft bake: 115 °C, 20 minutes. Align and expose (Mask 4): 2 minutes. Develop (MF 319): 30 seconds + 30 seconds. Box oven hard bake: 115 °C, 10 minutes.

32. **Sputtering deposit Pd**: 5 mtorr, 100 watts, 100 Å Ti, then 500 Å Pd

33. **Lift off Pd**: strip photoresist in acetone, rinse cold DI water 10 minutes, blow dry.

34. **P-clean**: M-pyrol, 95 °C, 10 minutes. Rinse cold DI 10 minutes. Blow dry.

35. **Low temperature oxide (LTO) deposit**: 300 sccm SiH_4, 75 sccm O_2, 500 mtorr, 425 °C, 3 hours (target: 3000 Å).

36. **Coat photoresist except tip end**: apply photoresist (Shipley 827), spin 0.5 second, evaporate 10 seconds, spin 2000~3000 rpm 30 seconds. Box oven hard bake: 115 °C, 20 minutes.

37. **RIE LTO on tip**: 25 sccm CF_4, 25 sccm CHF_3, 500 mtorr, 300 watts, 25 °C, 3 minutes.

38. **Strip photoresist**: M-pyrol, 95 °C, 10 minutes primary, 10 minutes secondary. Rinse cold DI 10 minutes. Blow dry.

39. **Photolithography**: apply photoresist twice (Shipley 827): 2000 rpm, 30 seconds. Box oven soft bake: 115 °C, 20 minutes. Align and expose (Mask 5): 2 minutes. Develop (MF 319): 30 seconds + 30 seconds. Box oven hard bake: 115 °C, 10 minutes.

40. **Sputtering deposit Au**: 5 mtorr, 100 watts, 100 Å Cr, then 500 Å Au.

41. **Lift off Pd**: strip photoresist in acetone, rinse cold DI water 10 minutes, blow dry.

42. **Photolithography**: apply photoresist twice (Shipley 827): 2000 rpm, 30 seconds. Box oven soft bake: 115 °C, 20 minutes. Align and expose (Mask 6): 2 minutes. Develop (MF 319): 30 seconds + 30 seconds. Box oven hard bake: 115 °C, 10 minutes.

43. **RIE LTO**: 25 sccm CF_4, 25 sccm CHF_3, 500 mtorr, 300 watts, 25 °C, 3 minutes.

44. **Strip photoresist**: M-pyrol, 95 °C, 10 minutes primary, 10 minutes secondary. Rinse cold DI 10 minutes. Blow dry.

45. **KOH etch Si** (front side protected by special holder): 45%(w) KOH, 80 °C, 6~7 hours. Rinse hot DI 10 minutes, rinse cold DI 10 minutes. Blow dry.

46. **RIE Si**: 40 sccm SF_6, 250 mtorr, 150 watts, 25 °C, etch to completely release cantilever.

REFERENCES

1. E. Doebelin, *Measurement Systems: Application and Design*, 3rd edtion, McGraw-Hill, New York, 1985.

2. S. Heng, and W. Z. Black, "Temperature mapping of localized hot spots on microelectronic chip surfaces," *J. Electron. Packaging*, vol. 113, 286(1991).

3. T. Q. Qiu, C. P. Grigoropoulos, and C. L. Tien, *Experimental Heat Transter*, 6, 231(1993).

4. K. Azar, J. R. Benson, and V. P. Manno, *IEEE 7th Annual Semiconductor Thermal Measurement & Management Symposium*, IEEE, New York, 23(1991).

5. R. Ostermeir, K. Brunner, G. Abstreiter, and W. Weber, "Temperature distribution in Si-MOSFET's studied by micro Raman spectroscopy," *IEEE Trans. Electron Devices*, ED-39, 858(1992).

6. G. Binning, H. Rohrer, Ch. Gerber, and E. Weibel, "Surface studies by scanning tunneling microscopy," *Phys. Rev. Lett.*, 49, 57(1982).

7. G. Binning, C. F. Quate, and Ch. Gerber, "Atomic force microscope," *Phys. Rev. Lett.*, 56, 930(1986).

8. S. Alexander, L. Hellemans, O. Marti, J. Schneir, V. Elings, P. K. Hansma, M. Longmire, and J. Hurley, "An atomic-resolution atomic-force microscope implemented using an optical lever," *J. Appl. Phys.*, 65, 164(1988).

9. G. Meyer, and N. M. Amer, "Novel optical approach to atomic force microscope," *Appl. Phys. Lett.*, 53, 1045(1992).

10. A. Majumdar, J. P. Carrejo, and J. Lai, "Thermal imaging using the atomic force microscope," *Appl. Phys. Lett.*, 62,2501(1993).

11. O. Nakabeppu, M. Chandrachood, Y. Wu, J. Lai, and A. Majumdar, "Scanning thermal imaging microscopy using composite cantilever probes," *Appl. Phys. Lett.*, 66, 694(1995).

12. R. J. Pylkki, P. J. Moyer, and P. E. West, "Scanning near-field optical microscopy and scanning thermal microscopy," *Jpn. J. Appl. Phys.:Part 1*, 33, 3785(1994).

13. A. Hammiche, H. M. Pollock, M. Song, and D. J. Hourston, "Sub-surface imaging by scanning thermal microscopy," *Meas. Sci. Technol.*, 7, 142(1996).

14. K. Luo, Z. Shi, J. Lai, and A. Majumdar, "Nanofabrication of sensors on cantilever probe tips for scanning multiprobe microscopy," *Appl. Phys. Lett.*, 68, 325(1996).

15. C. M. Mate, G. M. McClelland, R. Erlandsson, and S. Chiang, "Atomic-scale friction of a tungsten tip on a graphite surface," *Phys. Rev. Lett.*, 59, 1942(1987).

16. Y. Martin, C. C. Williams, and H. K. Wickramasinghe, "Atomic force microscope-force mapping and profiling on a sub 100-Å scale," *J. Appl. Phys.*, 61, 4723(1987).

17. Y. Martin, and H. K. Wickramasinghe, "Magnetic imaging by 'force microscopy' with 1000 Å resolution," *Appl. Phys. Lett.*, 50, 1455(1987).

18. J. E. Stern, B. D. Terris, H. J. Mamin, and D. Rugar, "Deposition and imaging of localized charge on insulator surface using a force microscope," *Appl. Phys. Lett.*, 53, 2717(1988).

19. D. Rugar, H. J. Mamin, and P. Guethner, "Improved fiber-optical interferometer for atomic force microscopy," *Appl. Phys. Lett.*, 55, 2588(1989).

20. T. R. Albrecht, and C. F. Quate, "Atomic resolution imaging of a nonconductor by atomic force microscopy," *J. Appl. Phys.*, 62, 2599(1987).

21. O. Marti, H. O. Ribi, B. Drake, T. R. Albrecht, C. F. Quate, and P. K. Hansma, "Atomic force microscopy of an organic monolayer," *Science*, 239, 50(1988).

22. T. R. Albrecht, S. Akamine, T. E. Carver, and C. F. Quate, "Microfabrication of cantilever styli for the atomic force microscope," *J. Vac. Sci. Technol.*, A8(4), Jul/Aug, 3386(1990).

23. J. Bryzek, K. Peterson, and W. McCulley, "Micromachines on the march," *IEEE Spectrum*, May, 20(1994).

24. O. Marti, B. Drake, and P. K. Hansma, "Atomic force microscopy of liquid-covered surface: atomic resolution images," *Appl. Phys. Lett.*, 51, 484(1987).

25. W. C. Young, *ROARK's Formulas for Stress and Strain*, 6th edition, McGraw-Hill, New York, 1989.

26. T. J. Seebeck, "Evidence for the Thermal Current from the Combination Bi-Cu by Its Action on the Magnetic Needle", *Ab. K. Akad. Wiss. Berlin*, 265, 1822(1821).

27. J. C. A. Peltier, "Nouvelles experiences sur la caloricite des courans electriques," *Ann. Chim. Phys. [2]*, 56, 371(1834).

28 W. Thomson, "Theory of thermoelectricity in crystals," *Trans. Edinburgh Soc.*, 21, 153(1847).

29. G. W. C. Kaye, and T. H. Laby, *Tables of Physical and Chemical Constants and Some Mathematical Functions*, Longman, London, 1973.

30. P. A. Kinzie, *Thermocouple Temperature Measurement*, Wiley, New York, 1973, p1.

31. A. Enver, *Digital Equipment Corporation*, private communication, 1996.

32. Yongxia Zhang, Yanwei Zhang, T. S. Sriram, and R. B. Marcus, "Formation of single tips of oxidation-sharpened Si," *Appl. Phys. Lett.*, vol.69, No.27, 4260(1996).

33. Yongxia Zhang, Yanwei Zhang, T. S. Sriram, and R. B. Marcus, "Formation of single tips of atomically sharp silicon," *the 43rd National Symposium of the American Vacuum Society*, Philadelphia, Pennsylvania, Oct.12-18, 1996.

34. K. E. Petersen, "Silicon as a mechanical material," *Proceedings of the IEEE*, vol. 70, No.5, 420(1982).

35. R. B. Marcus, T. S. Ravi, T. Gmitter, K. Chin., D. Liu, W. J. Orvis, D. R. Ciarlo, C. E. Hunt, and J. Trujillo, "Formation of silicon tips with < 1 nm radius," *Appl. Phys. Lett.*, 56(3), 236(1990).

36. T. S. Ravi, R. B. Marcus, and D. Liu, "Oxidation sharpening of silicon tips," *J. Vac. Sci. Techno.*, B9(6), 2733(1991).

37. J. Brugger, R. A. Buser, and N. F. de Rooij, "Silicon cantilevers and tips for scanning force microscopy," *Sensors and Actuators A*, 34, 193(1992).

38. M. Wendman, *Digital Instruments, Inc.*, private communication, 1995.

39. A. S. Grove, *Physics and Technology of Semiconductor Devices*, Wiley, New York, 1967, pp23-31.

40. D. B. Kao, J. P. McVittie, W. D. Nix, and K. C. Saraswat, "Two-dimensional Thermal oxidation of silicon---I. Experiments," *IEEE Trans. Elect. Dev.*, ED-34, 1008(1987).

41. R. C. Davis, C. C. Williams, and P. Neuzil, "Micromachined submicrometer photodiode for scanning probe microscopy," *Appl. Phys. Lett.*, 66, 2309(1995).

42. R. C. Davis, C. C. Williams, and P. Neuzil, "A micromachined submicrometer photodiode for scanning probe microscopy," *the 8th International Conference on Solid-State Sensors and Actuators, and Eurosensors IX*, Stockholm, Sweden, June 25-29, 1995, p667.

43. H. Seidel, L. Csepregi, A. Henberger, and H. Baumgartel, "Anisotropic etching of crystalline silicon in alkaline solutions---I. Orientation dependence and behavior of passivation layers," *J. Electrochem. Soc.*, vol.137, No.11, 3612(1990).

44. H. Seidel, "The mechanism of anisotropic,electrochemical silicon etching in alkaline solution," *IEEE Solid-State Sensor and Actuator Workshop*, Hilton Head Island, SC, 1990, p86.

45. B. Puers, and W. Sansen, "Compensation structures for convex corner micromachining in silicon," *Sensors and Actuators*, A21-A23, 1036(1990).